FINAL REPORT

Studies of the Spectra of the Vertical Fluxes of Momentum, Heat, and Moisture in the Atmospheric Boundary Layer

DA TASK 3A99-27-005-08

Dr. Harrison E. Cramer
Dr. Frank A. Record
Mr. James E. Tillman

oject Supervisor — Dr. Henry G. Houghton

Division of Sponsored Research
Massachusetts Institute of Technology
Meteorology Department
Round Hill Field Station
South Dartmouth, Mass.

Under Contract Number
DA-36-039-SC-80209

For
METEOROLOGY DEPARTMENT
U. S. ARMY ELECTRONIC PROVING GROUND
Fort Huachuca, Arizona
April 1962

FINAL REPORT

STUDIES OF THE SPECTRA OF THE VERTICAL FLUXES OF MOMENTUM, HEAT, AND MOISTURE IN THE ATMOSPHERIC BOUNDARY LAYER

DA Task 3A99-27-005-08

Dr. Harrison E. Cramer
Dr. Frank A. Record
Mr. James E. Tillman

Project Supervisor - Dr. Henry G. Houghton

Division of Sponsored Research
Massachusetts Institute of Technology
Meteorology Department
Round Hill Field Station
South Dartmouth, Massachusetts

Under Contract Number
DA-36-039-SC-80209

for

METEOROLOGY DEPARTMENT
U. S. ARMY ELECTRONIC PROVING GROUND
Fort Huachuca, Arizona
April 1962

SUMMARY

DA TASK 3A99-27-005-08, Micrometeorology (USAEPG)
TITLE: Final Report - "Studies of the Spectra of the Vertical Fluxes of Momentum, Temperature, and Moisture in the Atmospheric Boundary Layer."
CONTRACTOR: Massachusetts Institute of Technology, Round Hill Field Station, South Dartmouth, Massachusetts

The broad objective of this task is to conduct empirical studies of the spectral composition of turbulent energy-exchange processes that occur between the atmosphere and the earth's surface. The necessary measurements of fluctuations in wind velocity, air temperature, and water vapor were made with specially-developed instrumentation and techniques, and recorded with an automatic data-handling system devised especially for this purpose. The report describes results obtained in three years of contractual effort.

An extensive program of measurements of the turbulent characteristics of the boundary layer under a variety of weather conditions was carried out during the spring and fall of 1961. Analysis of the data permits an evaluation of the influence of these conditions on the spectra of the various energy fluxes. Results reported include spectral and co-spectral analyses of the fluctuation data from 14 one-hour experiments.

Of the 14 experiments for which spectral and co-spectral estimates were determined, eight are at a height of 16 m above ground level and contain information on the X, Y, Z components of wind velocity and air temperature. The remaining six experiments contain like information measured simultaneously at heights of 16 and 40 m. The estimates refer to the frequency band from about 0.5 to 0.002 cycles/sec, the upper limit being set by the resolution time of the measurement system and the lower limit determined by the length of the observation period.

The results indicate the following tentative conclusions concerning the transfer processes occurring within the atmospheric boundary layer.

1) Power spectra of the wind-velocity components and air temperature exhibit a minus four-thirds or minus five-thirds power law dependency on frequency.

2) The spectral analyses show that under stable thermal stratification, the bulk of the turbulent energy for the X, Y, Z components of wind velocity and air temperature is generally found within the limits of the spectral band investigated. During periods of thermal instability, the energy maxima of the spectra for air temperature and the horizontal components of wind velocity occur at frequencies below 0.003 cycles/sec.

3) Co-spectra of the vertical fluxes of momentum and air temperature show an approximate inverse-square dependency on frequency at the high frequency end of the band investigated. There is evidence that the co-spectra of the vertical temperature flux contain two maxima under thermally unstable stratification - one at intermediate frequencies and another, possibly larger, peak at low frequencies. The data clearly show that the temperature flux in the direction of the mean flow cannot be ignored as in common practice, for it generally exceeds the vertical temperature flux by a factor of two.

4) The co-spectral analyses confirm the expected shift in peak energy toward higher or lower frequencies as thermal stratification becomes increasingly stable or unstable, respectively.

Intensive analysis of the bulk of the turbulence measurements recorded during 1961 is continuing under a basic research grant. Additional measurements will be made as required for other heights and roughness regimes. Spectral and co-spectral studies will be extended to investigate frequencies below 0.003 cycles/sec.

This report contains no recommendations.

METEOROLOGY DEPARTMENT
USAEPG

TABLE OF CONTENTS

LIST OF ILLUSTRATIONS

LIST OF TABLES

I. SUMMARY OF PREVIOUS WORK UNDER THE CONTRACT

Measurement techniques appropriate for an extensive empirical investigation of the spectral composition of turbulent energy exchange processes occurring in the atmospheric boundary layer are available from previous work under the contract and have been described in detail in the Annual Report (Cramer, Record, Tillman, and Vaughan, 1961). In brief, the over-all instrumentation comprises a fast-response system for simultaneous measurements of the fluctuations in wind-velocity components, air temperature, and moisture at two heights above ground level; and, a slow-response system for supporting measurements of radiation, vertical profiles of mean wind speed, wet- and dry-bulb temperature, soil temperature, and other quantities requisite for calculations of the boundary-layer heat budget. Transducers for the fast-response instrumentation comprise bead-thermistor anemometers, lightweight mechanical bivanes, and platinum-wire resistance thermometers. The development of an infrared humidity transducer is continuing. The fast-response system also includes automatic data-handling components for obtaining simultaneous measurements of the outputs of ten transducers at intervals of about 1 sec; these analog data are encoded in binary-digital form and entered on punched paper tape. The tape is later decoded and the data punched in decimal-digital form on IBM cards and also printed out by an electric typewriter. The present capacity of the data-handling system is adequate for about 2 hr of operation at a sampling rate of one complete set of data per second. Power spectra and cospectra are obtained from machine analyses of the punched-card data following established statistical procedures.

Sixteen 1-hr field experiments utilizing the complete slow-response system and one level of fast-response instrumentation, installed at a height of 16 m above the ground, were carried out during the latter part of 1960. These observations served a dual purpose of providing both a thorough operational check of the entire measurement system and a representative set of fluctuation data for preliminary spectral and cospectral analyses. As a result of these initial field trials, some changes were made in the measurement and analysis techniques. These are described below. In general, however, no major modifications were necessary.

II. MODIFICATIONS IN EXPERIMENTAL TECHNIQUES DURING 1961

As a result of the experience gained during the initial field experiments, several modifications were made to improve the reliability of the data-handling apparatus. The original sampling rate of one complete observation per second was changed to one observation each 1.2 sec, thereby permitting a reduction in the operation rate of the tape punch from 22 to 18 punches per second. Studies of the paper-tape punching mechanism with a stroboscope by C. S. Lin at the Lincoln Laboratory of the Massachusetts Institute of Technology indicated erratic operation at rates above 20 punches per second. Another change in the punching mechanism involves the use of an additional set of contacts on the channel D relay of the programmer (see the Annual Report, p. 85) to prevent the punch coils from being energized except during the interval immediately preceding the punching operation. If the punch coils remain energized for an appreciable time interval after the metal pins have been removed from the paper, the pins become locked in the punching position and the same information will be punched on the tape during the next punch cycle. This feature of the punch operation was responsible for some repetitions in the data for the earlier experiments. No errors of this type have been detected since the modification was effected.

The cadmium-sulfide photoresistive cells used in the encoding programmer of the data-handling system behaved erratically during the initial field trials. Cell resistances exhibited variations of the order of 50 percent during extended periods of high illumination and the amount of instability was found to vary widely among individual cells. This variability has been significantly reduced by selecting relatively stable cells and monitoring their resistance; also, the circuitry has been modified to reduce the effect of variations in cell resistance on the operation of the programmer. Since these changes, no programming errors due to this factor have been noted.

The wind-velocity transducers initially comprised two bead thermistors in opposite arms of a bridge circuit, one of the thermistors being exposed to the air stream and the other being shielded from the air stream but exposed to ambient air temperature (see p. 9 in the Annual Report). The purpose of the dual thermistors was to ensure bridge balance at zero flow velocity in the presence of changes in the

ambient air temperature. Experience demonstrated that the shielded thermistor was largely superfluous in the present application and it has been replaced by a fixed resistor. The bridge is balanced immediately prior to the start of each field experiment; changes in ambient air temperature during a field trial are usually small and do not significantly affect the anemometer calibration. The Philbrick operational amplifiers in the wind-velocity circuits have been modified to provide a high-voltage output for driving Esterline-Angus recorders. Two recorders have been fitted with special gears so that the chart speed matches that of the Minneapolis-Honeywell recorders used to record data from the other fast-response transducers. Previously, no visual records of fluctuations in wind velocity were available.

The length of the observation period for individual experiments has been increased from 1 to 2 hr. The longer period is essential to studies of low-frequency fluctuations and also permits greater freedom in selecting 1-hr data sequences that conform best to the ideal requirement of an approximate steady state during the measurement period.

Three cup anemometers and three azimuth wind-direction vanes have been added to the slow-response tower installation to provide quasi-continuous recordings of mean wind speed and direction fluctuations at heights of 2, 8, and 40 m above the ground. These data furnish background information on the hourly and diurnal changes in the gross turbulence structure that is useful in relating the detailed patterns revealed by the analysis of the field experiments to larger-scale atmospheric circulation patterns. The cup anemometers utilize low-torque d.c. generators; wind speed and wind direction are recorded on Esterline-Angus milliammeters.

III. EXPERIMENTAL DATA OBTAINED DURING 1961

A total of forty-six individual field experiments were carried out during 1961. All of these experiments utilized two levels of fast-response instrumentation at heights of 16 and 40 m, respectively. Eight 1-hr experiments were conducted during the late spring and early summer. Thirty-eight experiments were carried out during the fall of 1961; twelve of these were of 2 hr duration and the remainder 1 hr in length. Of the total of fifty-eight hours of observations, approximately 32 hr were obtained during the daytime in the presence of unstable thermal stratification, 18 hr at night during stable stratification, and the remaining 8 hr refer to near-neutral stratification. Ten hours of data are identified with over-water trajectories or mixed land-water trajectories. The rest of the observations refer to trajectories over a land surface. Complete spectral and cospectral analyses are available for six of the above experiments; the remainder data are currently being processed. It is not to be expected that all of the observations will prove satisfactory due to occasional equipment failures and departures of the gross meteorological factors from approximate steady-state conditions. However, it appears that a minimum of twenty-five satisfactory two-level experiments will be available for analysis.

During the last two field experiments of 1961, a microwave refractometer provided on a loan basis by Dr. J. R. Bauer of the Lincoln Laboratory of the Massachusetts Institute of Technology was installed at the 16-m level. The output of the instrument was fed into the humidity channel of the data-handling system and also to an Esterline-Angus chart recorder. Studies of the chart records indicate a gross variation in the refractive index of the order of 1 N unit during 1 hr. This is equivalent to a change of vapor pressure of about 0.25-mb. Vapor pressure fluctuations ranging from 0.1 to 1 mb have been reported by Swinbank (1951).

IV. DEVELOPMENT OF THE INFRARED HYGROMETER

Several modifications have been made during the past year in the infrared-hygrometer system described in the Annual Report. The cam shown in Figure 19 of this report has been replaced by a long eccentric shaft and the oscillating arm has been removed in favor of a cam follower mounted close to the filter pivot. The cam follower is made of a durable plastic material ("Delrin" manufactured by the E. I. duPont de Nemours Company) that provides a reasonably quiet and long-lived operation of the filter assembly.[1] The variac previously used to operate the source lamp of the hygrometer has been replaced by a 10-turn, wire-wound potentiometer; prior to this substitution, the Variac was a limiting factor in the resolution of the system. The potentiometer drives a d.c. amplifier that controls the lamp intensity.

The electronic portion of the infrared system has been significantly modified. A transistorized voltage regulator has been provided for the lamp power supply thus providing a stable energy source free of objectionable electrical noise. The output of the lamp power supply feeds the power input of a transistorized d.c. voltage and power amplifier. The amplifier output, which supplies the source lamp, is controlled by the voltage across the potentiometer and the potentiometer shaft is positioned by the servo motor. Since the input impedance of the power amplifier can be set at several megohms, it may be controlled by low-power electronic or electro-mechanical demodulators and other relatively high impedance sources.

All of the electronics up to the servo-motor driver stage have been redesigned using only solid state components for improved reliability and freedom from hum pickup. The servo-motor driver amplifier has not been transistorized since it will be replaced in the future by an all-electronic or simple electro-mechanical device. Tests of the present amplifier indicate that the noise level, in a 2 cycles sec^{-1} frequency interval centered on 60 cycles sec^{-1}, is about 25 percent of the noise level of the Kodak PbS detector with a 15-microampere bias through the cell. Batteries provide a low-noise power source for the preamplifier and the PbS photocell bias. The type of transistor used in the pre-

[1] This material was suggested by R. S. Borgeshani of the Polaroid Corporation.

amplifier is a Fairchild 2N1613, selected for high gain at low collector currents. The use of wire-wound resistors in the cell-bias circuits in place of deposited-carbon resistors significantly reduces the amount of electrical noise. At present, the PbS photocell is the limiting circuit element.

The maximum sensitivity of an infrared hygrometer system similar to the present system has been calculated. The calculations assume that the instrument compares the absorption in the 1.38 micron band with the transmission in a nearby band transparent to water vapor. In the present system, the filter angle is not quite wide enough to move the transmission path completely out of the water-vapor absorbing band. Due to this factor and the uncertainties in estimating the appropriate lamp area, lamp operating temperature, water-vapor absorption, and other parameters, the calculations may be one order of magnitude in error. The theoretical noise level of the system is equivalent to a peak-to-peak error in water vapor concentration of 0.001 g m^{-3}. Noise-level measurements of the present system for periods of operation in excess of 15 min show a peak-to-peak error of 0.08 and 0.19 g m^{-3}, respectively, at water vapor densities of 9.2 and 10.9 g m^{-3}. The lamp operating temperature for the 9.2 g m^{-3} water-vapor density was probably about 3000 K while a somewhat lower temperature is indicated for the other test. Thus, the noise level of the system appears to be very sensitive to the lamp temperature. The present technique for operating the hygrometer permits an adjustment in lamp temperature so that high operating temperatures can be used over a wide range of water vapor densities. However, there is no compensation for wide fluctuations in water vapor density that occur during the period of operation and the possibility exists that the noise level of the system may vary widely under these conditions. Further tests are required to determine the significance of these variations in lamp temperature.

V. ANALYSIS OF EXPERIMENTAL DATA

A. Data available for analysis

Complete spectral and cospectral analyses are available for fourteen 1-hr field experiments. Eight of the experiments, carried out during the fall of 1960, contain information on the fluctuations in air temperature and the orthogonal components of wind velocity at a height of 16 m above ground level. The remaining six experiments, conducted during 1961, include fluctuation data at both 16 and 40 m above ground level. A sampling rate of one complete fast-response observation per second was used in Runs 7B through 20; in the other experiments, the rate was one complete observation each 1.2 sec due to the adjustment in the paper-tape punch mentioned in Part II above. Gross weather conditions during the fourteen experiments are summarized in Table 1. It should be noted that the mean wind flow during eleven of the 1-hr observation periods was over a relatively smooth land surface. In Run 8, the trajectory was principally over water except for a distance of about 50 m directly upwind from the tower; the turbulent structure at the 16 m level does not appear to have been significantly affected by this short travel distance from the shoreline to the tower installation. In Runs 7B and 40, the direction of the mean flow was roughly parallel to the shoreline and the effective trajectory was over both land and water surfaces. During Run 15, the thermal stratification changed from a slight temperature lapse to a slight inversion as a result of the diurnal changeover. Vertical profiles of mean wind speed, dry- and wet-bulb temperature, and soil temperature for the various experiments are presented in Tables A1 through A3 of the Appendix.

B. Gross turbulence statistics

Gross turbulence statistics for the selected 1-hr experiments are entered in Table 2. Prior to the calculations shown in the table, long-period fluctuations and trends were removed from the raw data sequences through the use of a 600-point running mean as part of a procedure for minimizing the occurrence of aliasing in the cospectral analyses (see Section V C, below). The steps involved in decoding the punched-card data, including the scaling equations and the trigonometric program for calculating the orthogonal wind-velocity components from bivane observations, have been described previously (see pp. 55-56 of the Annual Report). The entries in Table 2 are in substantial agreement with similar statistics derived from measurements made by the Round Hill research team

Table 1. Summary of gross weather conditions during selected field experiments. Mean wind speed $\bar{V}$, wind direction $\bar{D}$, and the standard deviations of azimuth angle σ_A and elevation angle σ_E are based on 1-hr records at a height of 16 m; values enclosed in parentheses refer to the 40-m level.

Run No.	Date	Time (EST)	Cloud Cover	Stratification	Trajectory
7B	11-22-60	1105-1204	Clear	Unstable	Land-Water
8	11-22-60	1939-2039	Clear	Stable	Water
9	11-23-60	1431-1531	Overcast	Neutral	Land
10	11-23-60	2000-2100	Clear	Stable	Land
12	11-23-60	2230-2330	Clear	Stable	Land
14	12- 2-60	1216-1317	Clear	Unstable	Land
15	12- 2-60	1430-1530	Clear	Neutral[+]	Land
16	12- 7-60	1206-1309	Partly Cloudy	Unstable	Land
20	7- 1-61	0035-0136	Clear	Stable	Land
38	10-16-61	1209-1315	Partly Cloudy	Unstable	Land
39	10-16-61	1427-1528	Clear	Unstable	Land
40	10-16-61	1902-2003	Clear	Stable	Land-Water
41	10-16-61	2044-2145	Clear	Stable	Land
42	10-16-61	2211-2312	Clear	Stable	Land

Run No.	$\bar{V}$ (m sec^{-1})	$\bar{D}$(deg)	σ_A (deg)	σ_E (deg)	Solar Radiation (cal cm^{-2} min^{-1})
7B	4.78	249	12.0	5.7	0.75
8	3.82	208	5.4	1.8	0
9	5.92	301	11.6	6.4	0.07
10	4.19	324	7.9	3.5	0
12	4.42	322	7.0	3.6	0
14	4.05	296	19.8	8.6	0.64
15	3.76	290	11.7	6.1	0.22
16	8.20	288	14.2	6.2	0.58
20	5.53 (7.31)	325	7.7 (5.7)	4.7 (3.2)	0
38	6.12 (6.48)	294	18.3(17.9)	7.4(10.4)	0.93
39	5.81 (6.69)	293	15.1(14.7)	7.1 (8.7)	0.46
40	3.67 (5.48)	253	4.7 (3.5)	3.2 (2.4)	0
41	5.03 (6.61)	280	7.0 (6.5)	4.6 (4.2)	0
42	4.21 (5.80)	291	7.3 (6.0)	5.2 (4.5)	0

[+] Slight lapse at start of run changing to slight inversion by end of run.

Table 2. Gross turbulence statistics from filtered fast-response data. Wind velocities are in m sec^{-1} and temperature is in Centigrade. Trends and low-frequency fluctuations have been removed as explained in the text. COS signifies in-phase covariance and QUAD signifies the quadrature covariance.

Run No.	7B(16m)	8(16m)	9(16m)	10(16m)	12(16m)
$\bar{U}$	4.78	3.82	5.92	4.19	4.42
σ_u	0.813	0.309	1.25	0.562	0.567
σ_v	0.894	0.239	1.11	0.430	0.410
σ_w	0.399	0.128	0.657	0.250	0.268
σ_T	0.224	0.082	0.024	0.127	0.147
$\sigma_{u/\bar{U}}$	0.170	0.081	0.207	0.134	0.128
$\sigma_{v/\bar{U}}$	0.187	0.063	0.187	0.103	0.093
$\sigma_{w/\bar{U}}$	0.083	0.033	0.111	0.060	0.061
$\overline{uT}$ (COS)	-0.1078	0.0148	-0.0061	0.0392	0.0457
(QUAD)	-0.0097	0.0032	0.0003	0.0035	0.0028
$\overline{wT}$ (COS)	0.0454	-0.0033	-0.0020	-0.0113	-0.0160
(QUAD)	-0.0017	0.0011	0.0016	0.0021	0.0039
$\overline{vT}$ (COS)	-0.0005	-0.0005	-0.0005	0.0068	-0.0012
(QUAD)	-0.0027	0.0007	0.0007	0.0007	-0.0001
$\overline{uv}$ (COS)	-0.0456	0.0015	-0.1752	0.0612	0.0346
(QUAD)	-0.0026	-0.0014	-0.0159	-0.0034	0.0024
$\overline{vw}$ (COS)	-0.0320	-0.0022	0.0118	-0.0121	-0.0045
(QUAD)	0.0067	-0.0027	-0.0061	0.0015	-0.0009
$\overline{uw}$ (COS)	-0.1189	-0.0166	-0.2537	-0.0502	-0.0585
(QUAD)	0.0187	0.0006	0.0483	0.0018	-0.0011
R (uT)(COS)	-0.59	0.59	-0.20	0.55	0.55
(QUAD)	-0.05	0.13	0.01	0.05	0.03
R (wT)(COS)	0.51	-0.31	-0.13	-0.35	-0.41
(QUAD)	-0.02	0.10	0.10	0.07	0.10
R (vT)(COS)	0.00	-0.02	-0.02	0.12	-0.02
(QUAD)	-0.01	0.03	0.03	0.01	0.00
R (uv)(COS)	-0.06	0.02	-0.13	0.25	0.15
(QUAD)	0.00	-0.02	-0.01	-0.01	0.01
R (vw)(COS)	0.09	0.07	0.02	0.11	0.04
(QUAD)	0.02	0.09	0.01	0.01	0.01
R (uw)(COS)	-0.37	-0.42	-0.31	-0.35	-0.39
(QUAD)	0.06	0.01	0.06	0.01	-0.01

Run No.	14 (16m)	15 (16m)	16 (16m)	20 (16m)	20 (40m)
$\bar{U}$	4.05	3.76	8.20	5.53	7.31
σ_u	0.959	0.635	1.55	0.783	0.684
σ_v	0.974	0.595	1.72	0.607	0.509
σ_w	0.562	0.373	0.813	0.453	0.399
σ_T	0.246	0.123	0.255	0.177	0.184
$\sigma_{u/\bar{U}}$	0.237	0.169	0.189	0.142	0.094
$\sigma_{v/\bar{U}}$	0.240	0.158	0.210	0.110	0.070
$\sigma_{w/\bar{U}}$	0.139	0.099	0.099	0.082	0.054
$\overline{uT}$ (COS)	-0.0438	-0.0264	-0.2410	0.0910	0.0774
(QUAD)	-0.0096	-0.0034	-0.0195	0.0117	0.0027
$\overline{wT}$ (COS)	0.0651	0.0082	0.0796	-0.0323	-0.0263
(QUAD)	0.0013	-0.0005	-0.0086	0.0070	0.0002
$\overline{vT}$ (COS)	-0.0137	-0.0203	-0.0557	0.0148	0.0138
(QUAD)	-0.0041	-0.0001	-0.0043	-0.0012	0.0016
$\overline{uv}$ (COS)	-0.0146	0.0024	-0.1412	0.0635	0.0692
(QUAD)	0.0045	-0.0032	-0.0623	-0.0144	-0.0007
$\overline{vw}$ (COS)	0.0968	0.0019	0.1047	-0.0278	-0.0296
(QUAD)	-0.0024	0.0029	-0.0520	-0.0011	0.0024
$\overline{uw}$ (COS)	-0.0624	-0.0692	-0.4847	-0.1582	-0.1056
(QUAD)	0.0197	0.0151	0.0995	0.0052	0.0023
R (uT)(COS)	-0.19	-0.34	-0.61	0.66	0.62
(QUAD)	-0.04	-0.04	-0.05	0.08	0.02
R (wT)(COS)	0.47	0.18	0.38	-0.40	-0.36
(QUAD)	0.01	-0.01	-0.04	0.09	0.00
R (vT)(COS)	-0.06	-0.28	-0.13	0.14	0.15
(QUAD)	-0.02	0.00	-0.01	-0.01	0.02
R (uv)(COS)	-0.02	0.01	-0.05	0.13	0.20
(QUAD)	0.00	-0.01	-0.02	-0.03	0.00
R (vw)(COS)	0.18	0.01	0.07	-0.10	-0.15
(QUAD)	0.00	0.01	-0.04	0.00	0.01
R (uw)(COS)	-0.12	-0.29	-0.39	-0.45	-0.39
(QUAD)	0.04	0.06	0.08	0.01	0.01

Run No.	38 (16m)	38 (40m)	39 (16m)	39 (40m)	40 (16m)
$\bar{U}$	6.12	6.48	5.81	6.69	3.67
σ_u	1.40	1.54	1.34	1.52	0.357
σ_v	1.71	1.61	1.23	1.38	0.292
σ_w	0.703	0.998	0.668	0.880	0.209
σ_T	0.375	0.303	0.195	0.201	0.105
$\sigma_{u/\bar{U}}$	0.229	0.238	0.231	0.228	0.097
$\sigma_{v/\bar{U}}$	0.279	0.248	0.212	0.206	0.080
$\sigma_{w/\bar{U}}$	0.115	0.154	0.115	0.132	0.057
$\overline{uT}$ (COS)	-0.2635	-0.2509	-0.1710	-0.2079	0.0222
(QUAD)	-0.0244	-0.0155	-0.0136	-0.0102	0.0016
$\overline{wT}$ (COS)	0.1220	0.1466	0.0428	0.0732	-0.0074
(QUAD)	-0.0027	-0.0008	-0.0032	-0.0038	0.0017
$\overline{vT}$ (COS)	-0.0796	-0.0015	0.0014	0.0411	0.0063
(QUAD)	-0.0033	0.0007	-0.0031	-0.0020	0.0004
$\overline{uv}$ (COS)	-0.3622	-0.2039	-0.1354	0.0617	0.0149
(QUAD)	-0.0406	-0.0310	-0.0322	-0.0179	-0.0047
$\overline{vw}$ (COS)	-0.0374	-0.1524	0.0000	-0.1143	-0.0106
(QUAD)	-0.0139	-0.0208	0.0059	-0.0105	-0.0042
$\overline{uw}$ (COS)	-0.2593	-0.6026	-0.3224	-0.5862	-0.0221
(QUAD)	0.0662	0.0297	0.0344	0.0194	0.0013
R (uT)(COS)	-0.50	-0.54	-0.65	-0.68	0.59
(QUAD)	-0.05	-0.03	-0.06	-0.03	0.04
R (wT)(COS)	0.46	0.48	0.33	0.41	-0.34
(QUAD)	-0.01	0.00	-0.02	0.02	0.08
R (vT)(COS)	-0.12	0.00	0.01	0.15	0.21
(QUAD)	-0.01	0.00	-0.01	-0.01	0.01
R (uv)(COS)	-0.15	-0.08	-0.08	0.03	0.14
(QUAD)	-0.02	-0.01	-0.02	-0.01	-0.04
R (vw)(COS)	-0.03	-0.10	0.00	-0.09	-0.17
(QUAD)	-0.01	-0.01	0.01	-0.01	-0.07
R (uw)(COS)	-0.26	-0.39	-0.36	-0.44	-0.30
(QUAD)	0.07	0.02	0.04	0.01	0.02

Run No.	40 (40m)	41 (16m)	41 (40m)	42 (16m)	42 (40m)
$\bar{U}$	5.48	5.03	6.61	4.21	5.80
σ_u	0.456	0.754	0.793	0.729	0.767
σ_v	0.319	0.562	0.632	0.524	0.580
σ_w	0.222	0.413	0.463	0.387	0.445
σ_T	0.114	0.160	0.159	0.144	0.149
$\sigma_{u/\bar{U}}$	0.083	0.150	0.120	0.173	0.132
$\sigma_{v/\bar{U}}$	0.058	0.112	0.096	0.124	0.100
$\sigma_{w/\bar{U}}$	0.040	0.082	0.070	0.092	0.077
$\overline{uT}$ (COS)	0.0319	0.0725	0.0839	0.0631	0.0742
(QUAD)	0.0025	0.0090	0.0025	0.0078	0.0055
$\overline{wT}$ (COS)	-0.0105	-0.0234	-0.0327	-0.0239	-0.0296
(QUAD)	0.0001	0.0048	-0.0003	0.0029	0.0035
$\overline{vT}$ (COS)	0.0076	0.0082	0.0070	0.0032	0.0089
(QUAD)	-0.0006	-0.0023	-0.0014	0.0017	0.0016
$\overline{uv}$ (COS)	0.0149	0.0246	0.0321	-0.0082	0.0272
(QUAD)	-0.0074	-0.0172	-0.0096	-0.0004	-0.0153
$\overline{vw}$ (COS)	-0.0073	-0.0172	-0.0475	-0.0066	-0.0244
(QUAD)	0.0012	-0.0104	0.0098	-0.0004	-0.0007
$\overline{uw}$ (COS)	-0.0384	-0.1083	-0.1311	-0.1185	-0.1330
(QUAD)	0.0013	0.0091	0.0100	0.0066	-0.0004
R (uT)(COS)	0.61	0.60	0.66	0.60	0.65
(QUAD)	0.05	0.05	0.02	0.07	0.05
R (wT)(COS)	-0.41	-0.35	-0.44	-0.43	-0.45
(QUAD)	0.00	0.07	0.00	0.05	0.05
R (vT)(COS)	0.21	0.09	0.07	0.04	0.10
(QUAD)	0.02	-0.02	-0.01	0.02	0.02
R (uv)(COS)	0.10	0.06	0.06	-0.02	0.06
(QUAD)	-0.05	-0.04	-0.02	0.00	-0.03
R (vw)(COS)	-0.10	-0.07	-0.16	-0.03	-0.09
(QUAD)	0.02	-0.04	0.03	0.00	0.00
R (uw)(COS)	-0.38	-0.35	-0.36	-0.42	-0.39
(QUAD)	0.01	0.03	0.03	0.02	0.00

during the Great Plains Program of 1953 (Lettau and Davidson, 1957). With respect to the gross temperature fluxes, it should be noted that the magnitude of the temperature flux in the direction of the mean flow $\overline{u}\overline{T}$ exceeds the vertical flux $\overline{w}\overline{T}$ in every case except one (Run 14). The cross wind temperature flux $\overline{v}\overline{T}$ is generally smaller than the other two fluxes but is the same order of magnitude as the vertical flux in approximately half the cases. The statistics for the gross momentum fluxes show that the vertical flux $\overline{u}\overline{w}$ is generally largest in absolute magnitude but, on occasion, one or both of the other fluxes may be the same order of magnitude. These results conflict with the usual assumption made in theoretical treatments of boundary-layer exchange phenomena that the horizontal fluxes of momentum and temperature are small in comparison with the respective vertical fluxes. The tabular entries also include estimates of the gross quadrature fluxes. The quadrature statistics indicate the contribution of fluctuations in two variates that are out-of-phase by one-quarter cycle; the conventional flux statistics measure only in-phase relationships. It is apparent that the magnitude of the quadrature contributions is generally negligible in comparison with gross in-phase contributions. This conclusion is supported by the quadrature correlation coefficients which are principally below the 95 percent confidence limit for significance.[1]

Calculations of the heat budget at the air-soil interface for the fourteen experiments are shown in Table A4 of the Appendix. For completeness, gross turbulence statistics obtained from the raw unfiltered experimental data (i.e., data from which long-period fluctuations and trends have not been removed by use of the 600-point moving average technique) similar to those in Table 2 above are presented in Table A5 of the Appendix.

C. Spectral analysis techniques

The spectral composition of the gross variances and covariances shown in Table 2 has been investigated by use of digital techniques based on procedures given by Blackmann and Tukey (1958). A detailed description of the various steps involved in the machine calculations may be found in

[1] See Dixon and Massey (1951, p. 327). The sample size for each experiment is about 3000 but the effective number of degrees of freedom is significantly smaller due to interdependence between sequential data points. The above argument assumes about 500 degrees of freedom and indicates that a sample correlation coefficient of 0.1 occurs about 10 percent of the time in random samples from a population in which the true correlation is zero.

the Annual Report (pp. 55-58). Empirical studies of the power spectra and cospectra of atmospheric properties are generally bandwidth limited due to the inability of a particular set of measurement techniques to treat the entire spectrum. Digital analysis of equally-spaced data points is subject to the following extreme bandwidth limits: a high-frequency limit of about $1/2\ \Delta t$ cycles sec^{-1} imposed by the sampling rate or time in seconds between consecutive data points Δt; and, a low-frequency bound near $10/L$ cycles sec^{-1} imposed by the total length to the observation period L in seconds. For the experiments listed in Table 2, Δt is either 1 or 1.2 sec and L is approximately 3000 sec. possible aliasing effects (see Blackman and Tukey, 1958, pp. 216-219) have been reduced in two ways. Prior to spectral analysis, the raw data sequences are differenced with respect to a 600-point unweighted moving average; this procedure eliminates contributions from trends and very low-frequency fluctuations. Also, undesirable high-frequency energy above $1/2\ \Delta t$ cycles sec^{-1} is removed from the transducer input signals by electrical filter networks (Figure 23 of the Annual Report for the transmission function of these networks).

The basic cospectral analysis program utilizes auto-covariances and covariances calculated for 60 lags from the differenced raw data sets mentioned above. Supporting information at high-frequencies is obtained from a 10-lag analysis of the same data sets and additional information on the shape of the spectra and cospectra at low frequencies is obtained from a 30-lag analysis of reduced data sets. The reduced sets are formed by summing and averaging consecutive 10-point blocks of the differenced sets. Bandwidths, sample sizes, approximate degrees of freedom, and confidence ratios (5 and 95 percent levels) associated with the various lags mentioned above are shown in Table 3. The confidence

Table 3. Bandwidths, sample sizes, approximate numbers of degrees of freedom, and 5 and 95 percent confidence ratios for the various lags used in the spectral analysis program. As mentioned in the text, Δt is either 1 or 1.2 sec, depending on the Run No.

Number of lags	10	30	60
Sample size	3000	300	3000
Bandwidth limits (cycles sec^{-1})	$1/2\ \Delta t$ - $1/20\ \Delta t$	$1/20\ \Delta t$ - $1/600\ \Delta t$	$1/2\ \Delta t$ - $120\ \Delta t$
Degrees of freedom	300	18	100
Confidence ratios	0.87 - 1.15	0.52 - 1.60	0.78 - 124

ratios are factors by which the spectral and cospectral estimates should be multiplied to delineate the range within which the true spectrum or cospectrum is expected to be found about 90 percent of the time. The final step in the cospectral analysis program involves adjustments in the estimates to compensate for the effects of the smoothing and filtering operations at frequencies within the bandwidth limits shown in Table 3.

D. Power spectra of the wind-velocity components and air temperature

The spectral composition of the fluctuations in wind velocity and air temperature is conveniently shown by graphs in which the product of the spectral density S(n) and the frequency n is plotted against the logarithm of the frequency. In this representation, which is usually termed the "logarithmic spectrum", areas under the spectral curve are proportional to the true energy or variance contributed per octave or logarithmic frequency interval. Comparison of spectra for various experiments is facilitated by transforming time frequencies n into space frequencies $n/\bar{U}$ since previous work has shown that the spatial pattern of turbulence at a fixed height is largely independent of the mean wind velocity $\bar{U}$ (Panofsky et al, 1958; Cramer, 1959; Lappe et al, 1959). For the wind-velocity spectra, the ordinate scale $S(n) \times n$ is normalized by dividing by the square of the mean wind velocity to obtain a dimensionless ratio. Since the surface shear stress is roughly proportional to the square of the mean wind velocity, this normalizing procedure is approximately equivalent to division by the vertical flux of momentum as indicated by the similarity theory (Monin and Obukhov, 1954).

Logarithmic spectra of the u-, v-, and w-components of wind velocity and of fluctuations in air temperature for the field experiments listed in Table 1 are shown in Figures 1a through 4d. The data points in the figures were obtained in the following manner. Time-frequency spectra were first plotted for each experiment using spectral estimates available from the analysis program described above. Lines of "best fit" were drawn by eye and representative estimates of $S(n) \times n$ (which has the dimensions of a variance were made at frequencies of 1/600, 1/300, 1/200, 1/100, 1/60, 1/40, 1/30, 1/25, 1/20, 1/15, 1/10, 1/5, and 1/2 cycles sec^{-1}. After conversion of time frequencies to space frequencies by use of Taylor's hypothesis (Taylor, 1938) and after division of the spectral estimates for the wind-velocity components by the square of the mean wind velocity $\bar{U}^2$, the results were entered in the figures and the individual points joined by straight lines. The highest frequency estimates (at $n = 1/2$ cycles sec^{-1}) should be considered only rough approximations due to possible aliasing effects and since, for the field

experiments conducted after Run No. 20, it was necessary to extrapolate from 1/2.4 to 1/2 cycles sec^{-1}. It should also be emphasized that the three lowest-frequency estimates (at n = 1/600, 1/300 and 1/200 cycles sec^{-1}) are significantly less precise than the data points at intermediate and high frequencies due to the small number of degrees of freedom available (see Table 3).

As expected, the spectral composition of the four meteorological variables changes significantly with the thermal stratification. Except for the vertical velocity spectra which will be discussed below, there is a shift of approximately one order of magnitude in the space frequency at which the maximum contribution to the variance occurs as the stratification changes from thermally stable to thermally unstable. During periods of strong insolation peak values of the logarithmic spectra for the u- and v-components of the wind velocity and the air temperature are found at wave numbers in the range from 0.001 to 0.0005 cycles m^{-1} (see Figures 1a, 1c, 2a, 2c, 4a, and 4c). At night, in the presence of thermally-stable stratification and a turbulence regime that is predominantly mechanical in nature, the maxima of the logarithmic spectra of the three variables occur at wave numbers from about 0.01 to 0.005 cycles m^{-1} (see Figures 1b, 1d, 2b, 2d, 4b, and 4d). The principal contributions to the variances of the three variables in near-neutral and stable atmospheres thus occur near the center of the logarithmic spectral band utilized in this study and the present technique generally is satisfactory for determining the characteristic form of the spectra. During the daytime, principal contributions to the variances occur at the low frequency end of the spectral band under investigation, presumably due to the presence of large convection cells. Additional measurements using appreciably longer lengths of record are needed to resolve the details of the shape of the spectra at these frequencies. In addition, it is likely that Taylor's hypothesis does not hold for large convective cells since their development and decay is clearly dependent on time and space (see Lappe et al, 1959). Thus, the space-frequency representation may not be appropriate. It appears that the absolute magnitude of the contributions to the three spectra within the mechanical turbulence regime (n = 0.01 to 0.005 cycles m^{-1}) differ approximately by a factor of two as the thermal regime changes from lapse to inversion. Consequently, it may be inferred that there is a positive convective contribution in lapse conditions and a negative contribution (due to thermal damping of mechanical turbulence) during inversions in this part of the spectrum.

Changes in the spectral composition of the vertical component of wind velocity with thermal stratification are considerably smaller than those for the other three variable. The general form of the logarithmic

w-spectra is determined largely by the height above ground of the observation point (Panofsky and Deland, 1959) but there is an orderly shift in the space frequency at which the maximum contributions occur as the thermal structure becomes increasingly stable or unstable. As shown in Figures 3a and 3c, the daytime spectral peaks occur at space frequencies from about 0.02 to 0.005 cycles m^{-1}. The peaks for the nighttime experiments, as shown in Figures 3b and 3d, are found generally at 0.05 to 0.02 cycles m^{-1}. It is apparent that the present measurement technique is not adequate for resolving the details of the shape of the w-spectrum at high frequencies during inversion conditions at either the 16- or 40-m level. A transducer capable of resolving frequencies of the order of 10 cycles sec^{-1} is needed to establish the detailed features of the high-frequency end of the w-spectrum in thermally-stable atmospheres at these heights. The effect of thermal stratification on the scale of the vertical velocity component has recently been discussed by Panofsky (1962). Measurements made in the Soviet Union show a significant shift in the peak frequency of the w-spectrum with stability at heights of 1 or 2 m above the surface. The absolute magnitude of the peak variance contributions during thermally-unstable stratification generally exceed the corresponding nighttime (thermally-stable) contributions by a factor of two.

Variations in the space frequency at which the maximum spectral contributions occur due to changes in the thermal structure are summarized in Figures 5a and 5b. In Figure 5a, estimates of the peak frequencies for each experiment have been plotted against the bulk Richardson Number or Stability Ratio calculated from the ratio of the difference in temperature (Centigrade) between heights of 8 and 2 m and the square of the mean wind speed (m^2 sec^{-2}) at a height of 4 m. The peak-frequency data are also plotted against hourly values of the standard deviation of azimuth wind direction in Figure 5b. In both plots, the peak w-frequencies at a height of 16 m vary in the extreme from about 0.05 cycles m^{-1} for very stable stratification to about 0.0067 cycles m^{-1} in extreme instability. It is interesting that the peak frequency in near-neutral stratification is 0.0125 cycles m^{-1} which corresponds to a wavelength of 80 m; this is equivalent to five times the height above ground in agreement with a previous prediction by Panofsky and Deland (1959). It appears that the peak frequencies at a height of 40 m are generally lower than those at 16 m, as expected, but the available data are insufficient to permit establishment of a quantitative relationship. In the case of the u-, v- and T-spectra, the variation in peak frequency with thermal stability is somewhat less regular than that for the w-spectra. As noted above, the peak frequencies in stable stratification differ by approximately one order of magnitude from the peak frequencies in unstable stratification. Also, the 40-m spectral peaks generally occur at lower space frequencies

than the corresponding peaks at a height of 16 m.

Two additional features of the experimental results should be mentioned. There is an interesting sequence of data comprising Runs 38 through 42, all obtained during one 11-hr period (1209-2312 EST on 16 October 1961). The first two experiments reflect the development and initial decay, respectively, of large-scale convective activity characteristic of fair-weather daytime regimes. During the transition from lapse to inversion, the turbulence is greatly reduced. The data for Run 40 show conditions associated with the formation of the nighttime inversion.[1] In Runs 41 and 42, the data show an intensification of the nighttime turbulence regime. Experience suggests that changes of this type in turbulent structure are typical during fair weather. Assuming this to be true, it is quite evident that steady-state conditions rarely exist for sampling times of the order of 1 hr due to large diurnal changes. The second feature of the data is the significant reduction in the intensity of the turbulence during Run No. 8 when the trajectory was over water rather than over land.

The general features of the spectral composition of the fluctuations in the wind-velocity components mentioned above are in agreement with the results of previous measurements which have been summarized by Priestley (1959), Panofsky and Deland (1959). Several investigators have noted the presence of double peaks during extreme thermal instability. Some of the spectra for the u- and v-components (see Figures 1a and 2a) at a height of 16 m indicate a possible separation of the mechanical and convective portions of the spectra at frequencies near 0.002 cycles m^{-1}, which supports the findings of Panofsky and McCormick (1954). The present data for the vertical velocity component, however, do not appear to contain the double peaks found by Webb (1955). This difference may be in part due to the very short observation (5 min) period employed by Webb.

For completeness, all of the logarithmic spectra have been replotted in terms of the logarithmic spectral density $S(n) \times \bar{U}$ or $S(n) / \bar{U}^2 \times \bar{U}$ and the logarithm of the space frequency. These double logarithmic graphs are useful in estimating power-law relationships that may exist in the spectra. The results are presented in Figures 6a through 9b. All of the spectra show an approximate fit to a $-4/3$ or $-5/3$ power law at the highest frequencies and, depending on the thermal stratification, the meteorological variable in question and the height, this dependence may extend to very low frequencies. Calculations of the absolute value of

[1] The reduced turbulence may be in part explained by the trajectory which was nearly parallel to the shoreline (see Table 1).

the power-law exponent range from about 1.40 to 1.60 and the arithmetic mean of all the estimates is about 1.50. This result is in general agreement with previous measurements by MacCready (1953), Jones (1957), and Suomi (1957) supporting an $n^{-5/3}$ law, as opposed to an n^{-2} law obtained from aircraft observations (Press, 1957). It should be pointed out that the peak logarithmic spectral frequencies discussed above indicate the low-frequency bound of the spectral band in which the power-law representation of the spectra may be expected to hold. Also, the peak frequencies of the logarithmic spectra for the vertical component of wind velocity delineate the low-frequency bound of the region in which there is approximate equivalence between the spectra of the three wind-velocity components. The data do not appear adequate for investigating the theoretical prediction that the energy of the v- and w- components should be 33 percent larger than the energy of the u-component for point measurements of isotropic turbulence (see Panofsky and Deland, 1959, p. 47). The data do show, however, that the magnitudes of all three components are approximately equivalent at high frequencies.

E. Cospectra of the vertical fluxes of momentum and temperature and of the temperature flux in the direction of mean flow

The cospectrum provides a measure of the contributions of the fluctuations in the product of two variables, within various frequency bands, to the gross covariance between the two variables just as the spectrum measures contributions to the total variance. The cospectrum may be interpreted in terms of a correlation coefficient that is a function of frequency since the cospectral estimates clearly depend on the amount of variation common to both variables. A very useful measure of the frequency dependence of the product of two variables x, y is provided by the coherence COH which is defined by the expression

$$\mathrm{COH}_{xy}(n) = \frac{\mathrm{COS}^2_{xy}(n) + \mathrm{QUAD}^2_{xy}(n)}{S_x(n)\, S_y(n)}$$

where (n) is the frequency, COS is the cospectral estimate, QUAD is the quadrature estimate and S_x and S_y are power spectral estimates. The form of the above expression is analogous to the square of a linear correlation coefficient since it represents the ratio of the square of a mean cross product and the product of two variances. The cospectral estimate measures only the in-phase relationship between the variates; the quadrature estimate measures the contribution of fluctuations in the two variates that are one-quarter cycle out-of-phase (see Panofsky and McCormick, 1954; Panofsky, 1962). Coherence diagrams thus show the

approximate percentage variation common to the two variates as a function of frequency.

Graphs of the coherence for the three most important fluxes (uw, wT, and uT) as shown by the correlation coefficients and relative amounts of turbulent energy entered in Table 2, are presented in Figures 10 through 23b for each of the field experiments. Estimates of the in-phase contributions COS and the quadrature contributions QUAD for each of the data points shown in the above figures are entered in Table A6 of the Appendix. Inspection of the entries in the table shows that the quadrature contributions are generally less than 10 percent of the in-phase contributions and thus may be neglected. As might be anticipated, the coherence at very high frequencies is effectively zero for uw and uT; wT values, although less than 0.1, may be significantly different from zero. In the presence of thermal instability, the maximum values of the coherence for all three fluxes are found at frequencies near 0.002 cycles sec^{-1}. The coherence values for uw at a height of 16 m in Run Nos. 14 and 38 do not follow this pattern (see Figures 15 and 19a); if the data are assumed correct, the results indicate that large-scale convection may on occasion produce a significant decrease in the vertical flux of momentum. In stable stratification, the coherence for uw and wT tends to reach a plateau at frequencies of .05 to .02 cycles sec^{-1}. The form of the coherence for the uT flux varies only slightly with stratification; the largest coherence values tend to be found at the low-frequency end of the spectrum in all thermal stratifications.

Logarithmic cospectral diagrams, similar to graphs of the logarithmic power spectra previously discussed, are presented in Figures 24a through 26d. Data points in the figures were obtained by the same procedure followed for the u-, v-, w-, and T-spectra. Cospectral estimates for the vertical flux of momentum uw have been normalized by dividing by the square of the mean wind velocity. The frequency dependence of the three cospectra exhibits a diurnal variation similar to that found for the spectra of the wind-velocity components and air temperature. During stable thermal stratification, peak frequencies for uw and wT at a height of 16 m occur between 0.02 and 0.005 cycles m^{-1} (Figures 24b and 25b); at a height of 40 m, the corresponding range of peak frequencies is from 0.01 to 0.002 cycles m^{-1} (Figures 24d and 25d). Maximum contributions to the uT cospectra in thermally stable atmospheres occur within the frequency band from 0.01 to 0.003 cycles m^{-1} (see Figure 26b); at a height of 40 m the peak frequency band is found between 0.005 and 0.0015 cycles m^{-1} (figure 26d). In all cases, the present measurement technique appears adequate for determining the characteristic form of the three cospectra.

In the presence of thermal instability, the maxima of the three cospectra shift toward low frequencies. The daytime peak frequencies for uw at a height of 16 m occur within the band from 0.002 to 0.0005 cycles m^{-1}; as shown in Figure 24a, there is some evidence of a relatively small secondary maximum between 0.02 and 0.005 cycles m^{-1} which corresponds to the limits of the peak band during stable stratification. The data for Run No. 9, in which the stratification was near-neutral, show a peak frequency within this range which is clearly due to mechanical turbulence. The two daytime cases at a height of 40 m (Figure 24b) exhibit very sharp maxima between 0.001 and 0.0005 cycles m^{-1}. The wT cospectra indicate a frequency dependence that is strikingly similar to that for uw if allowance is made for the collapse of the temperature spectrum in near-neutral stratification. Three of the 16-m cases in Figure 25a show well-defined double maxima, one between 0.01 and 0.005 cycles m^{-1} and a low-frequency peak near 0.001 cycles m^{-1}. The two cases at 40 m (Figure 25c) indicate peak frequencies at about 0.0005 cycles m^{-1}. The principal contributions to the uT cospectra in unstable thermal stratification (Figures 26a, 26b) occur without exception between 0.001 and 0.0005 cycles m^{-1}. In contrast to the uw and wT diagrams for the 16-m level, which indicate important cospectral contributions within the mechanical turbulence regime, the uT diagrams show only very minor contributions during unstable stratification in the band from 0.02 to 0.005 cycles m^{-1}. Variations in the peak frequencies of the three cospectra with changes in stability are summarized in Figures 27a and 27b where the Stability Ratio and hourly values of the standard deviation of azimuth wind direction, respectively, are used as indicators.

Double logarithmic diagrams of the cospectra for the three fluxes are presented in Figures 28a and 30b. The principal feature of these data is the rapid decrease in cospectral density at high frequencies which follows an inverse-square law rather than the minus four-thirds or minus five-thirds law shown by the u-, v-, w-, and T-spectral densities. The tendency for a rapid decrease in the uw cospectra at high frequencies has previously been noted by Panofsky and McCormick (1954).

VI. DISCUSSION OF RESULTS AND SUGGESTIONS FOR FUTURE RESEARCH

It should be emphasized that the results described above are preliminary and are based on the analysis of only a fraction of the available experimental data. Also, in the relatively brief time available for studying these data, principal attention has been focussed on the general form of the spectra and cospectra of the characteristic air properties investigated. With these qualifications, the following tentative conclusions may be stated: Power spectra of the wind-velocity component (u, v, and w) and air temperature show a minus four-thirds or minus five-thirds power law dependency on frequency at the highest frequencies studied. Cospectra of the vertical fluxes of momentum and temperature and of the temperature flux in the direction of the mean flow show an inverse-square dependency at these frequencies. Logarithmic spectral and cospectral diagrams show that the principal contributions to the variances and covariances of these meteorological parameters, in stable thermal stratification, occur at wavelengths of 20 to 500 m. The present measurement techniques are satisfactory for resolving the spectral composition of all parameters except the vertical component of wind velocity (and, possibly, the lateral component v) in extreme stability.

In unstable thermal stratification, major contributions to the u-, v-, and T-spectra and to the uw-, wT- and uT-cospectra occur at wavelengths of 500 to 2000 m. The 1-hr observation periods utilized in the present study are too short to permit reliable estimates of the shape of the spectra and cospectra at wavelengths larger than 1 or 2 km. Major contributions to the spectrum of the vertical component of wind velocity in unstable stratification occur at wavelengths of 50 to 200 m and there is a regular shift in the wavelength at which the maximum contribution occurs as the stratification becomes increasingly stable or unstable. In near-neutral stratification, the maximum contribution occurs at a wavelength equivalent to about five times the height of the observation point above ground level. The height dependence of the various spectra and cospectra cannot be established on the basis of the results thus far available. However, it is apparent that the peak contributions at the 40-m level occur at longer wavelengths than the corresponding contributions at a height of 16 m. The cospectra for the vertical temperature flux show two maxima in extreme thermal instability; one peak occurs at a wavelength of about 100 m, presumably due to mechanical

turbulence, and the other peak occurs at a wavelength of about 1 km where large-scale convection is predominant.

It is usually assumed in descriptions of boundary-layer transfer processes that the horizontal fluxes of characteristic air properties are negligible in comparison with the vertical fluxes (Priestley, 1959, p. 1). The data obtained in this study show very clearly that the temperature flux in the direction of the mean flow generally exceeds the temperature flux along the vertical by a factor of two. Similar results were obtained by the Round Hill research team at O'Neill, Nebraska in 1953 (see Lettau and Davidson, 1957). It is suggested that this large horizontal temperature flux is principally due to the presence of large convective elements transported near ground level from relatively great heights and swept past the point of measurement embedded in quasi-horizontal flow. Due to the presence of the ground, the temperature and horizontal momentum of these large eddies is conserved to a much larger degree than their vertical momentum. In effect, the $u\overline{T}$ flux is a result of vertical exchange; the exchange, however, occurs at some distance upwind from the point of observation.

Analysis of the experimental data is continuing under a basic research grant. Once the spectral and cospectral analyses are completed, the results should be compared with the predictions of the similarity theory along the lines pursued by Takeuchi (1962) in his studies of the O'Neill, Nebraska structure measurements. Additional field experiments will be conducted to extend the data to greater heights and different roughness regimes; also, considerably longer sampling periods of the order of 3 hr are required to establish the features of the spectra and cospectra at low frequencies in the presence of extreme thermal instability. Finally, it is already apparent that studies of the high-frequency part of the vertical-velocity spectrum in stable atmospheres require the development and use of instrumentation capable of responding to frequencies of the order of 10 cycles sec^{-1}.

ACKNOWLEDGEMENTS

The authors wish to acknowledge the very important contributions to the work described in this report by the following members of the research team at the Round Hill Field Station: George Fontes, Harry Geary, John Luby and James Peers. Also, credit for handling the details of the machine spectral analysis program should be given to Mr. W. D. Ohmstede, Sgt. George L. Doughty and SP 4 P. Schmelzer of the Meteorology Department at Fort Huachuca.

ILLUSTRATIONS

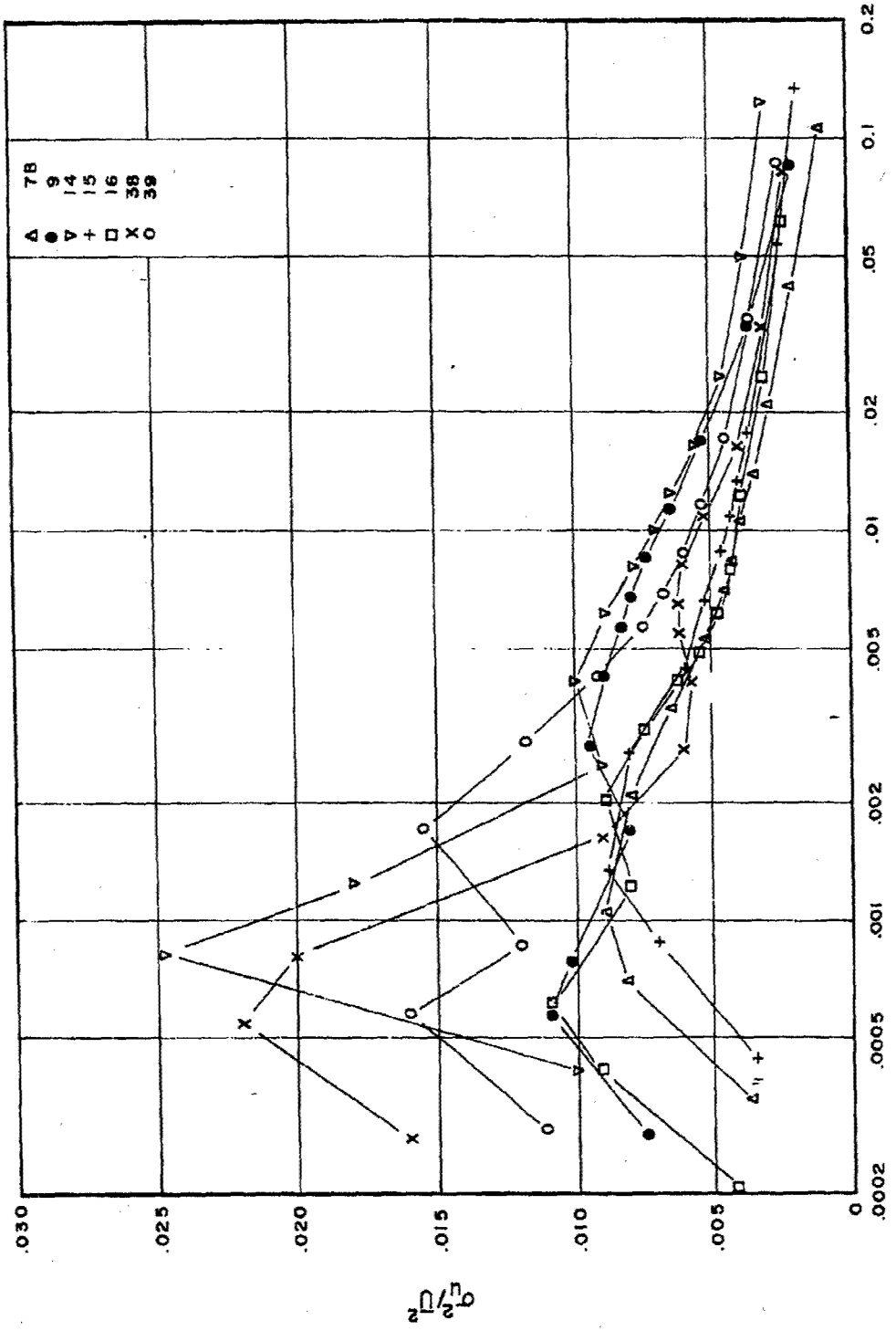

Fig. 1a. Logarithmic power spectra of the u-component of wind velocity at a height of 16 m for the daytime experiments.

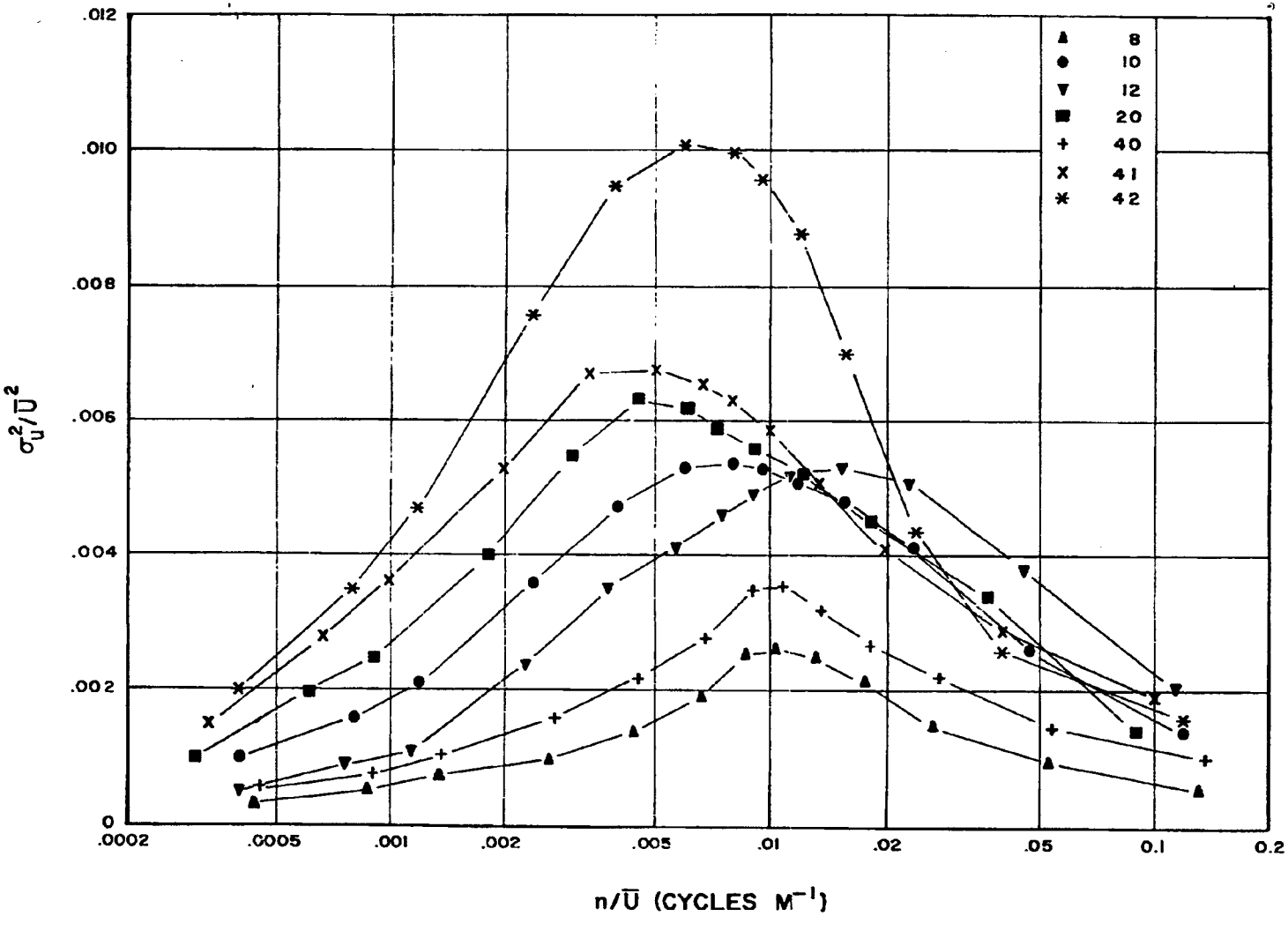

Fig. 1b. Logarithmic power spectra of the u-component of wind velocity at a height of 16 m for the nighttime experiments.

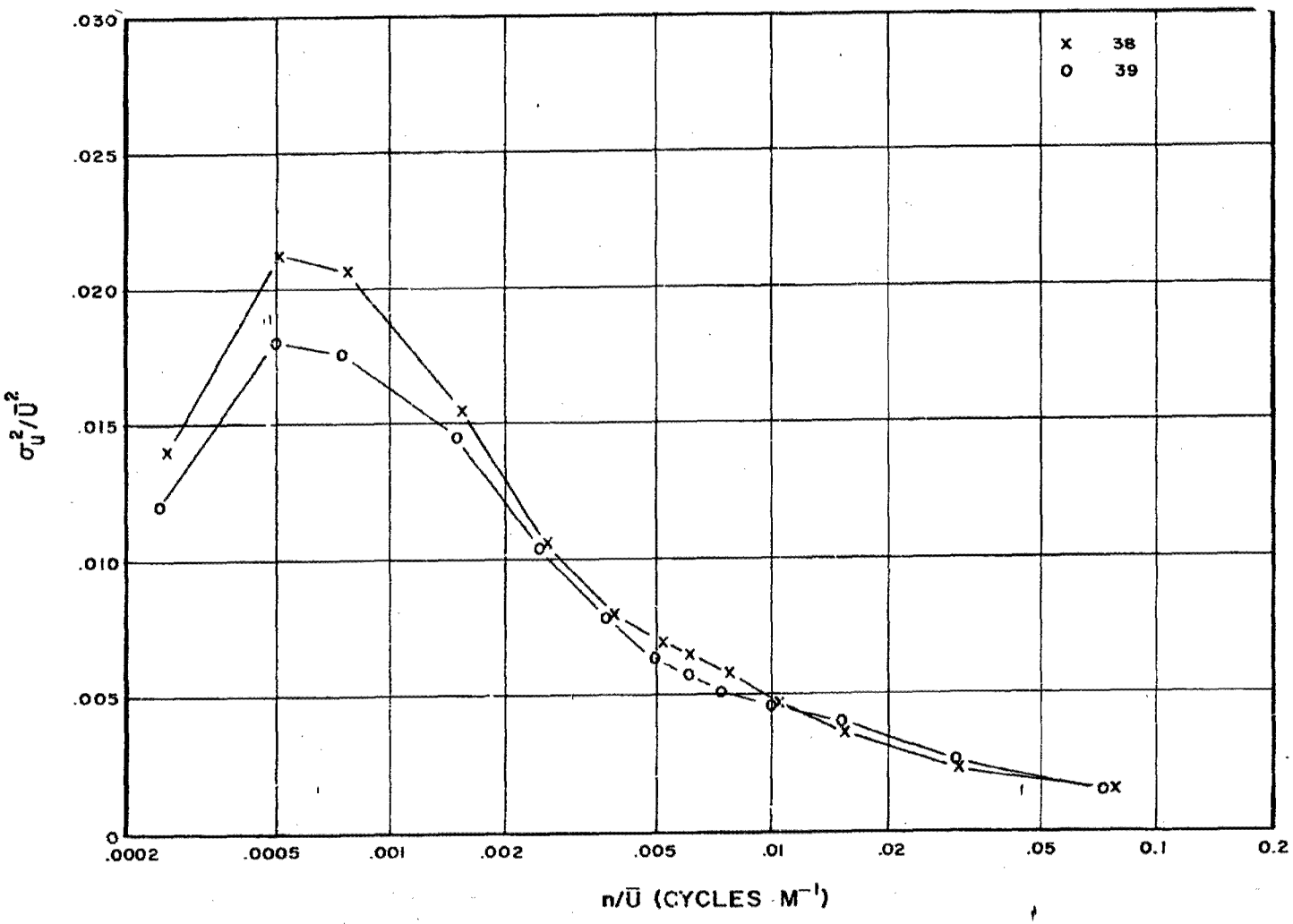

Fig. 1c. Logarithmic power spectra of the u-component of wind velocity at a height of 40 m for the daytime experiments.

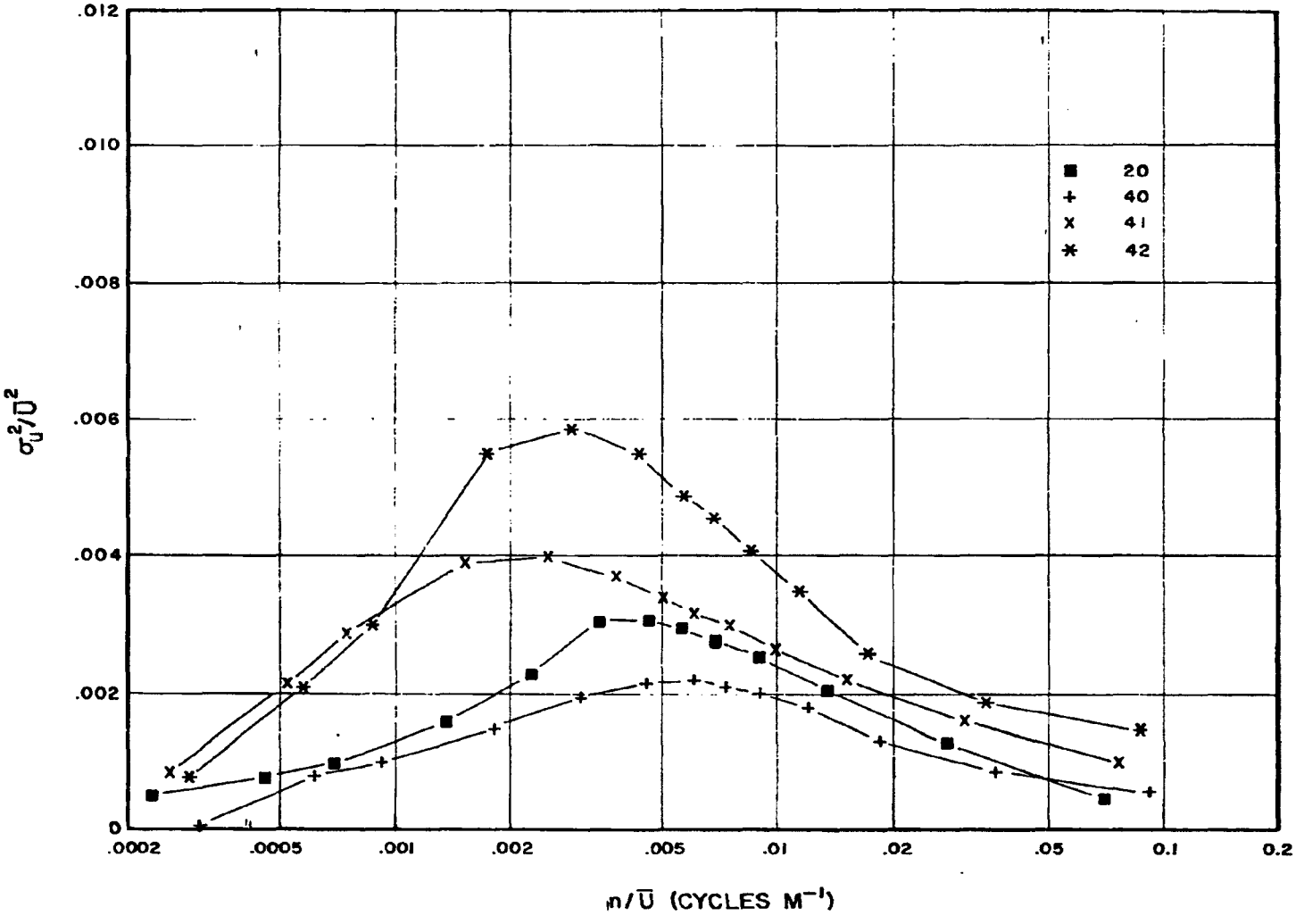

Fig. 1d. Logarithmic power spectra of the u-component of wind velocity at a height of 40 m for the nighttime experiments.

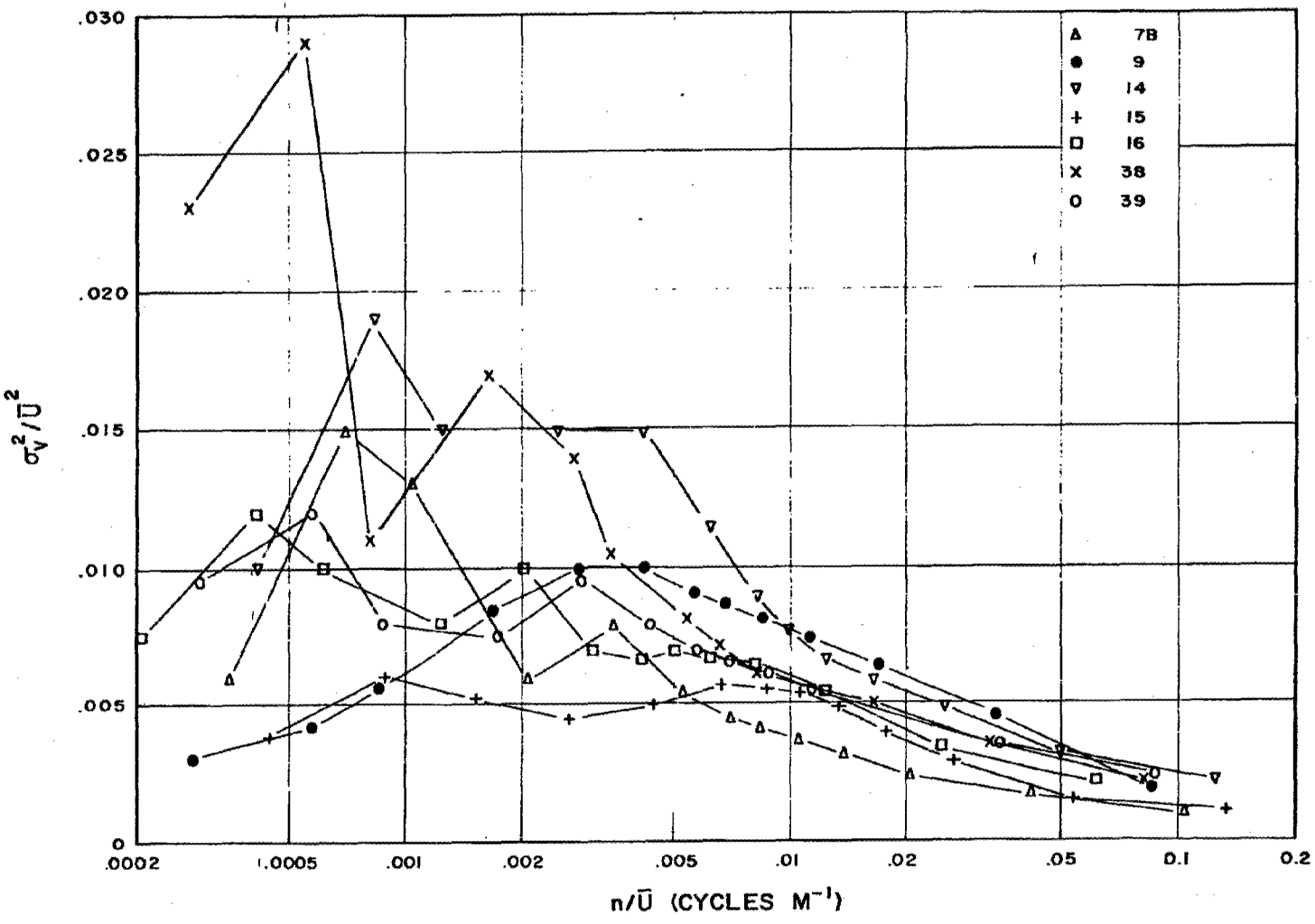

Fig. 2a. Logarithmic power spectra of the v-component of wind velocity at a height of 16 m for the daytime experiments.

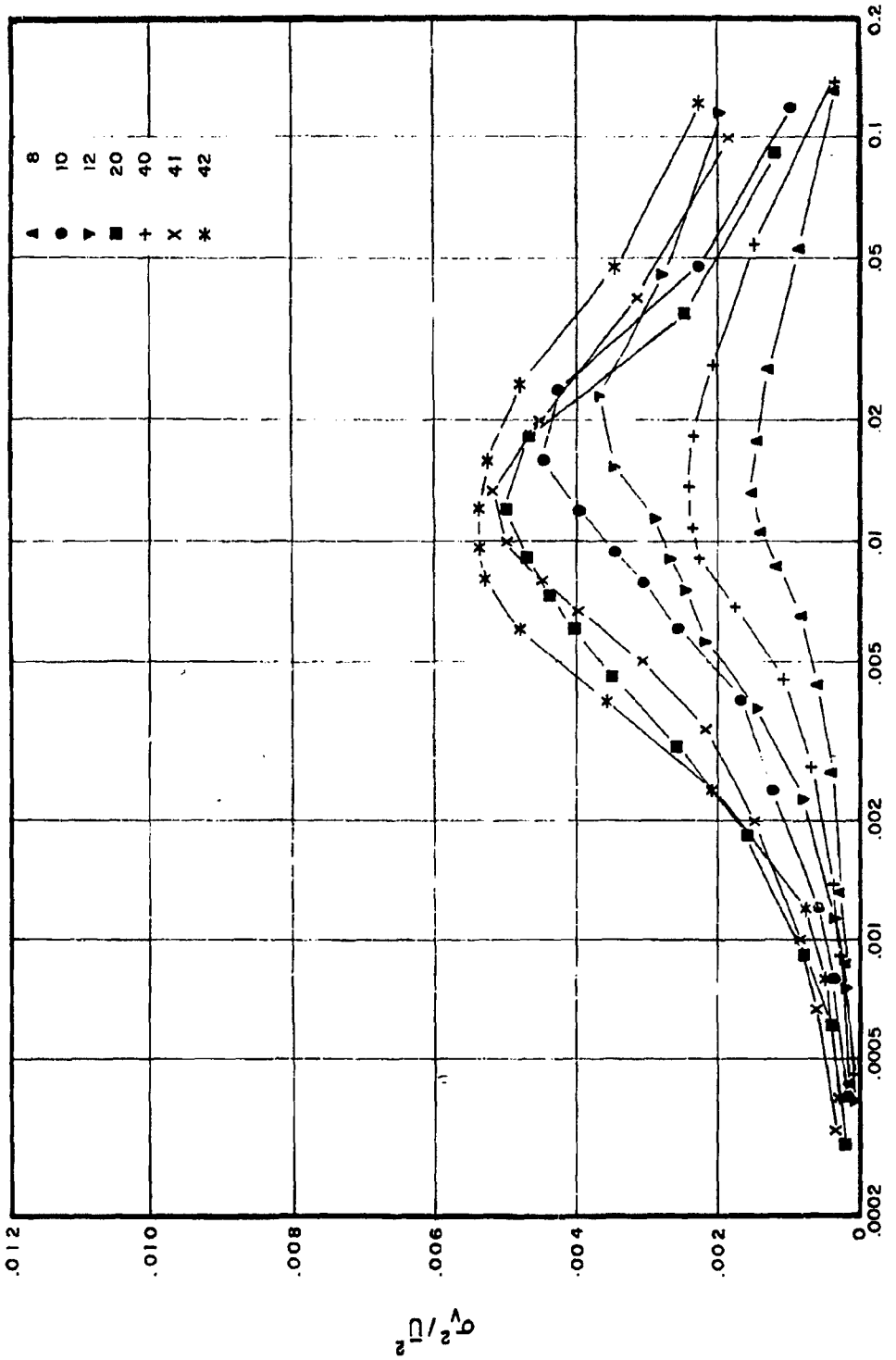

Fig. 2b. Logarithmic power spectra of the v-component of wind velocity at a height of 16 m for the nighttime experiments.

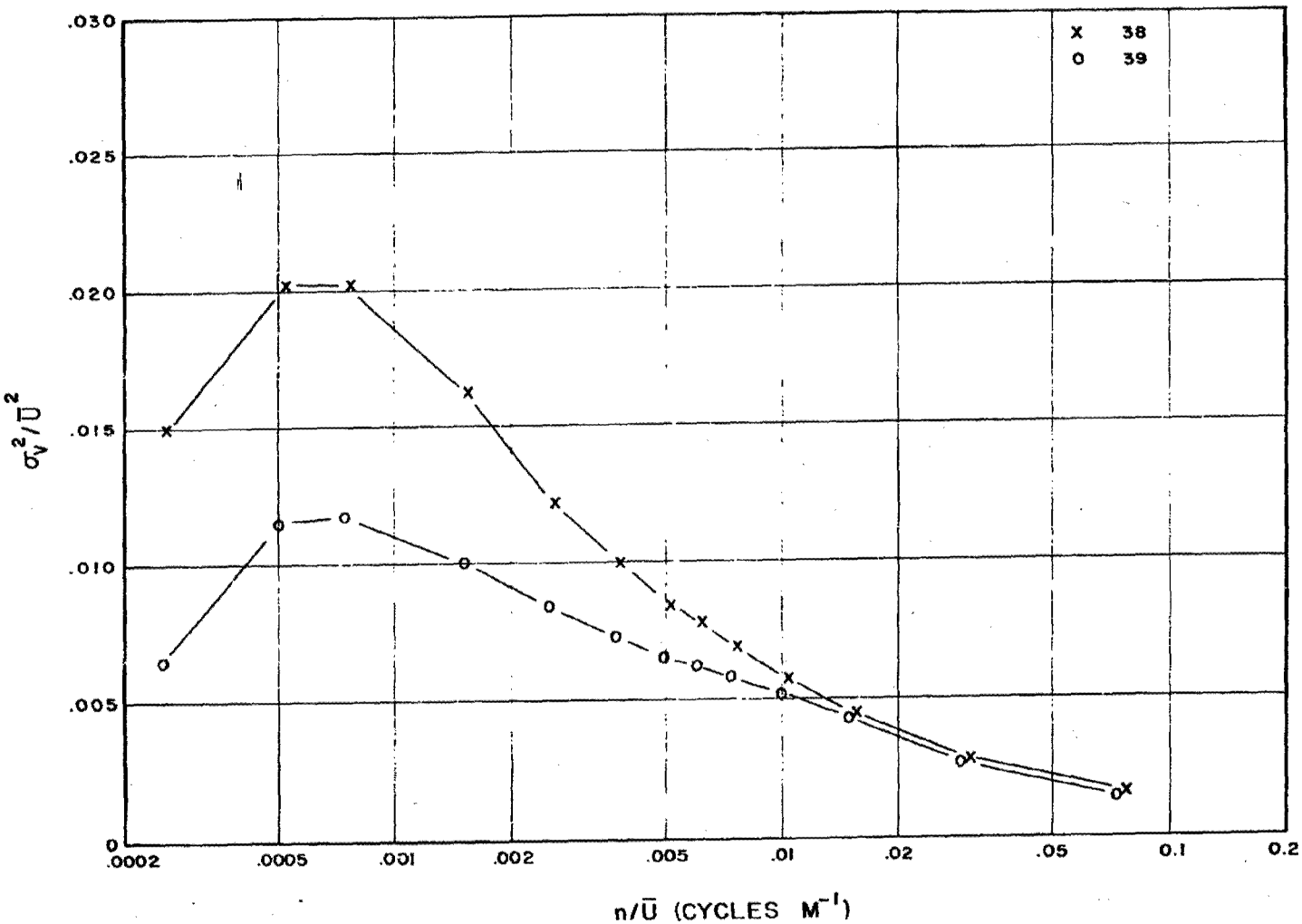

Fig. 2c. Logarithmic power spectra of the v-component of wind velocity at a height of 40 m for the daytime experiments.

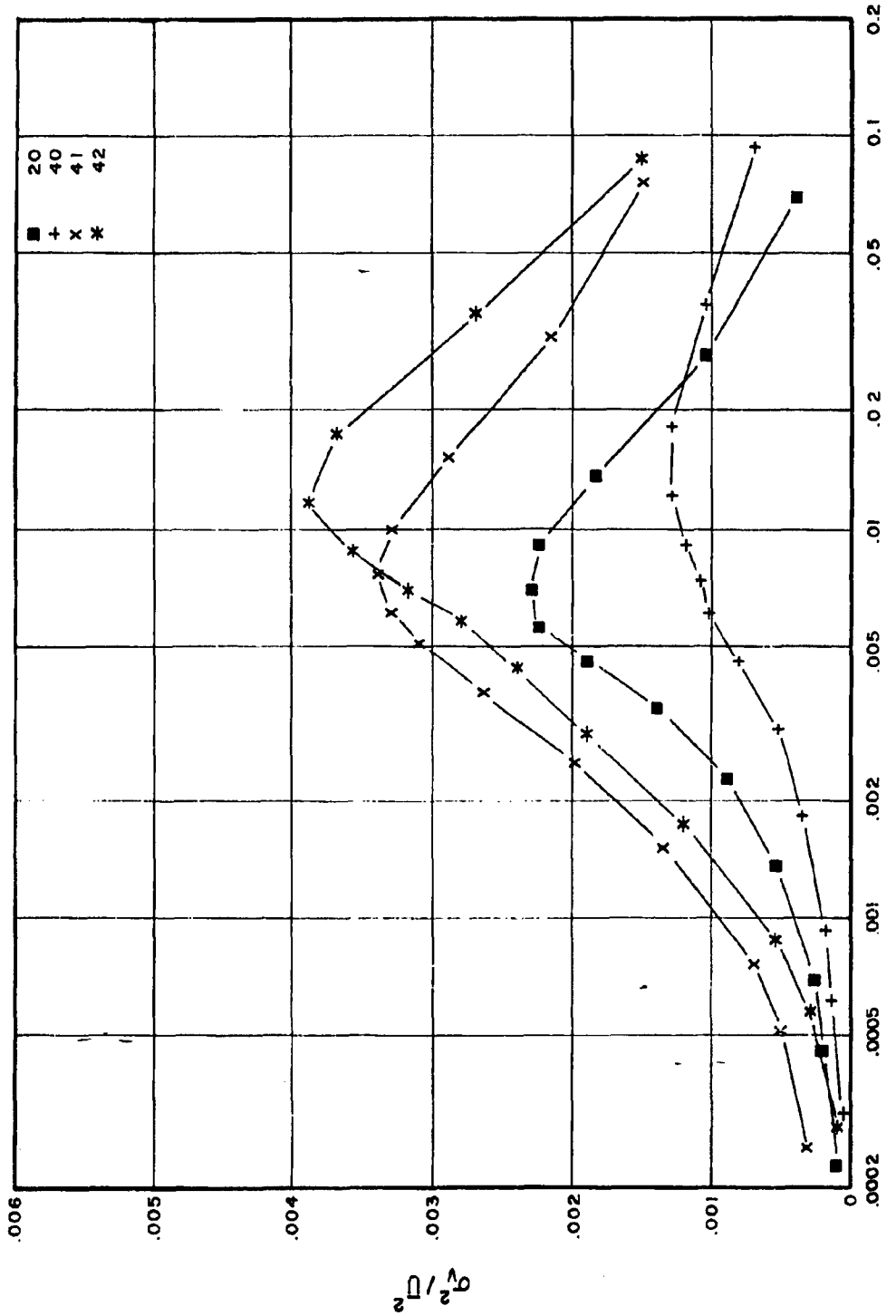

Fig. 2d. Logarithmic power spectra of the v-component of wind velocity at a height of 40 m for the nighttime experiments.

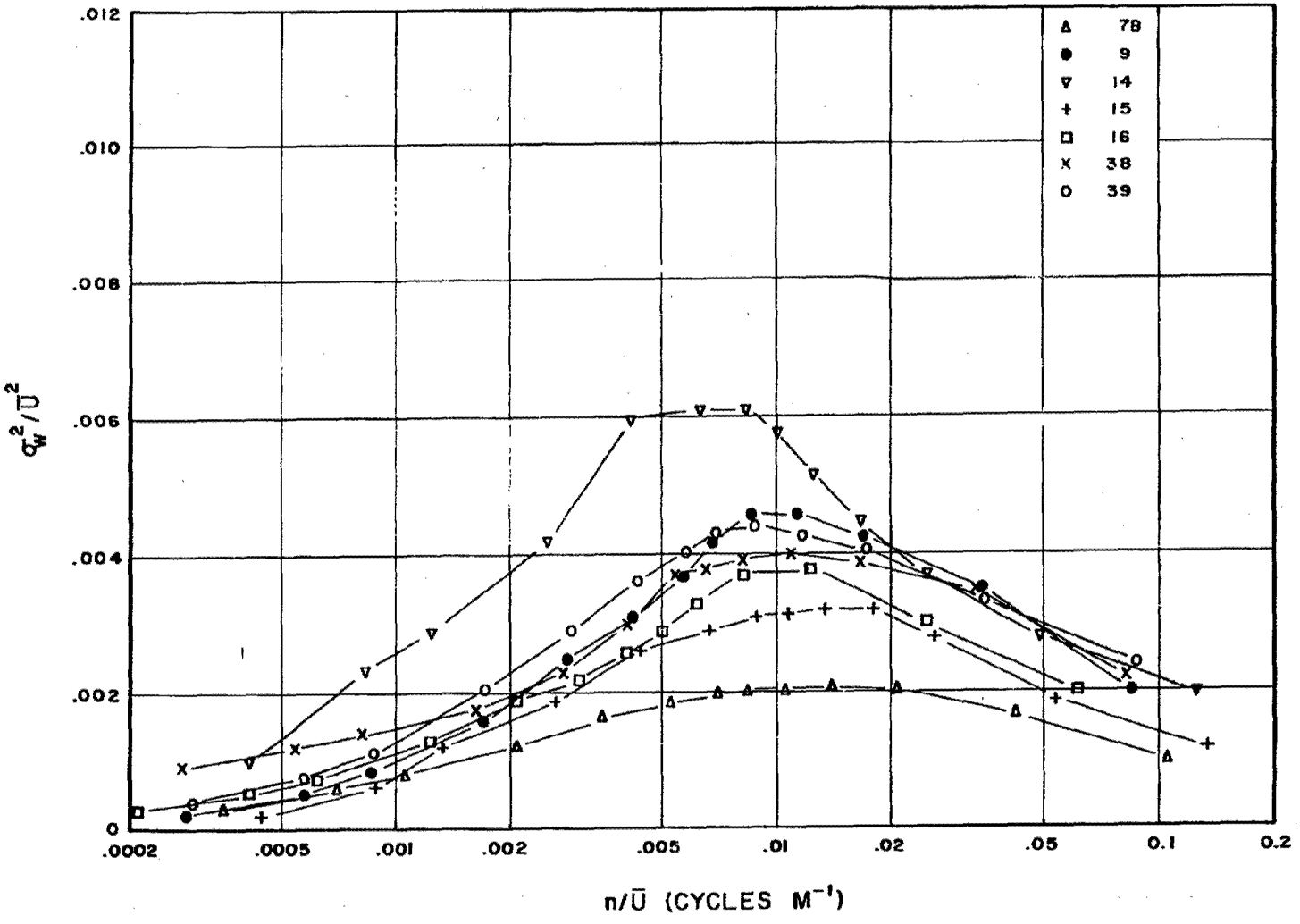

Fig. 3a. Logarithmic power spectra of the w-component of wind velocity at a height of 16 m for the daytime experiments.

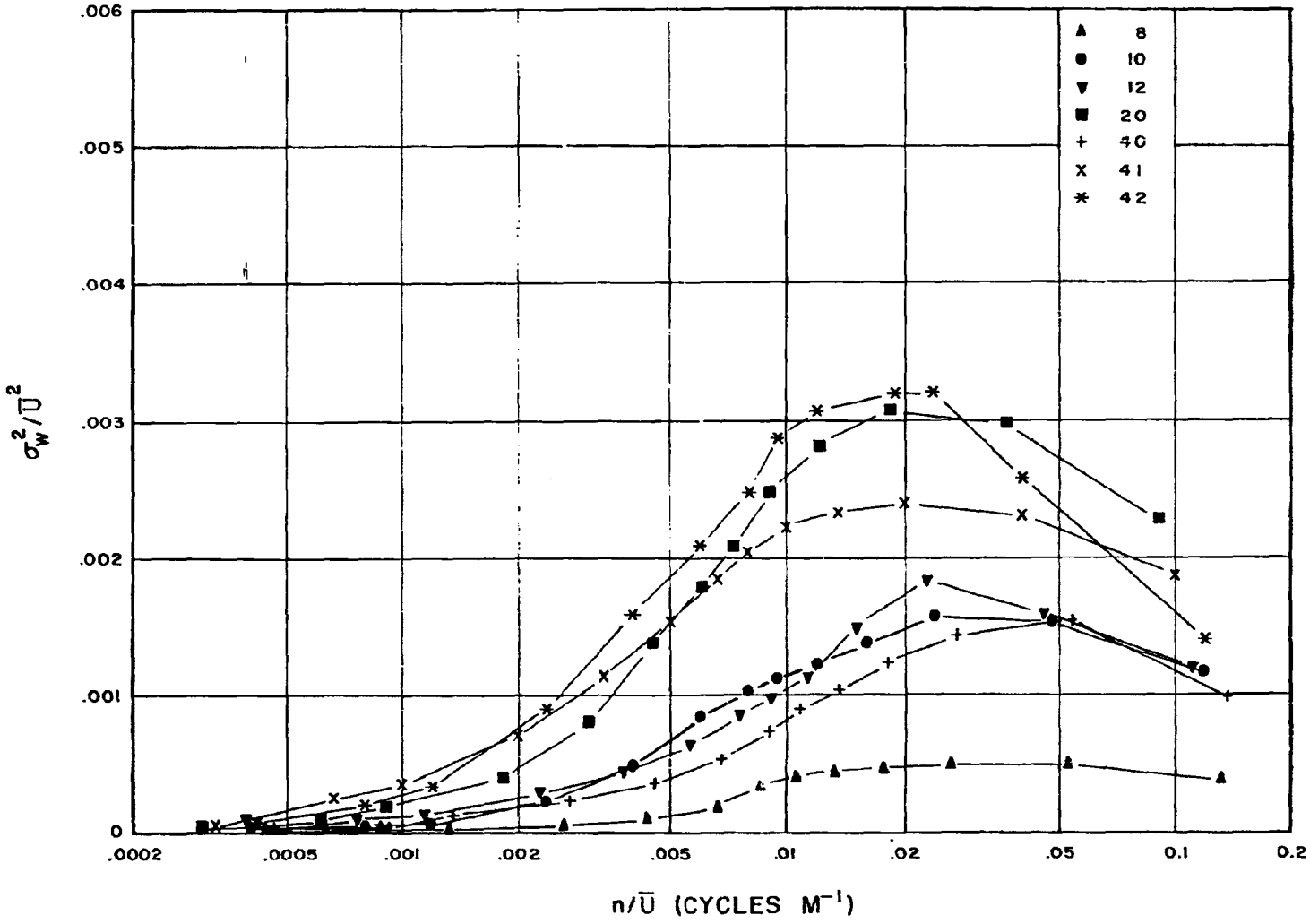

Fig. 3b. Logarithmic power spectra of the w-component of wind velocity at a height of 16 m for the nighttime experiments.

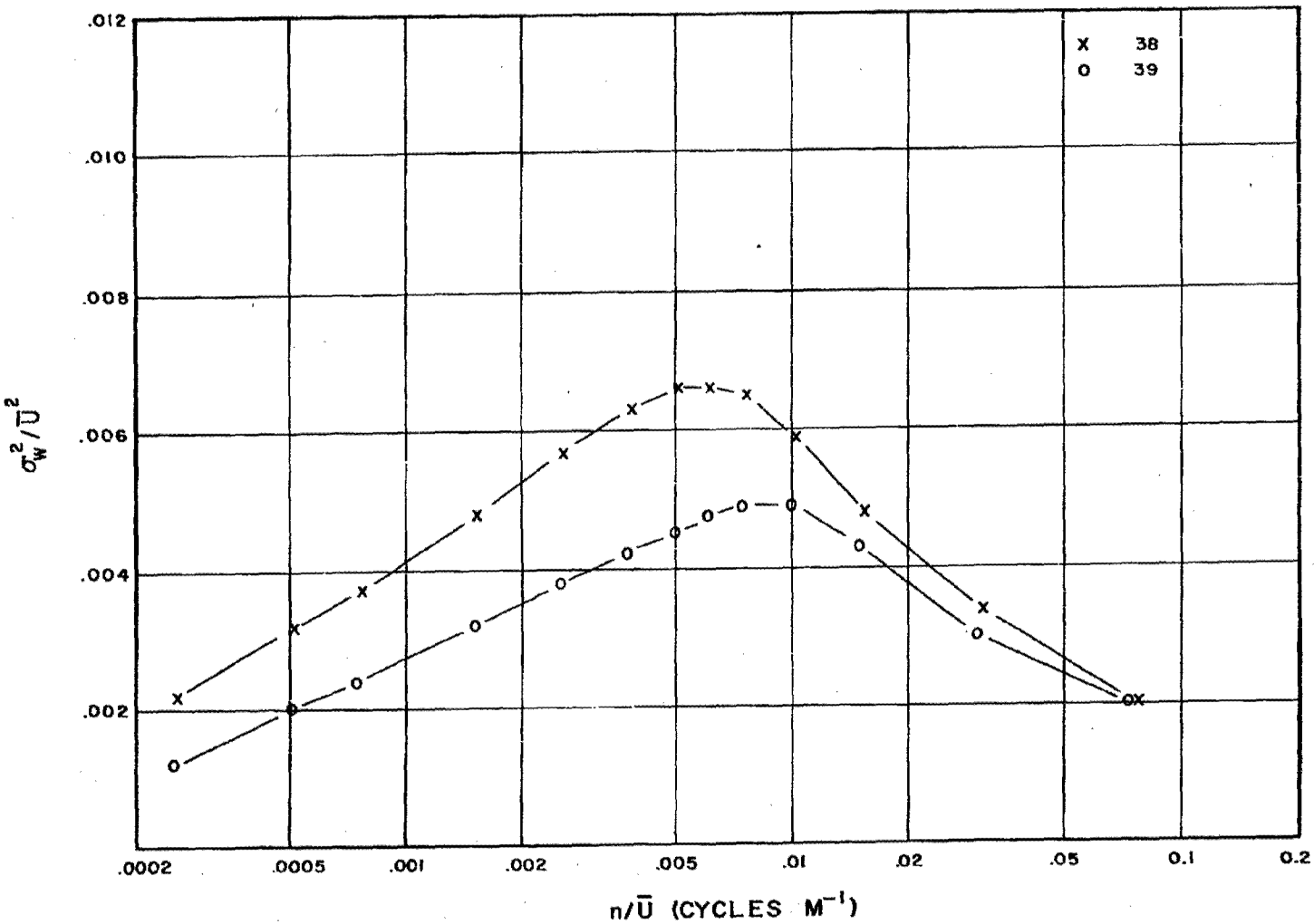

Fig. 3c. Logarithmic power spectra of the w-component of wind velocity at a height of 40 m for the daytime experiments.

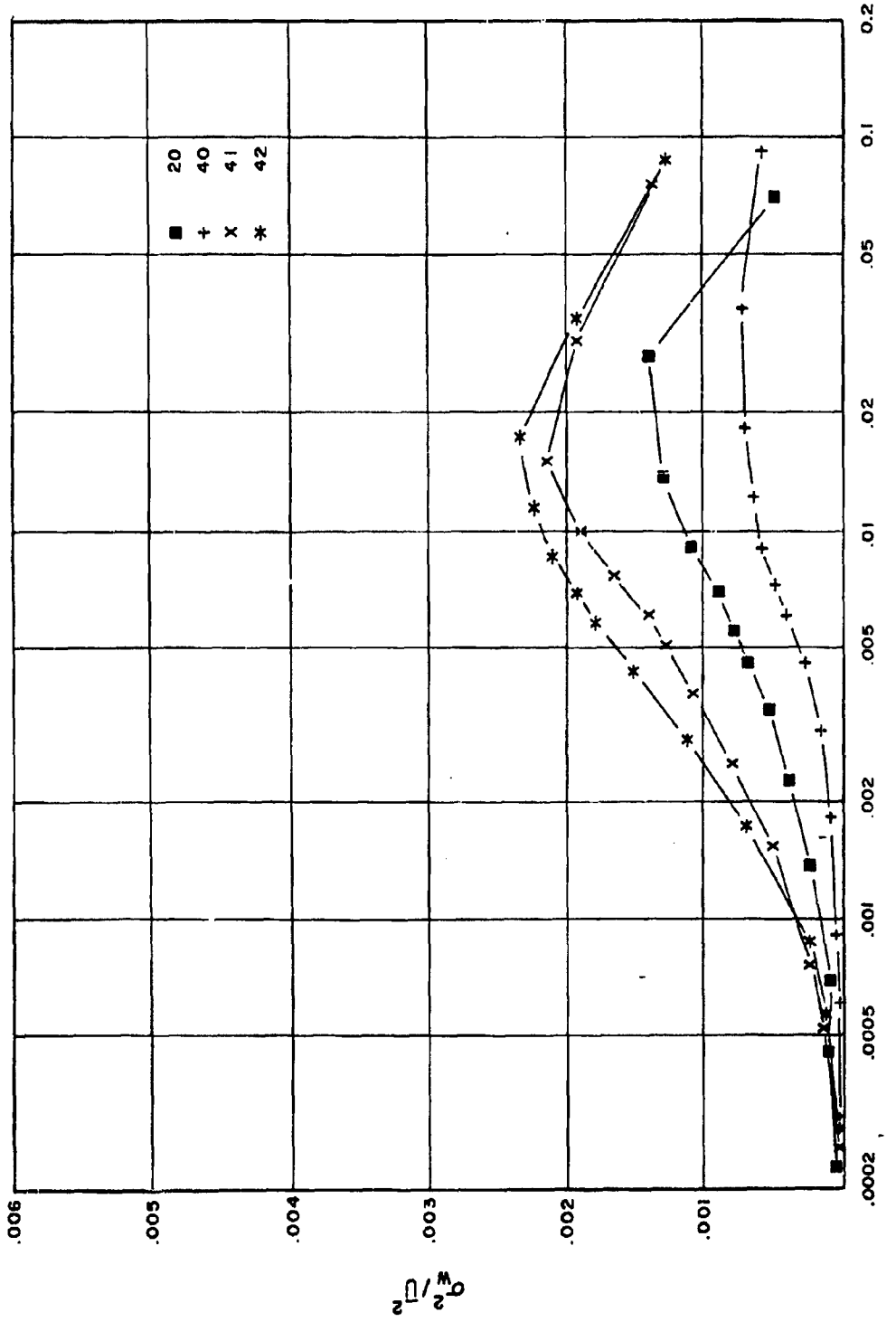

Fig. 3d. Logarithmic power spectra of the w-component of wind velocity at a height of 40 m for the nighttime experiments.

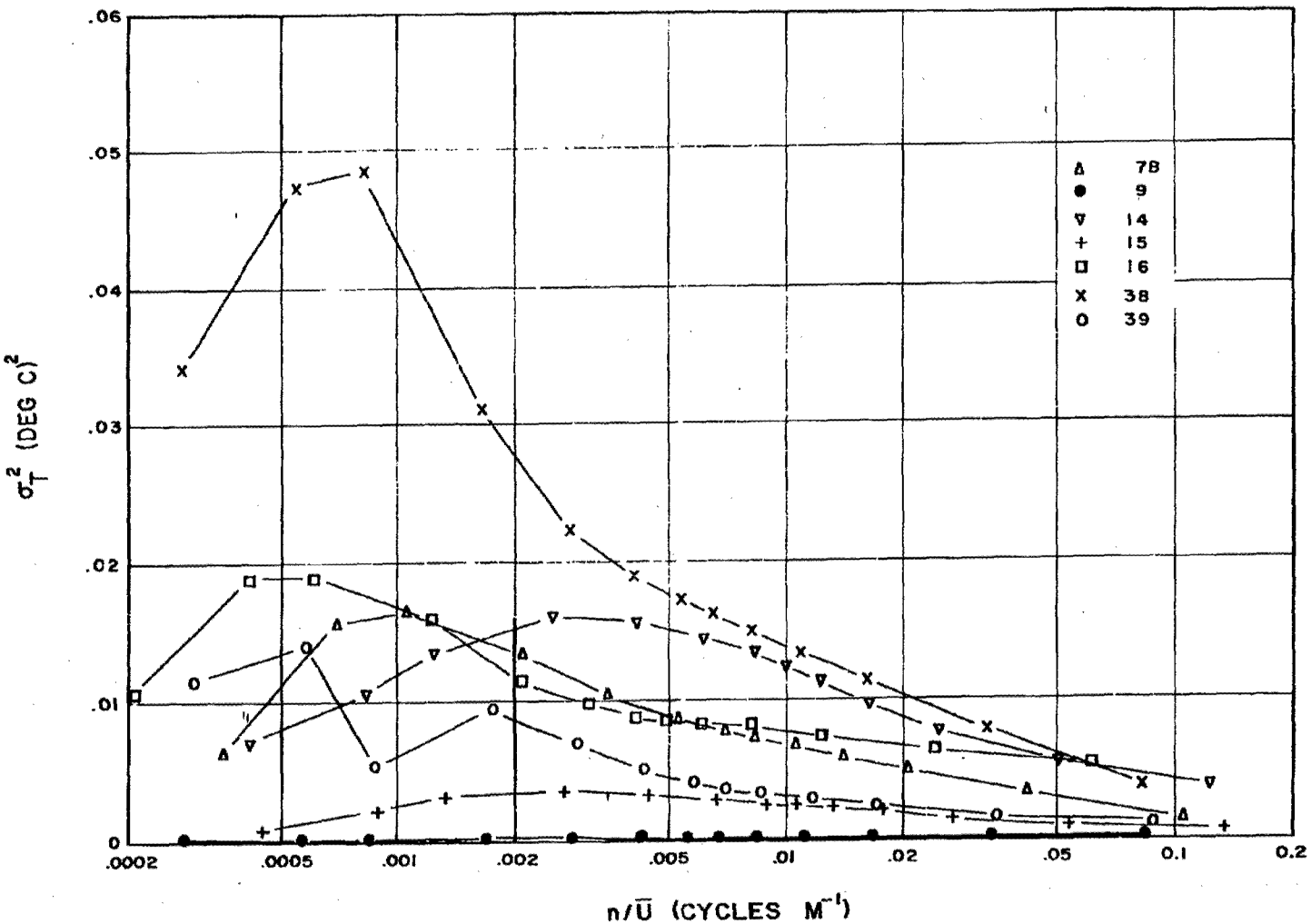

Fig. 4a. Logarithmic power spectra of air temperature at a height of 16 m for the daytime experiments.

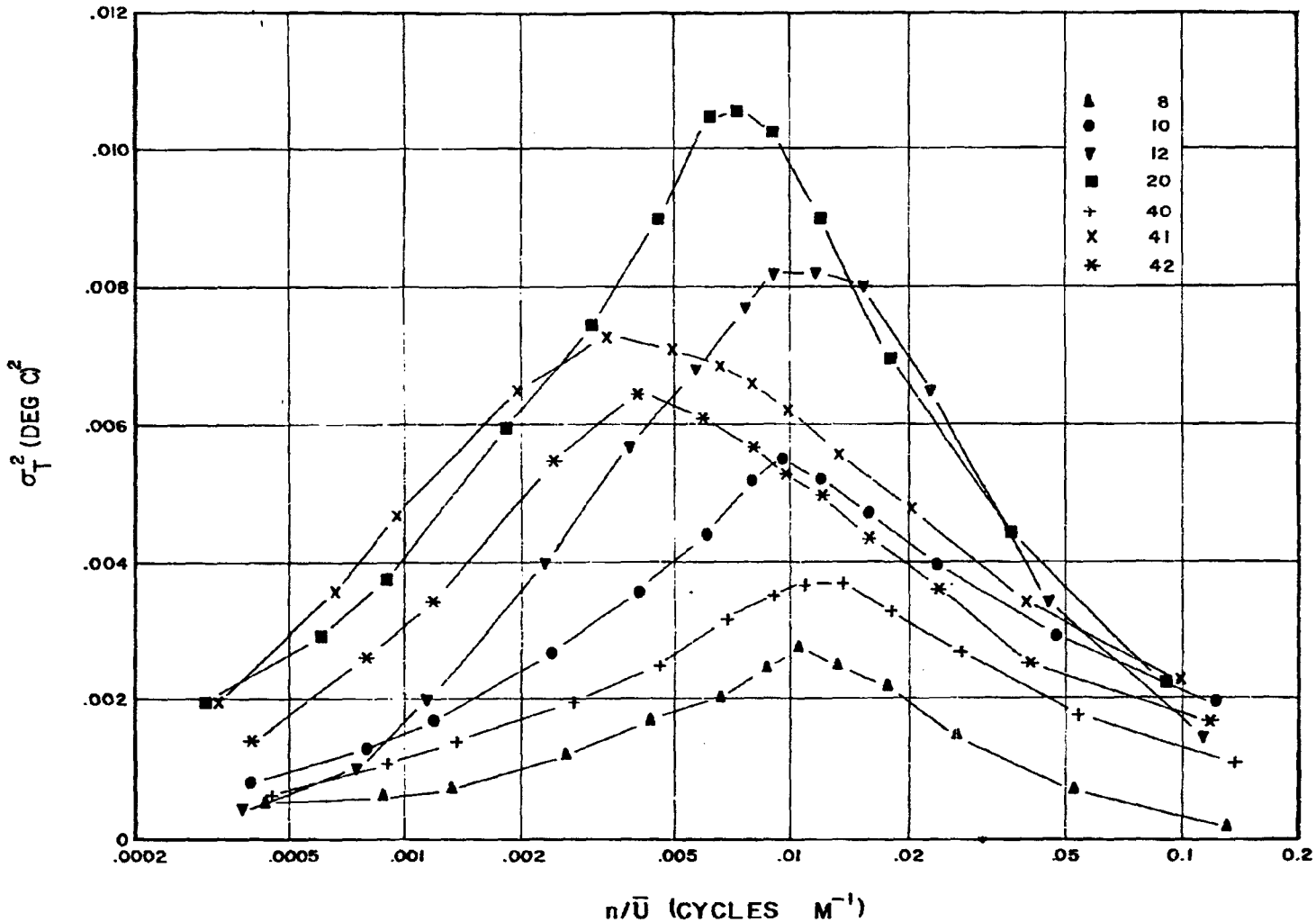

Fig. 4b. Logarithmic power spectra of air temperature at a height of 16 m for the nighttime experiments.

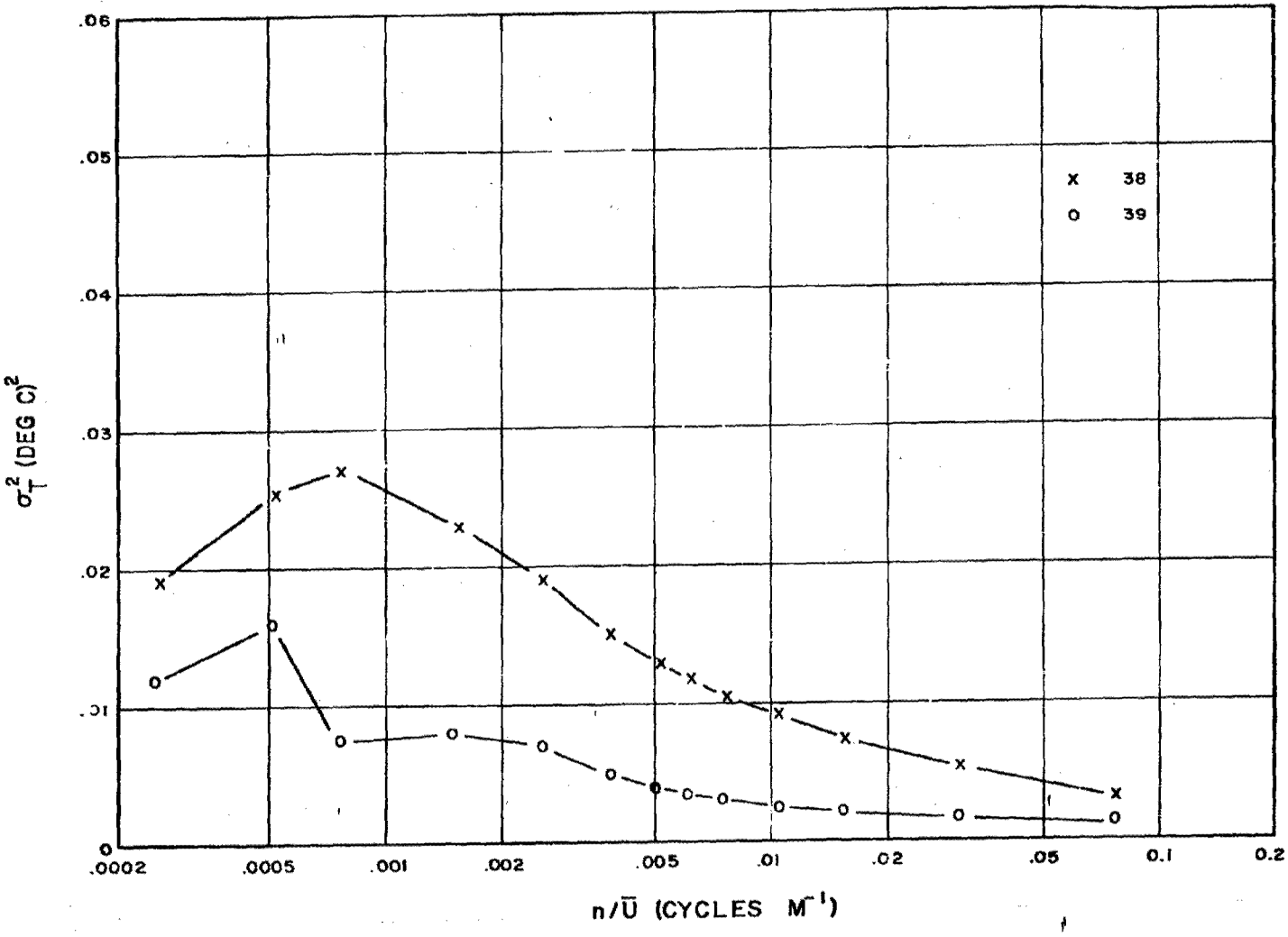

Fig. 4c. Logarithmic power spectra of air temperature at a height of 40 m for the daytime experiments.

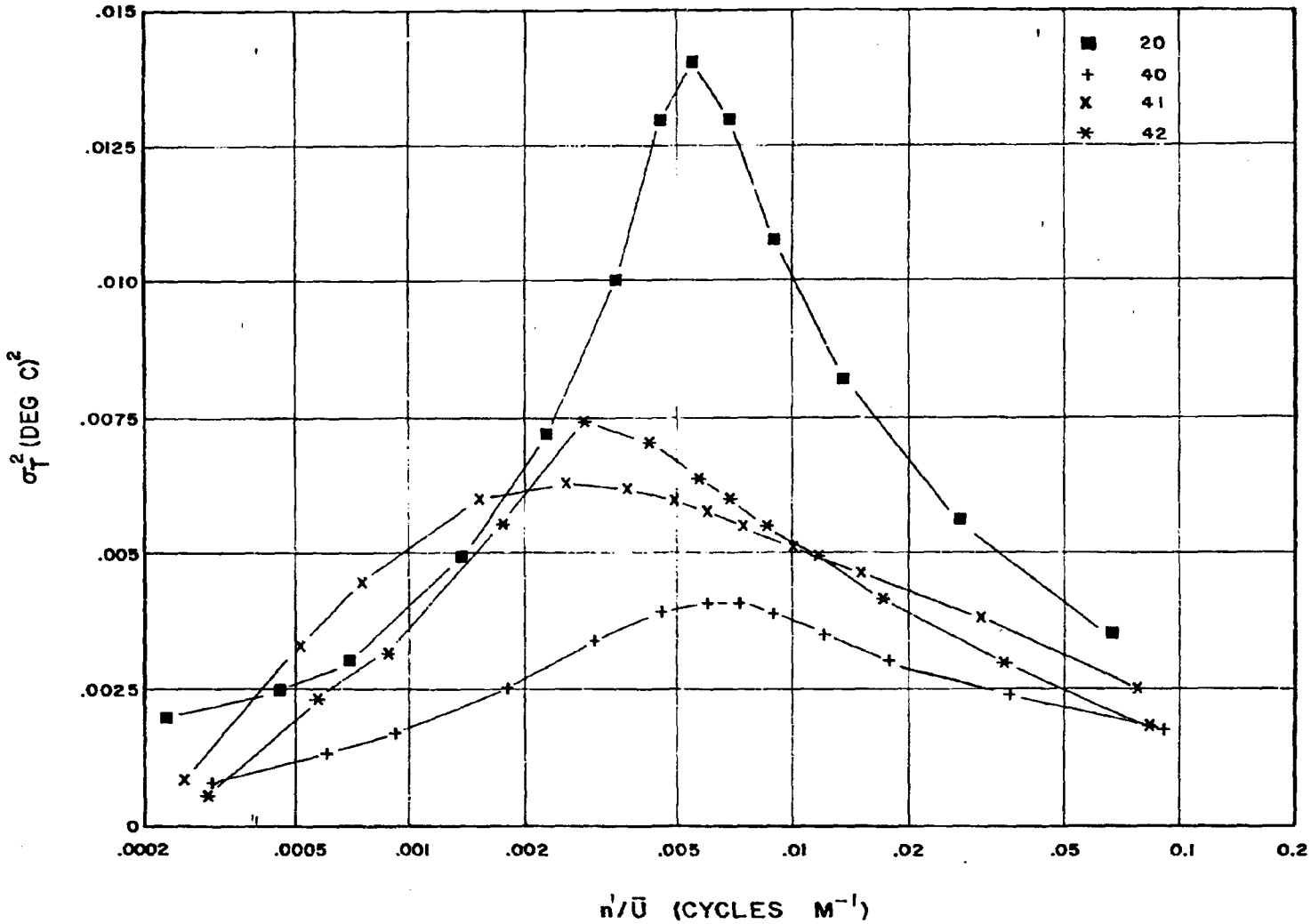

Fig. 4d. Logarithmic power spectra of air temperature at a height of 40 m for the nighttime experiments.

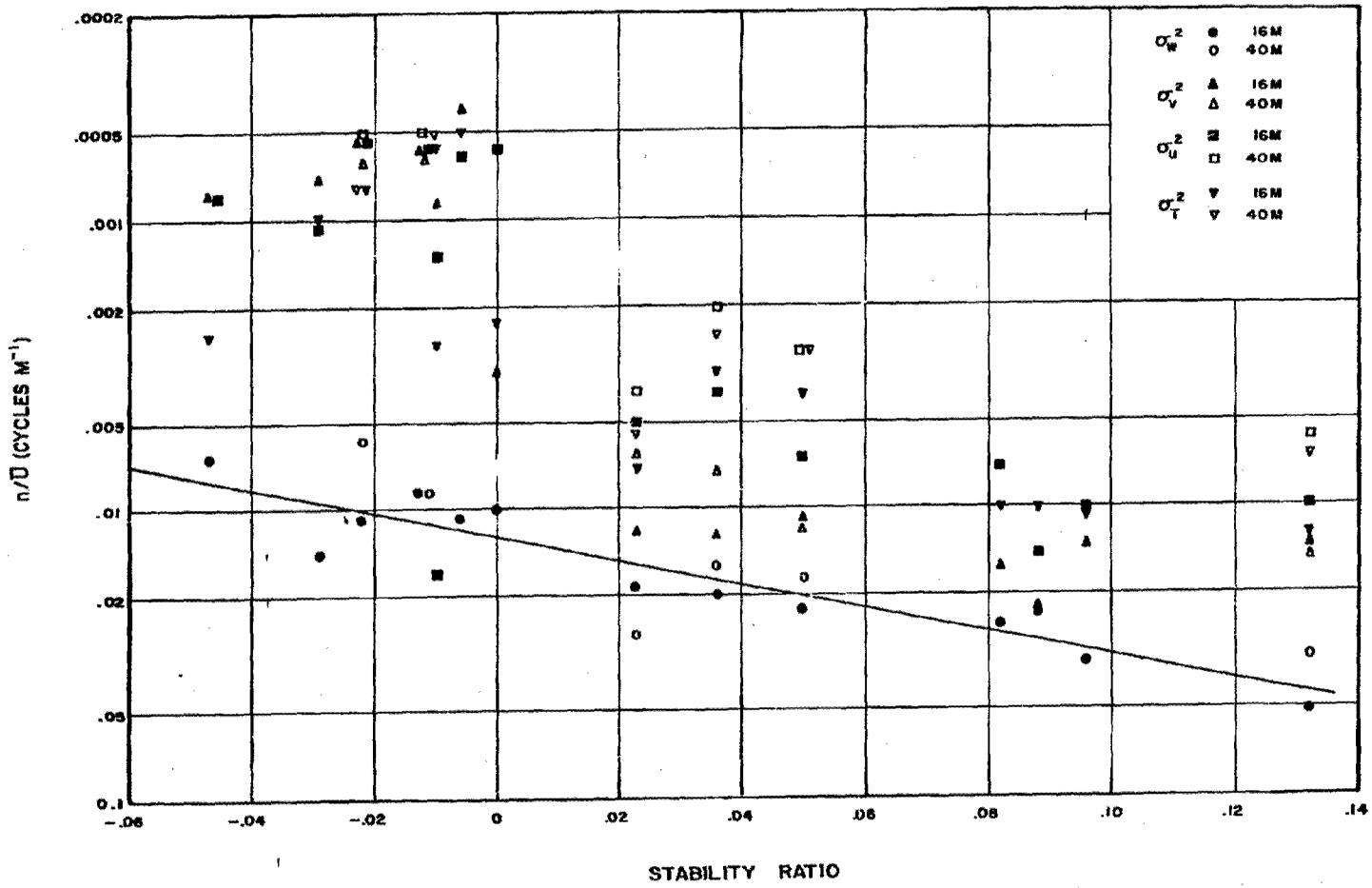

Fig. 5a. Peak frequencies of the u-, v-, w-, and T-spectra versus the Stability Ratio. Solid line was fitted by eye to the w peak data at a height of 16 m.

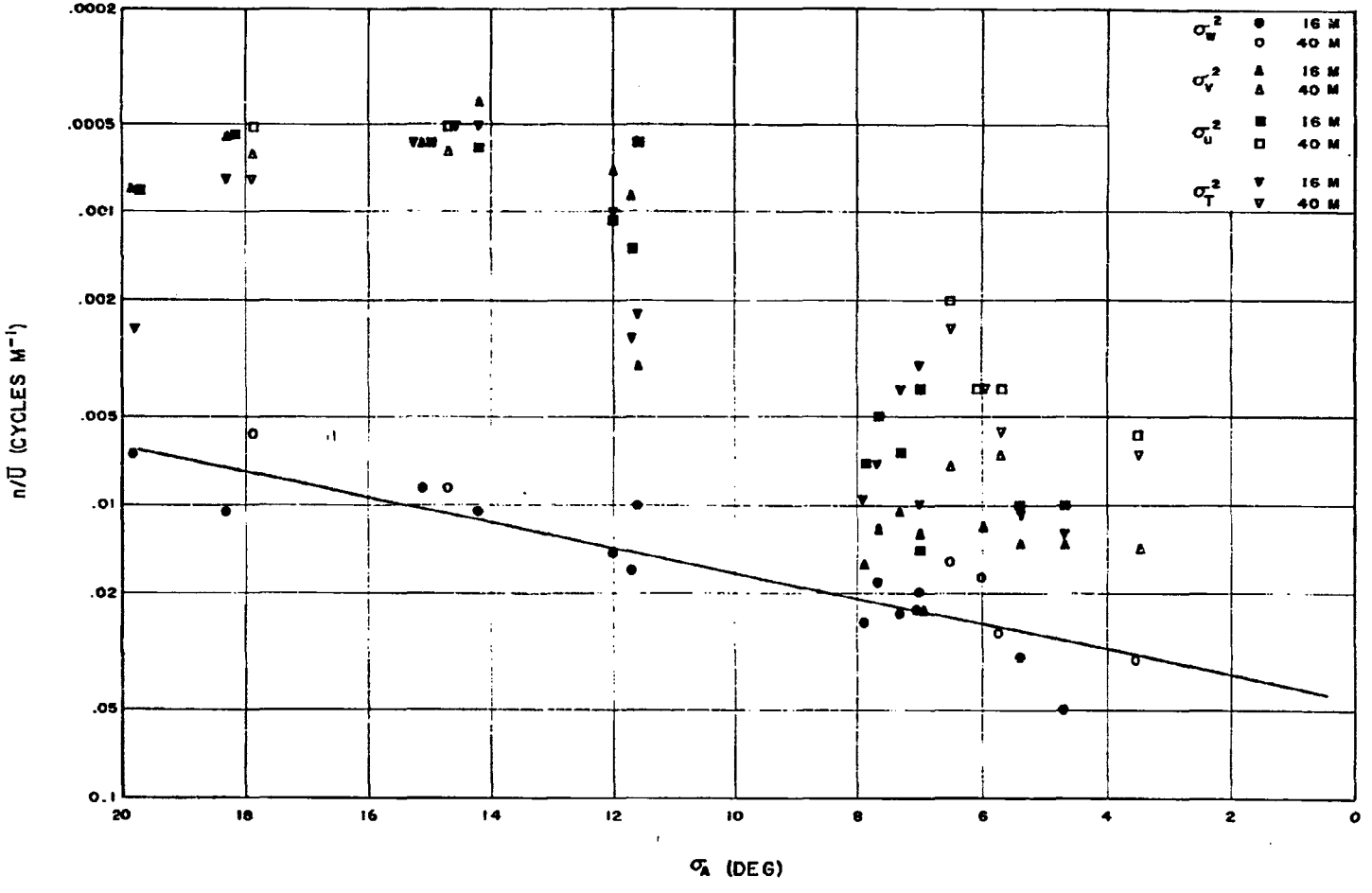

Fig. 5b. Peak frequencies of the u-, v-, w-, and T-spectra versus the standard deviation of the azimuth wind direction. Solid line was fitted by eye to the w peak data at a height of 16 m.

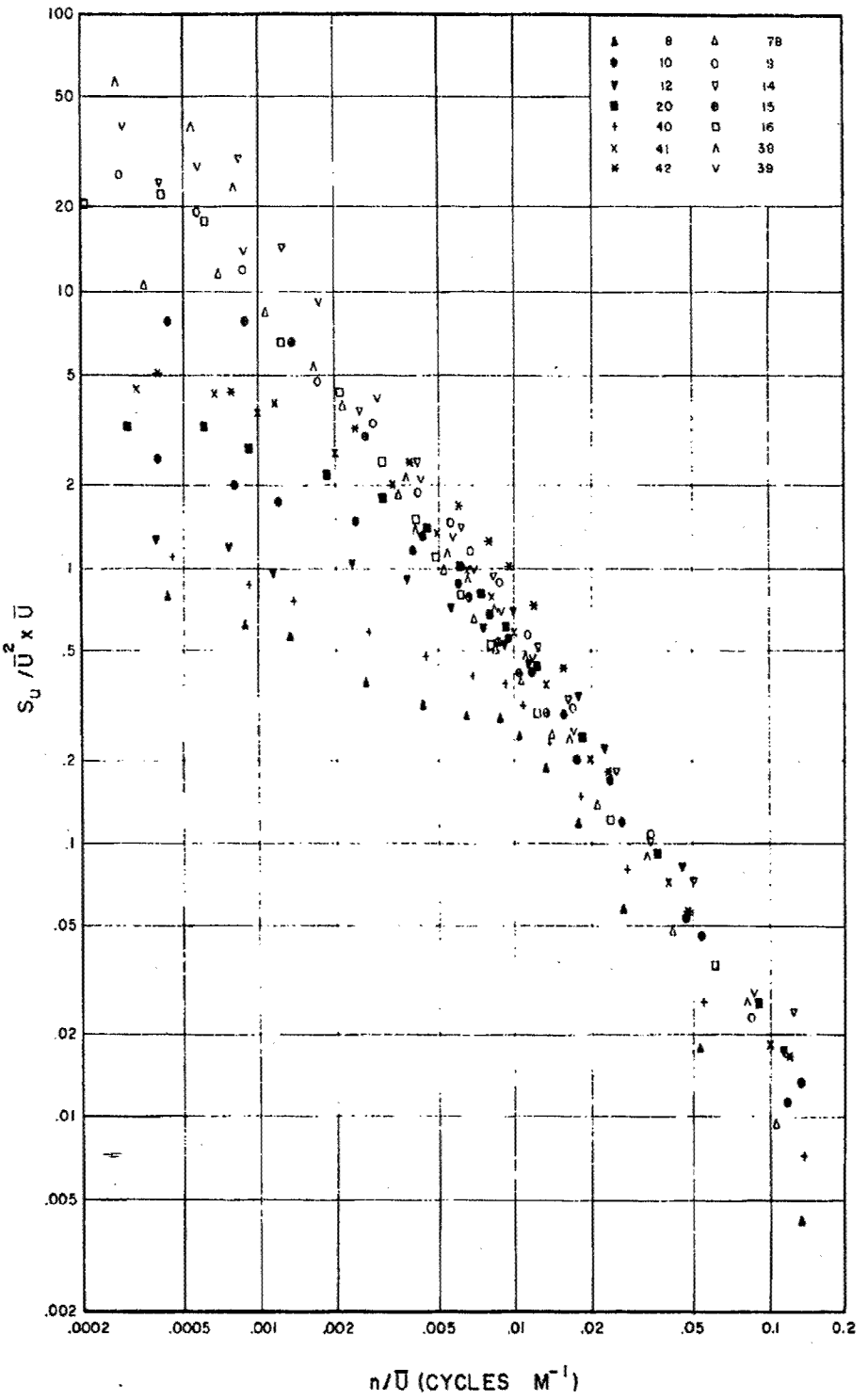

Fig. 6a. Spectral density of the u-component of wind velocity at 16 m.

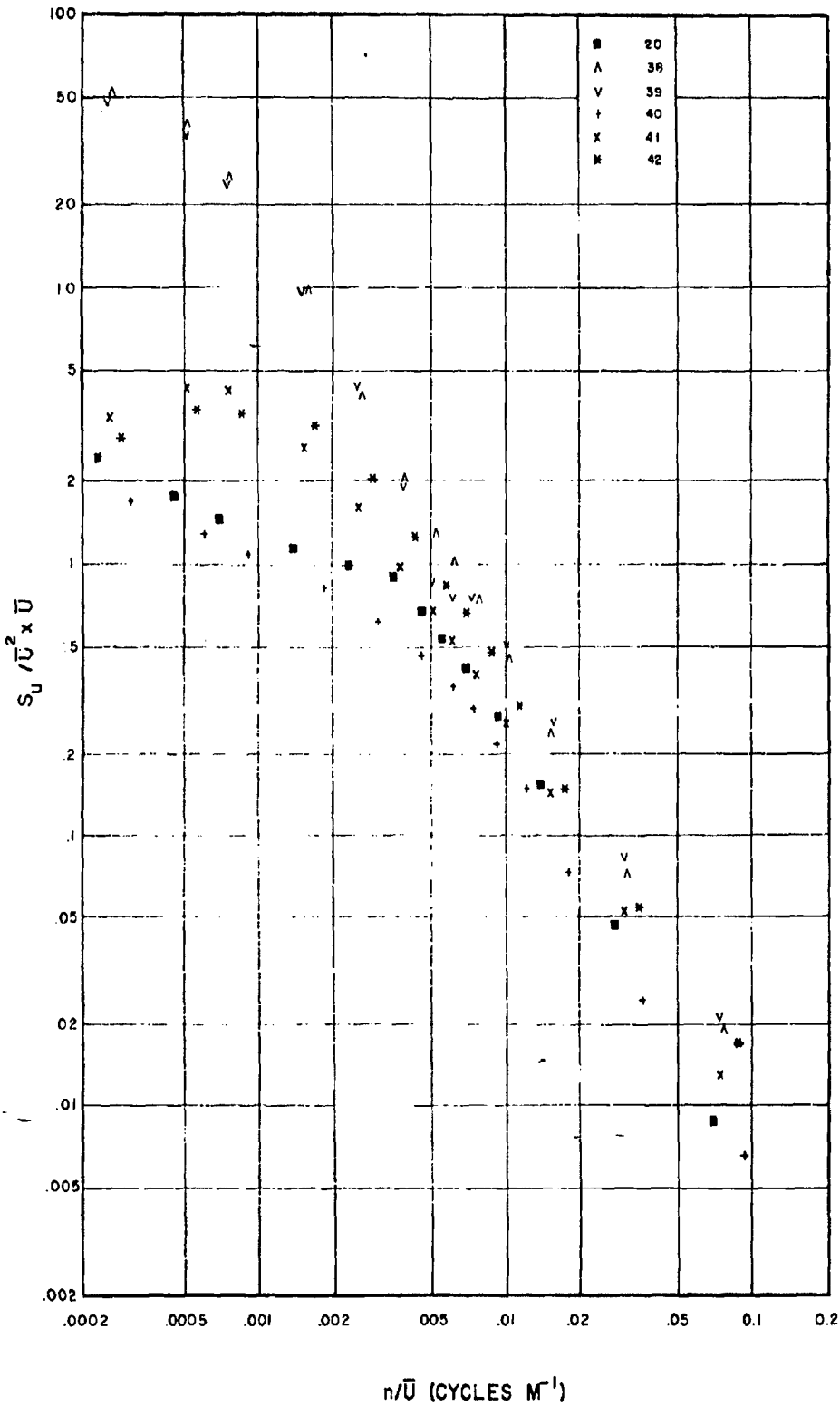

Fig. 6b. Spectral density of the u-component of wind velocity at 40 m.

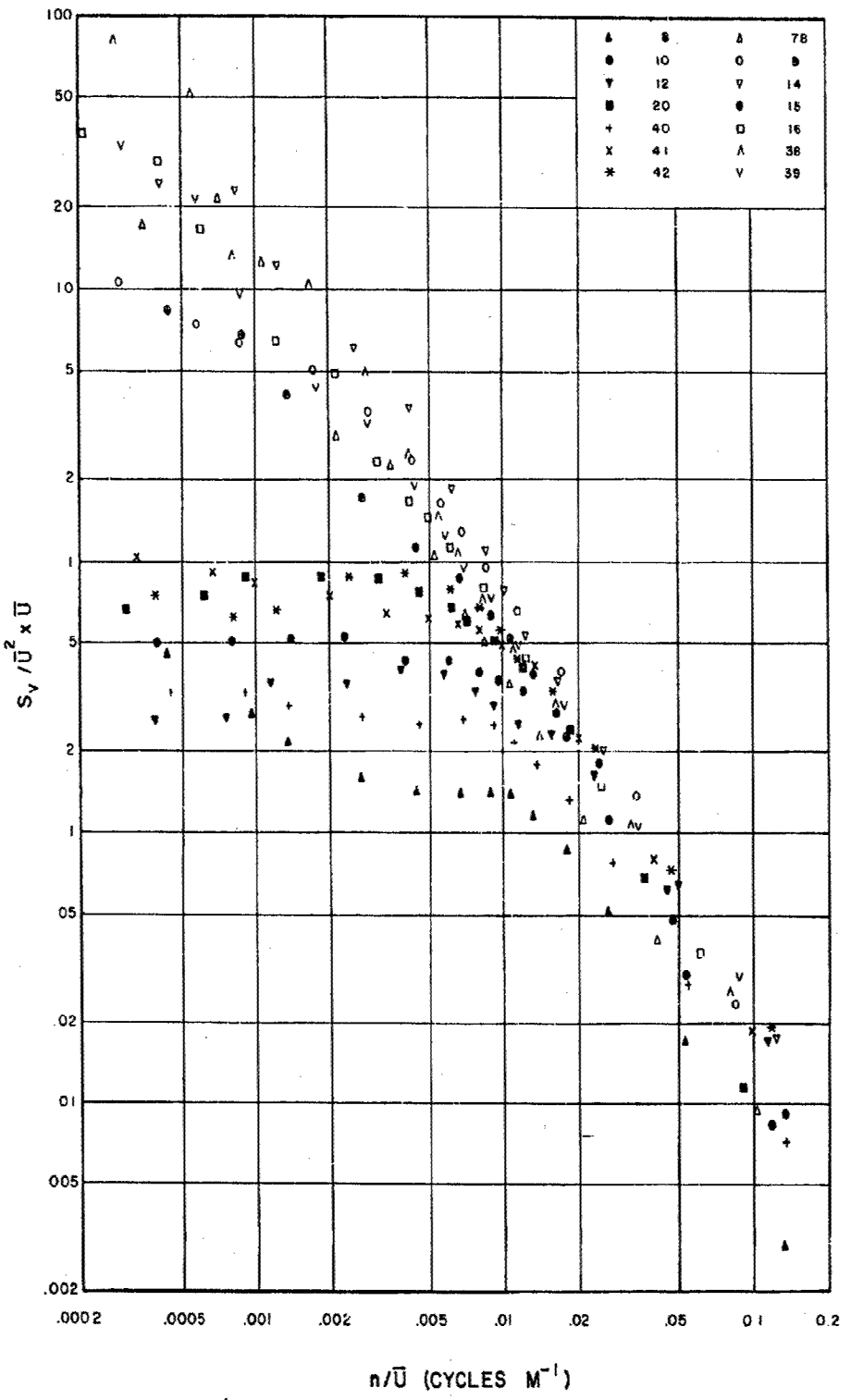

Fig. 7a. Spectral density of the v-component of wind velocity at 16 m.

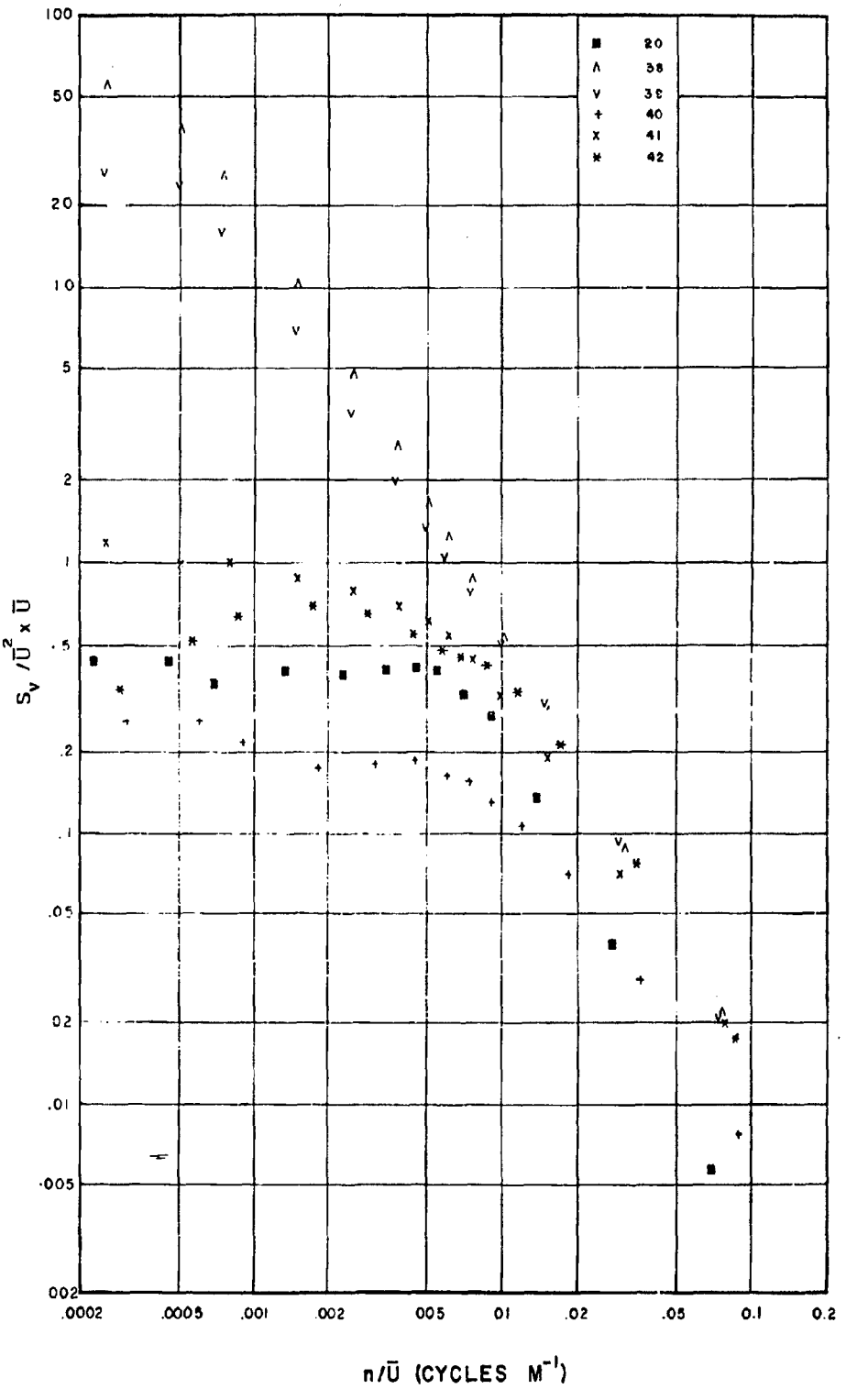

Fig. 7b. Spectral density of the v-component of wind velocity at 40 m.

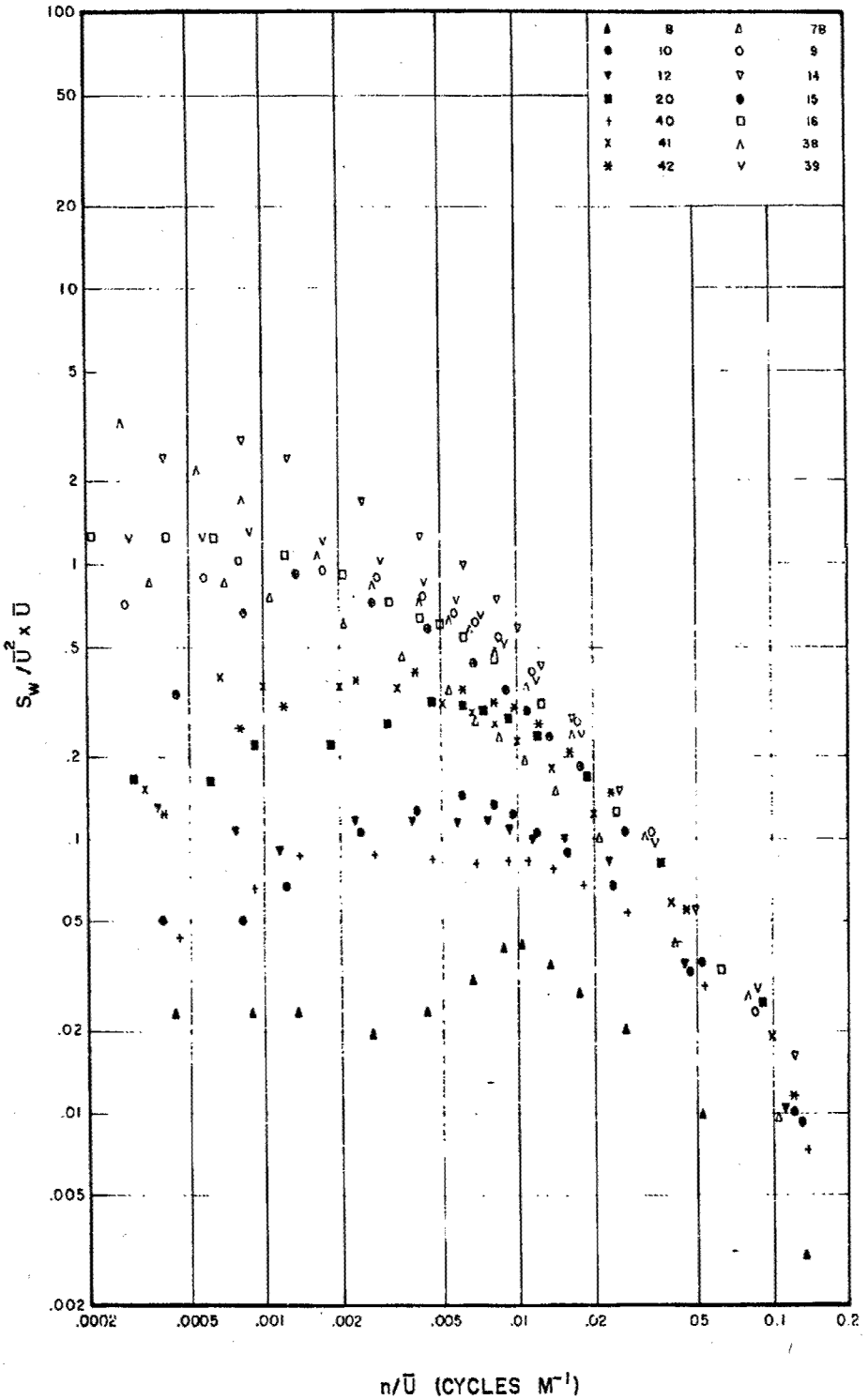

Fig. 8a. Spectral density of the w-component of wind velocity at 16 m.

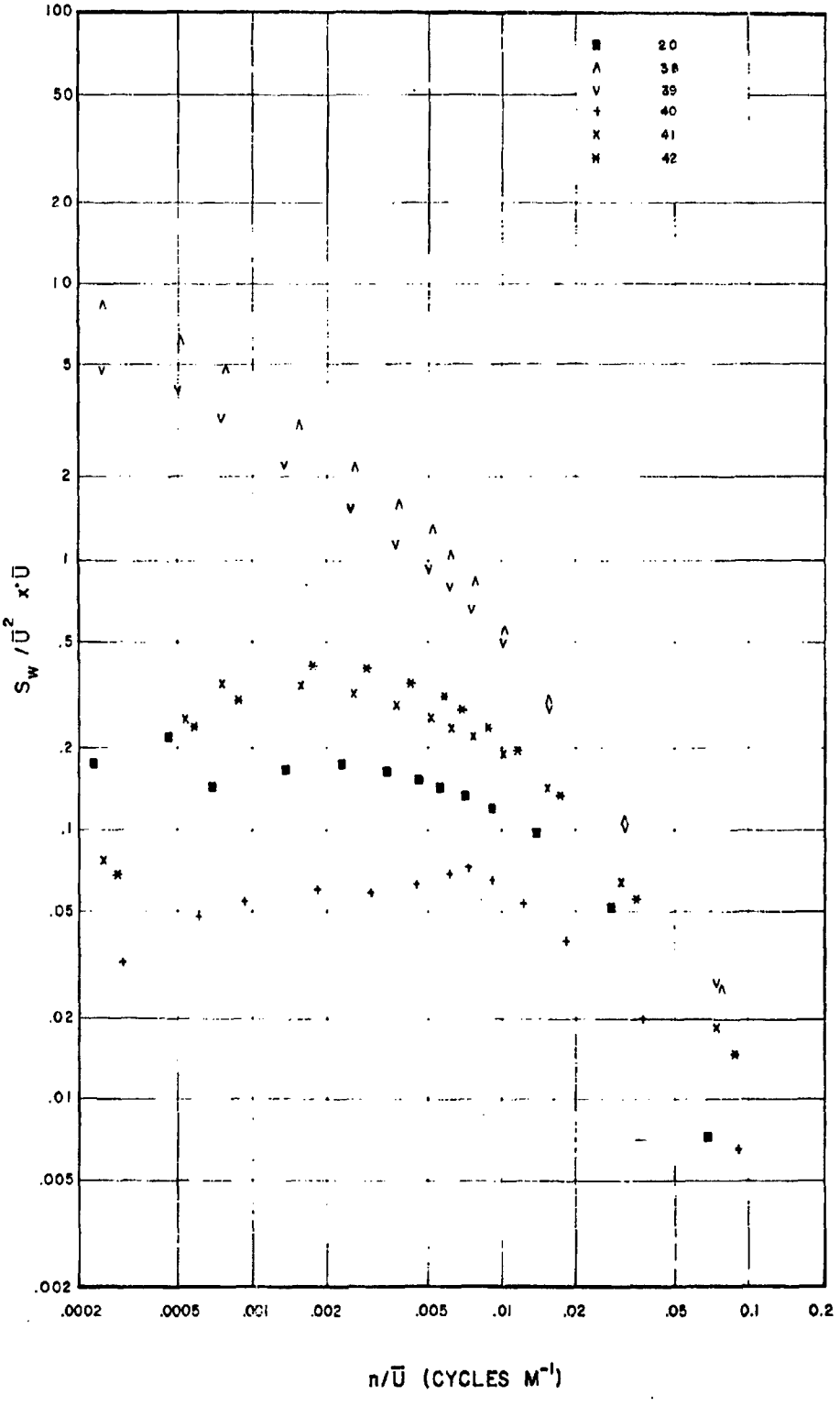

Fig. 8b. Spectral density of the w-component of wind velocity at 40 m.

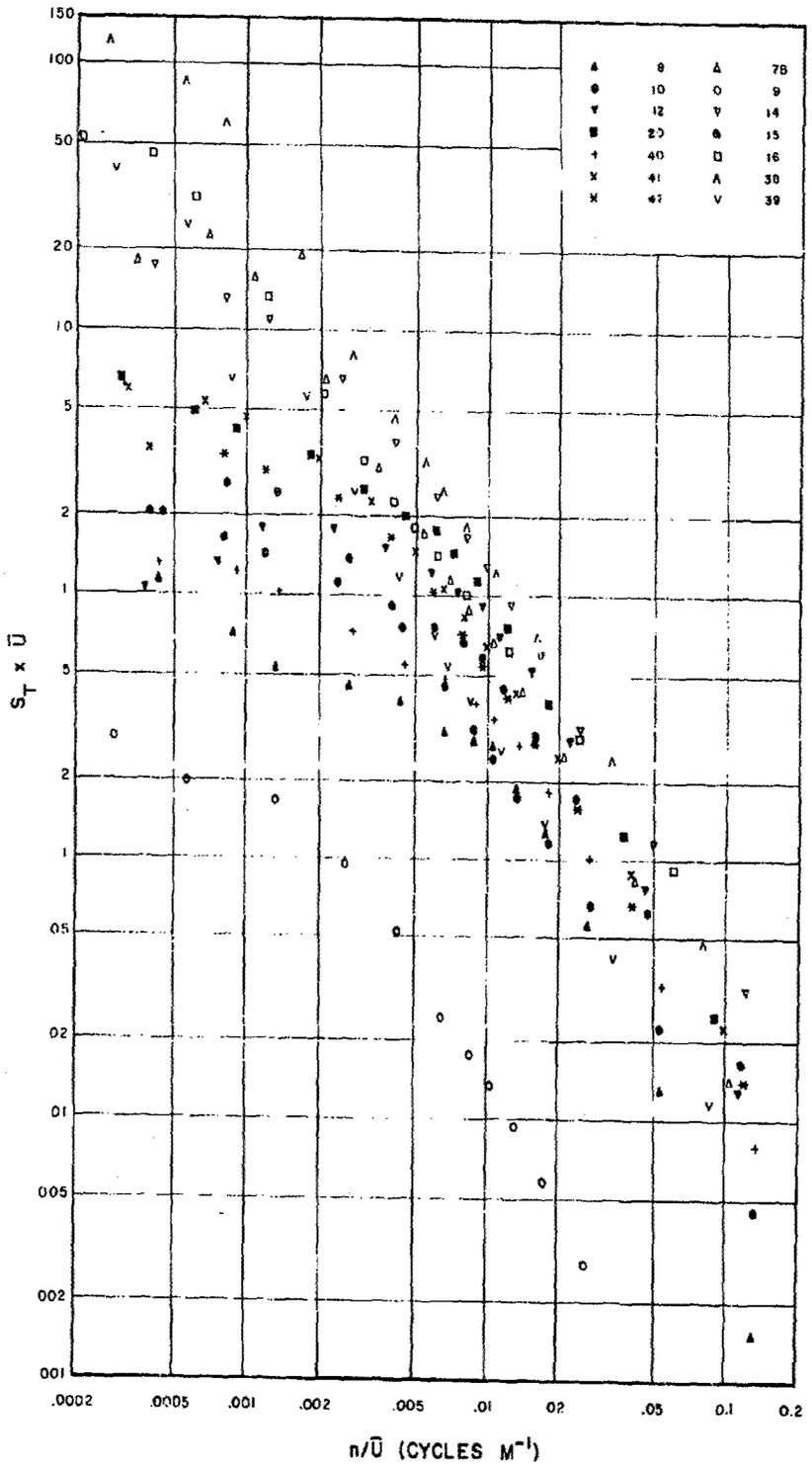

Fig. 9a. Spectral density of air temperature at 16 m.

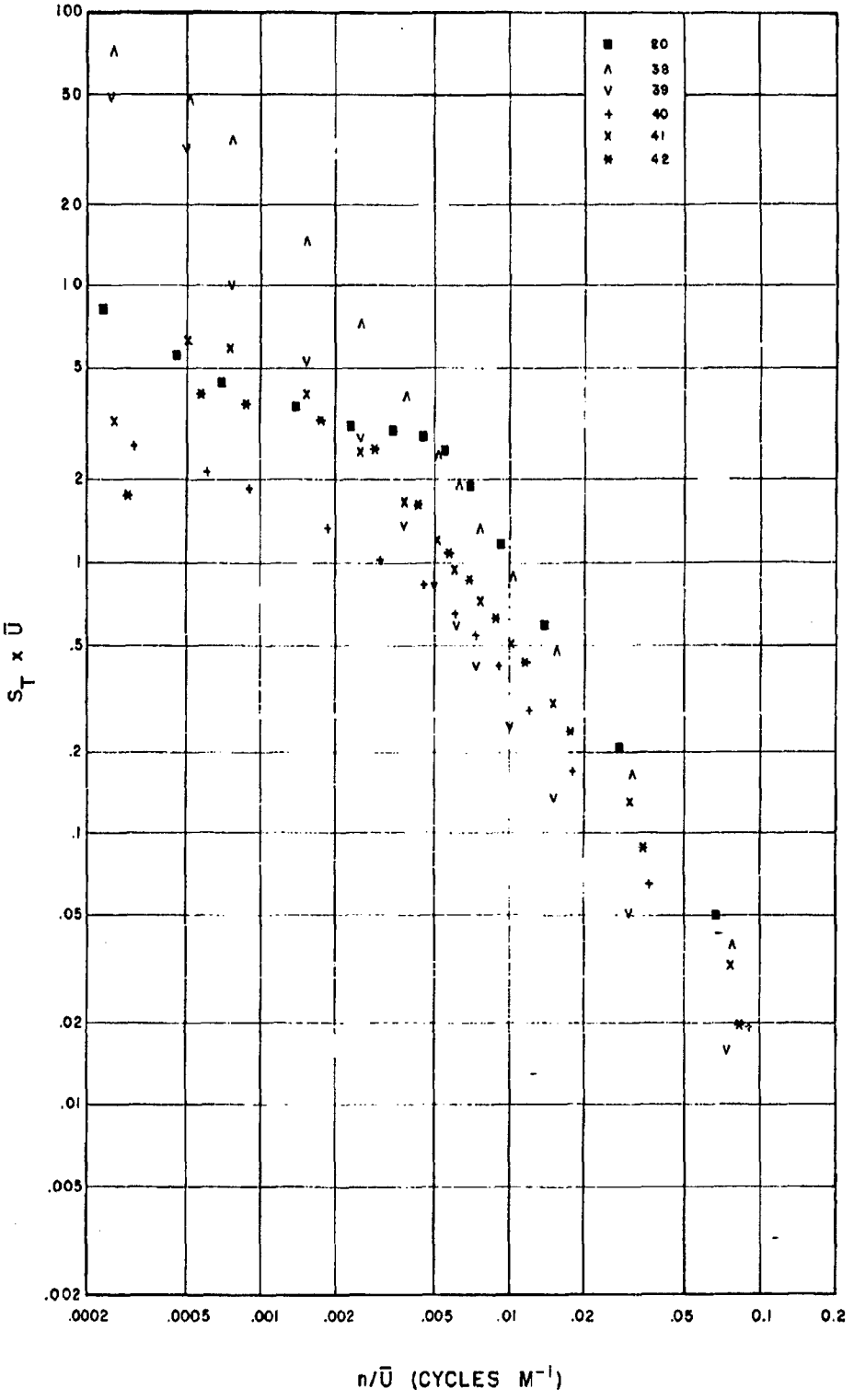

Fig. 9b. Spectral density of air temperature at 40 m.

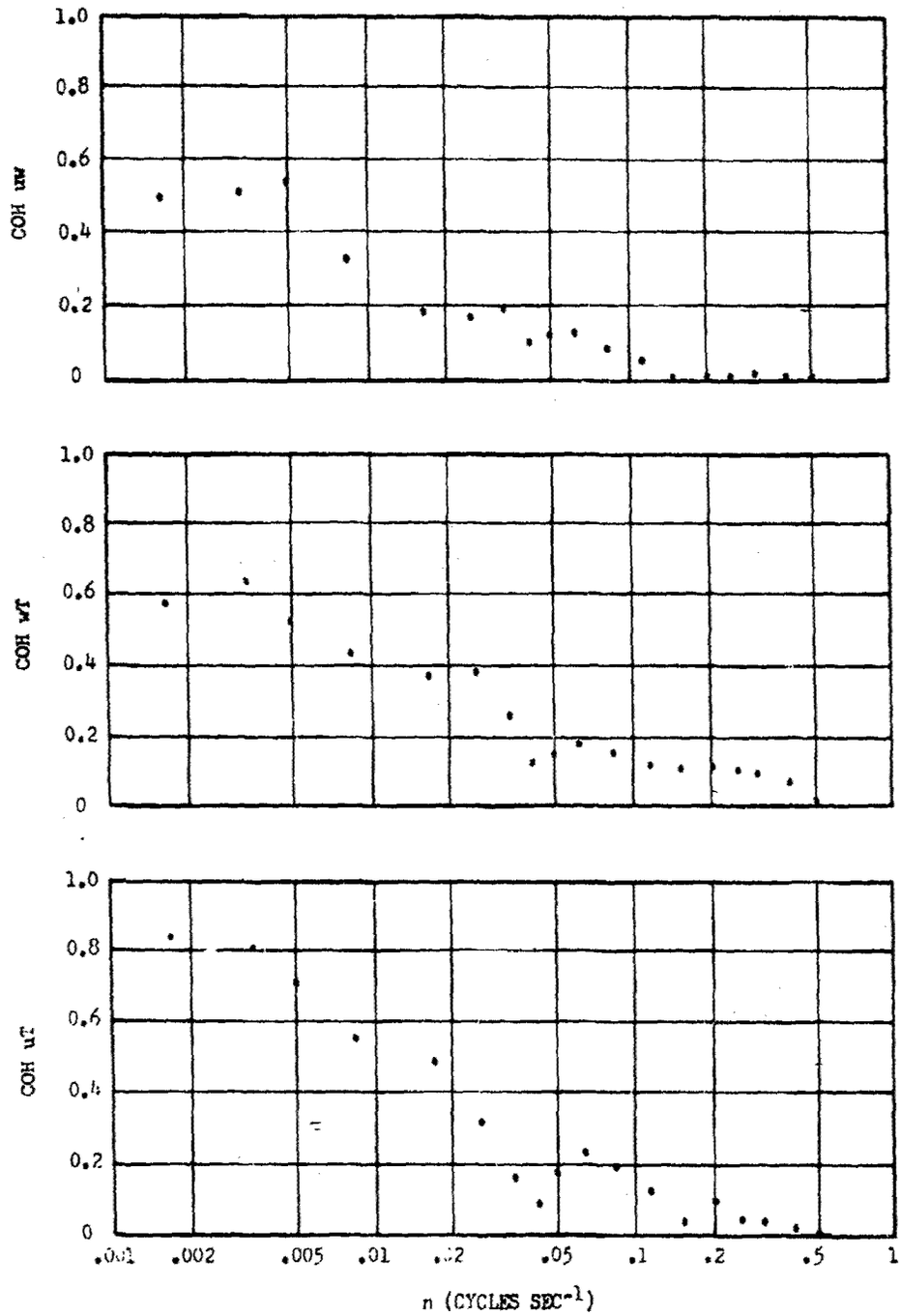

Fig. 10. Coherence diagrams at a height of 16 m for Run No. 7B.

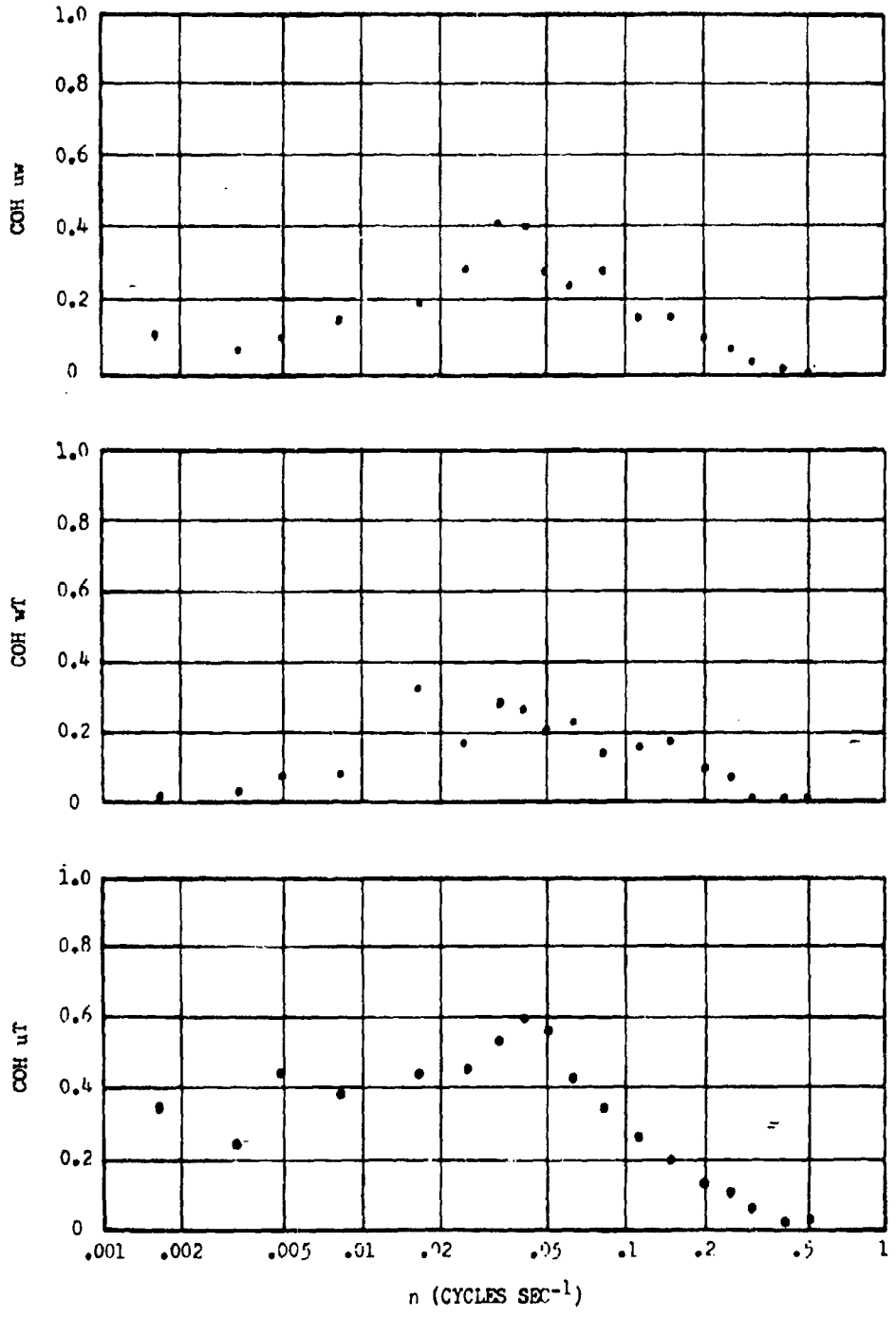

Fig. 11. Coherence diagrams at a height of 16 m for Run No. 8.

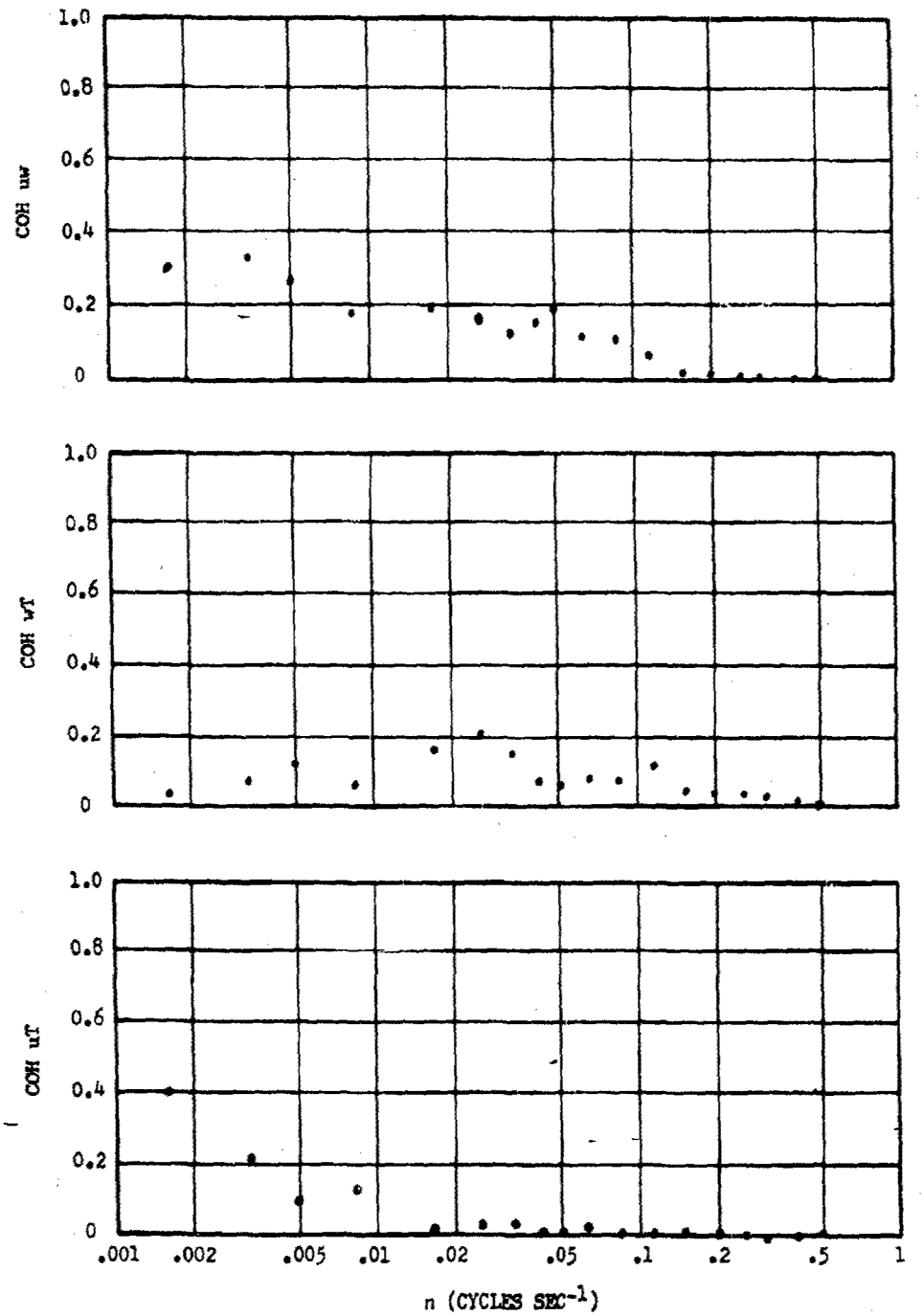

Fig. 12. Coherence diagrams at a height of 16 m for Run No. 9.

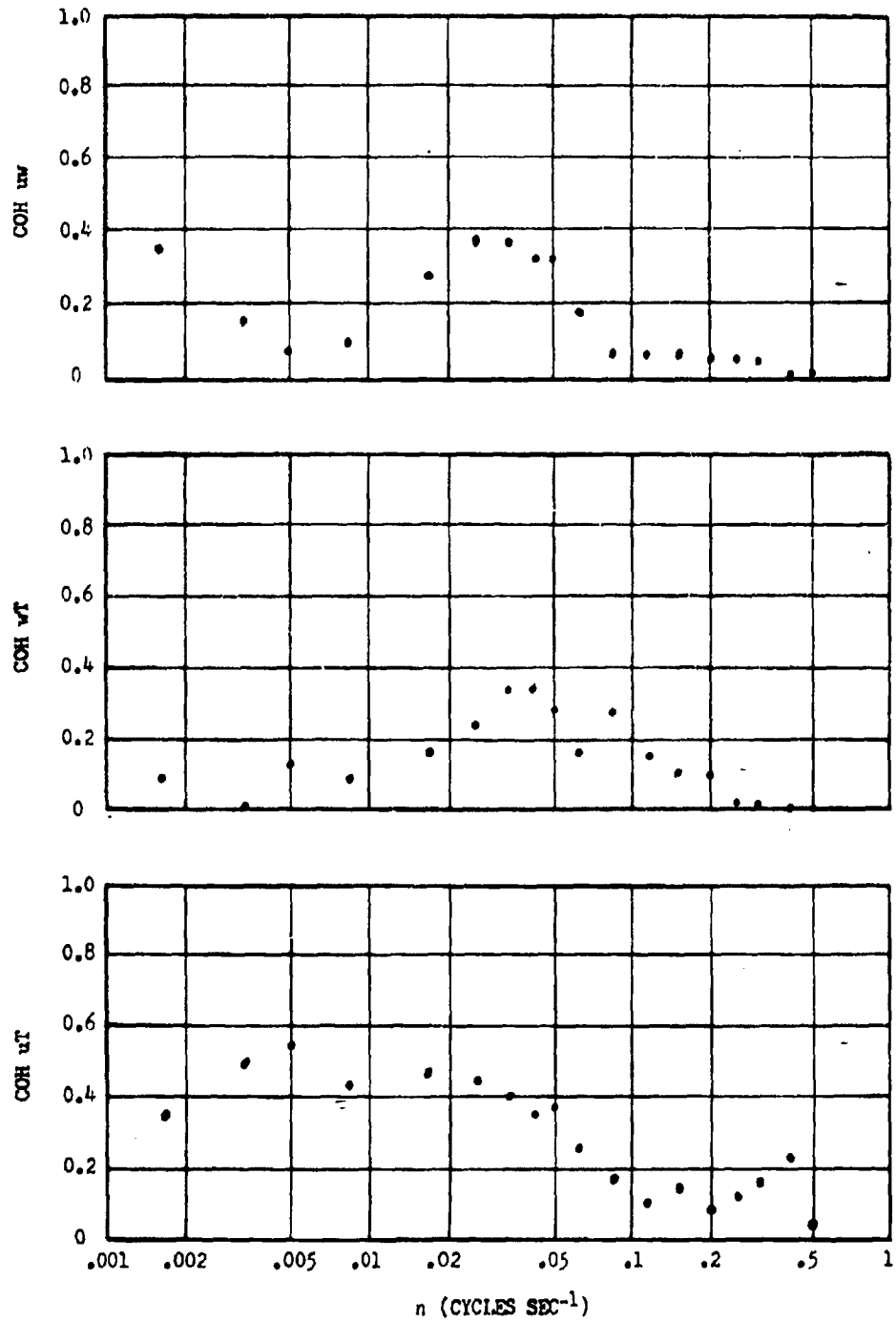

Fig. 13. Coherence diagrams at a height of 16 m for Run No. 10.

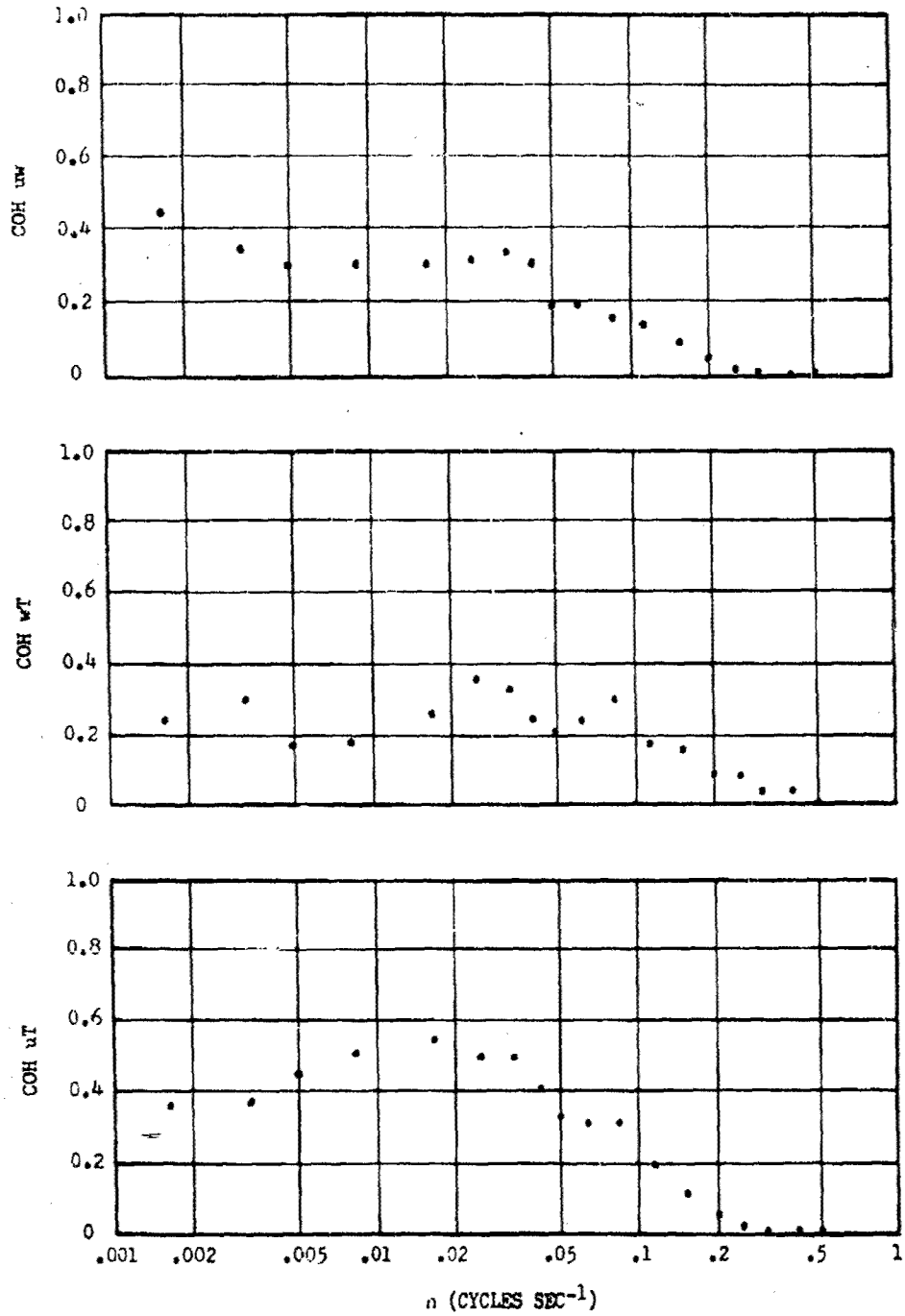

Fig. 14. Coherence diagrams at a height of 16 m for Run No. 12.

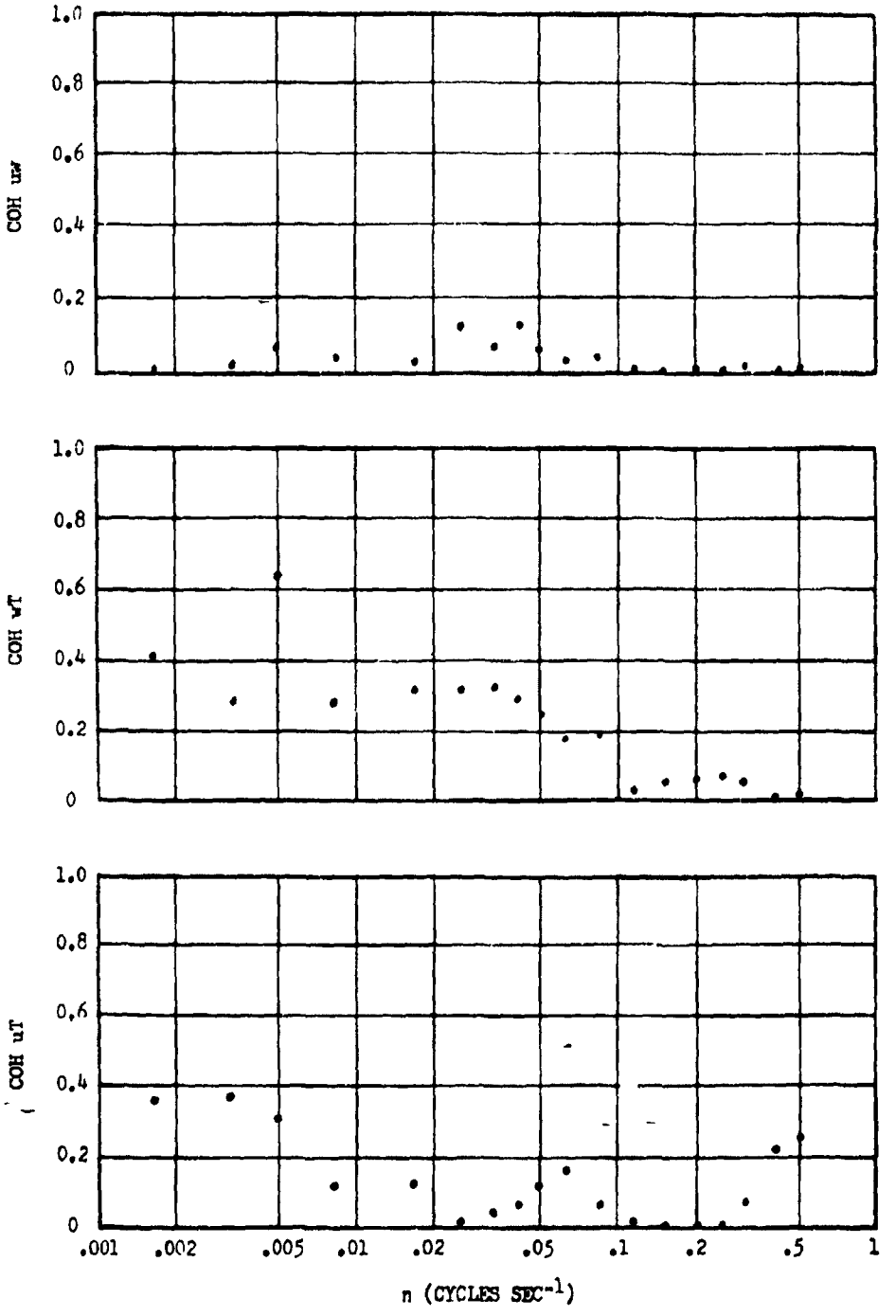

Fig. 15. Coherence diagrams at a height of 16 m for Run No. 14.

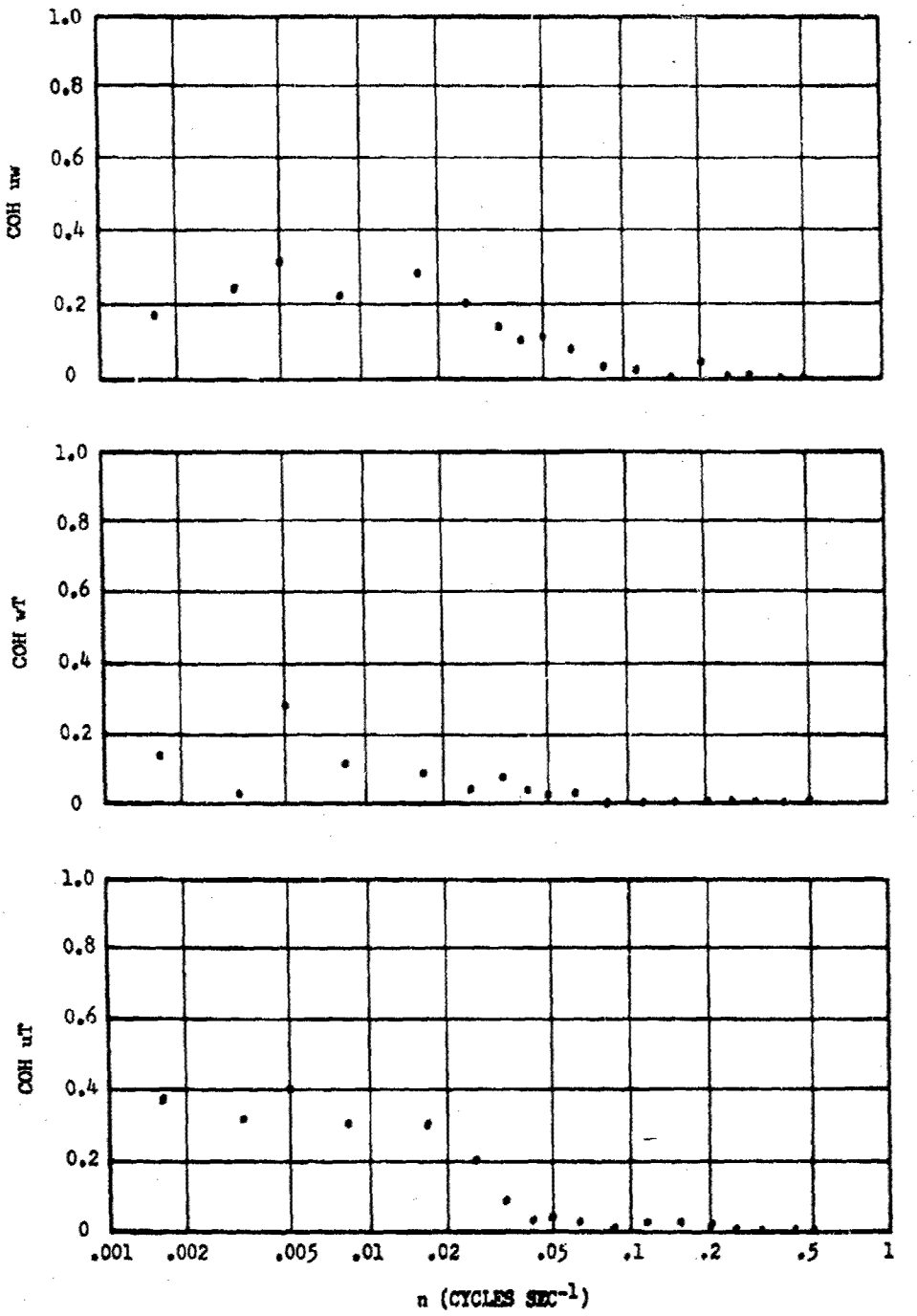

Fig. 16. Coherence diagrams at a height of 16 m for Run No. 15.

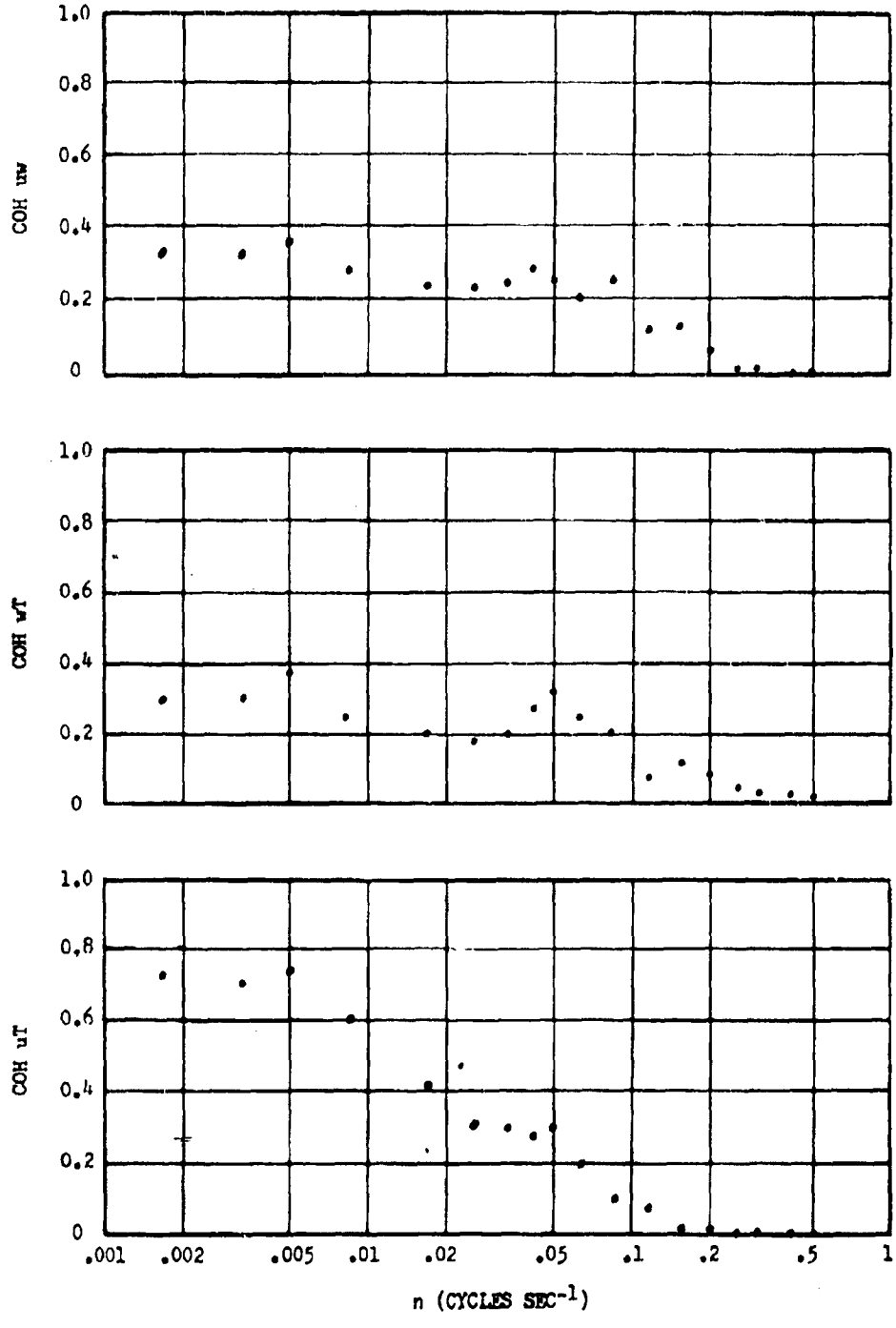

Fig. 17. Coherence diagrams at a height of 16 m for Run No. 16.

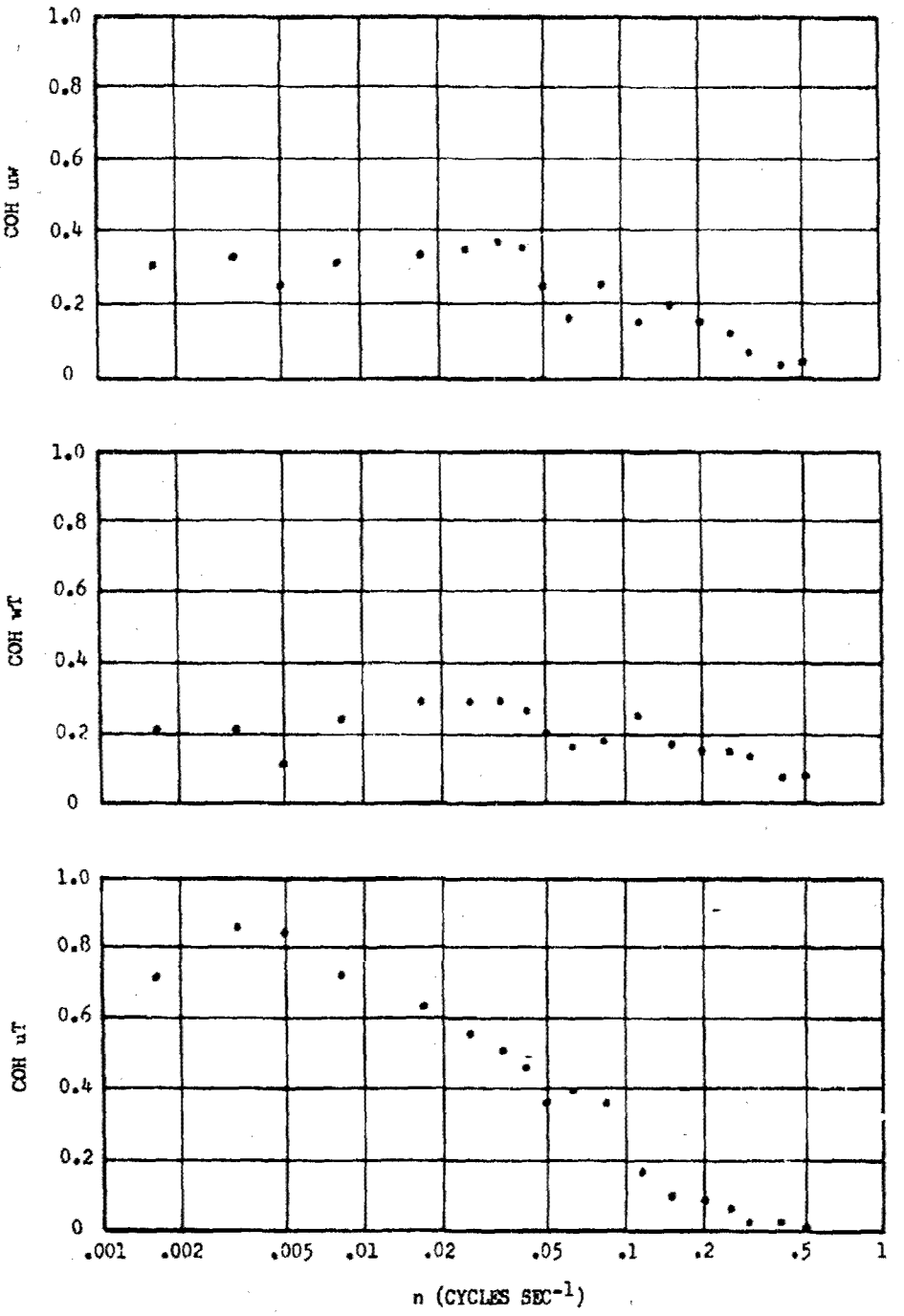

Fig. 18a. Coherence diagrams at a height of 16 m for Run No. 20.

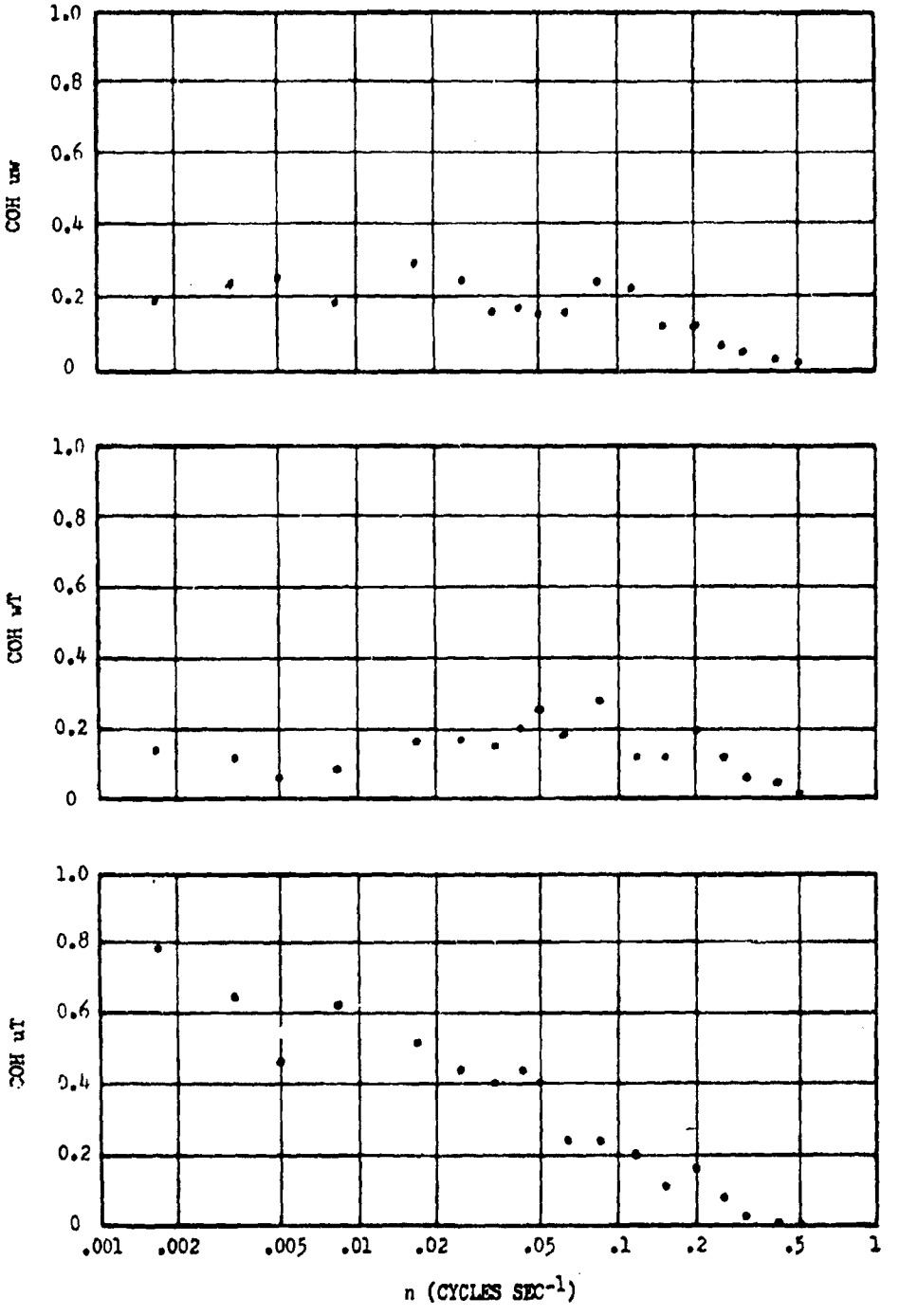

Fig. 18b. Coherence diagrams at a height of 40 m for Run No. 20.

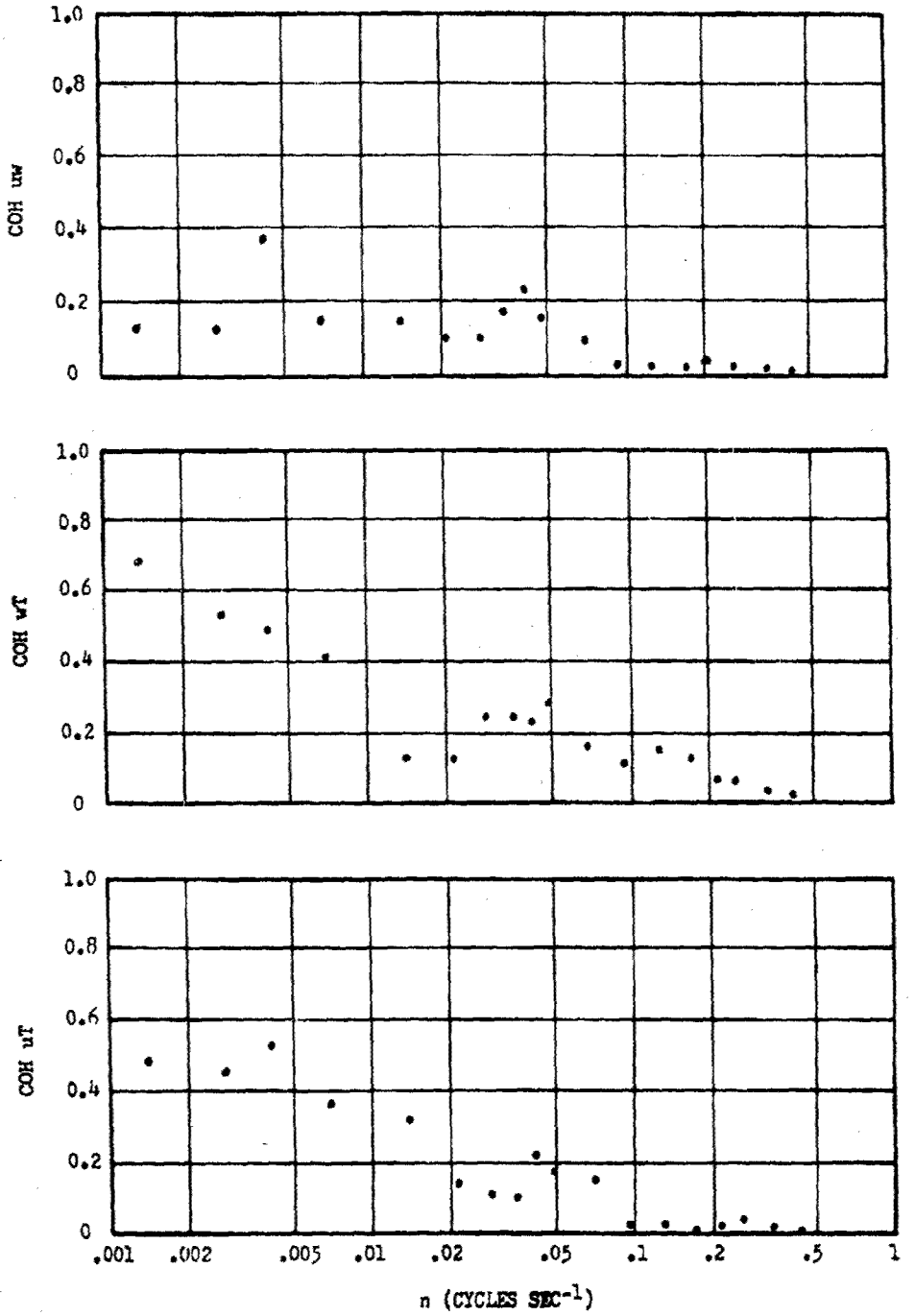

Fig. 19a. Coherence diagrams at a height of 16 m for Run No. 38.

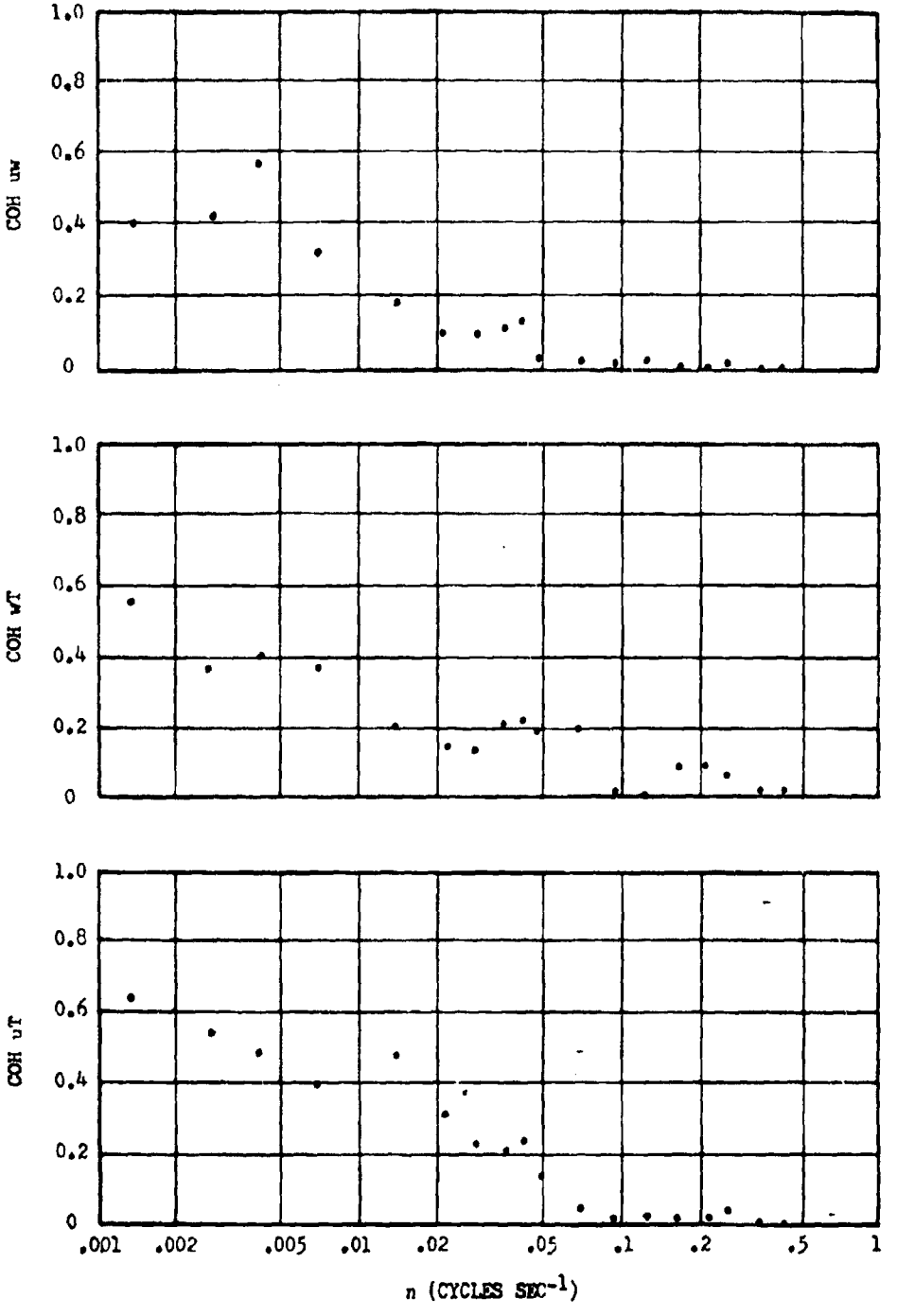

Fig. 19b. Coherence diagrams at a height of 40 m for Run No. 38.

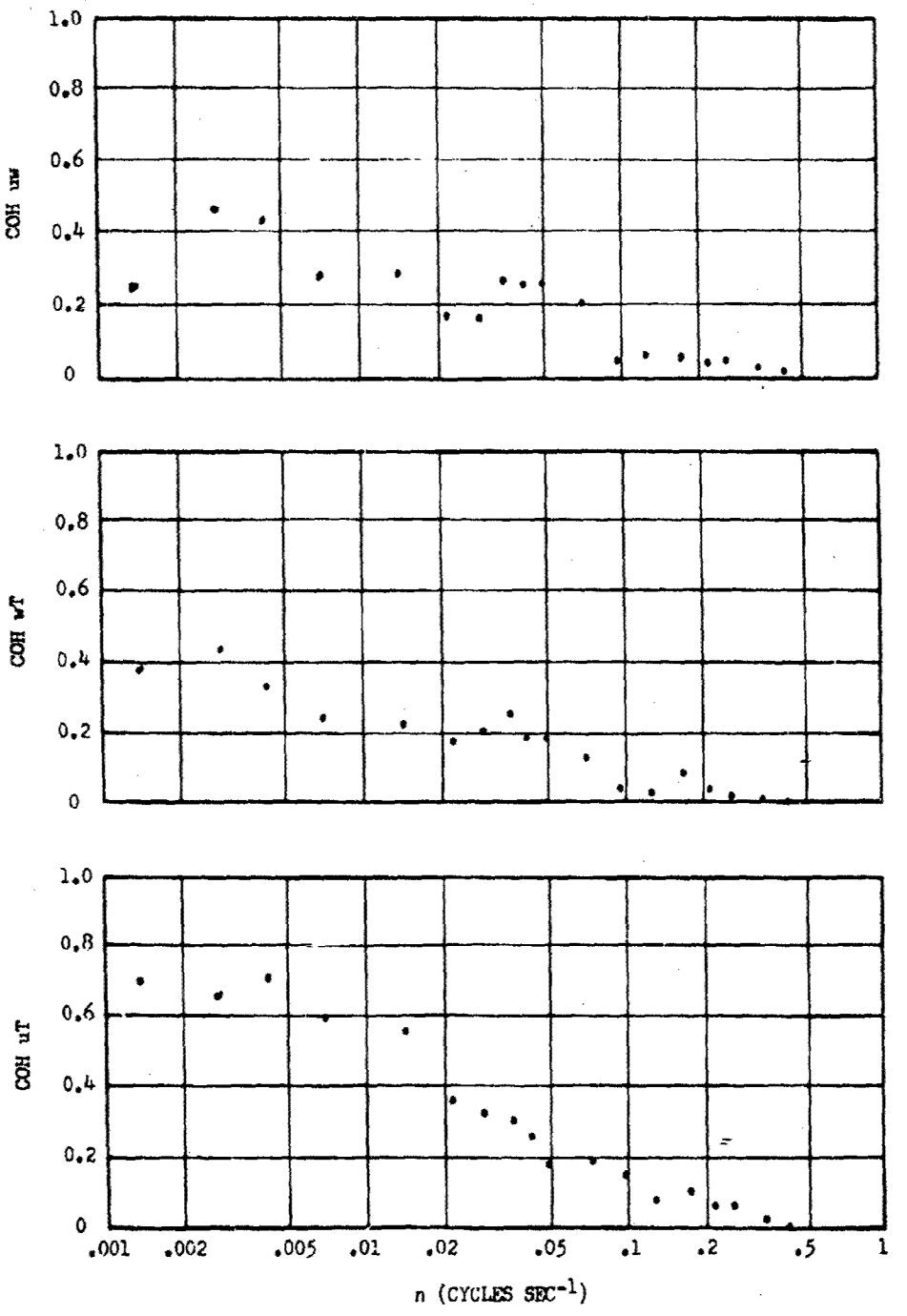

Fig. 20a. Coherence diagrams at a height of 16 m for Run No. 39.

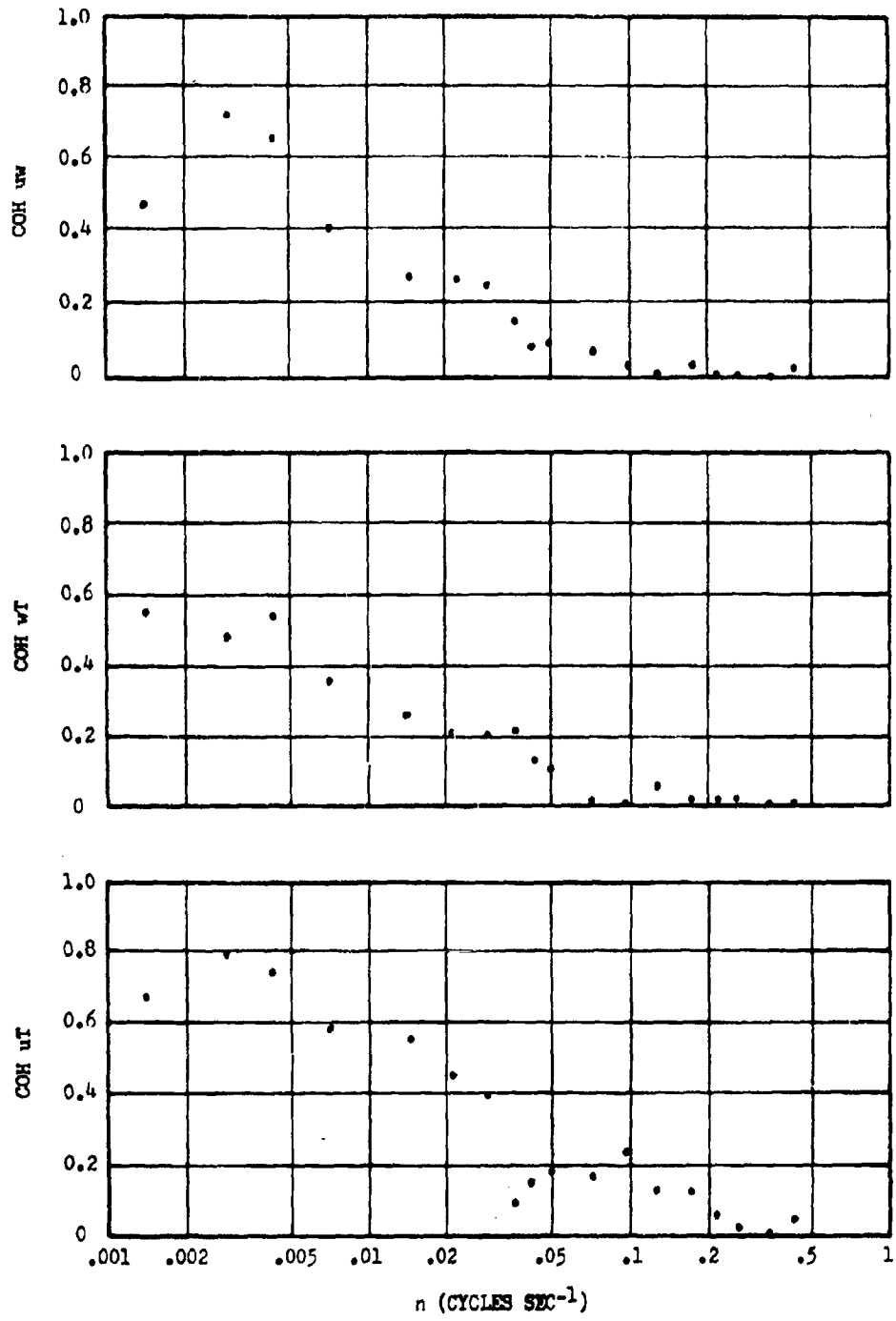

Fig. 20b. Coherence diagrams at a height of 40 m for Run No. 39.

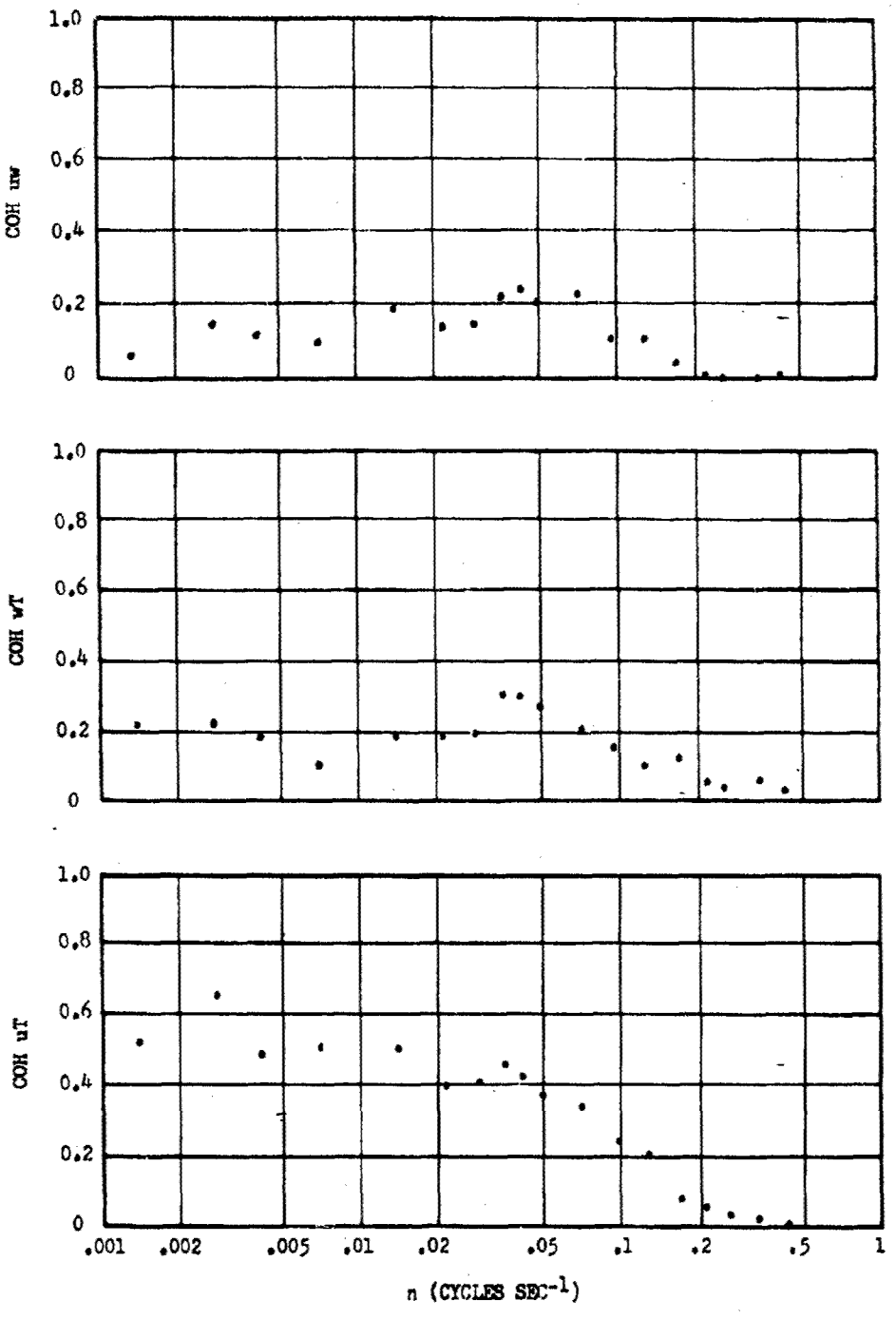

Fig. 21a. Coherence diagrams at a height of 16 m for Run No. 40.

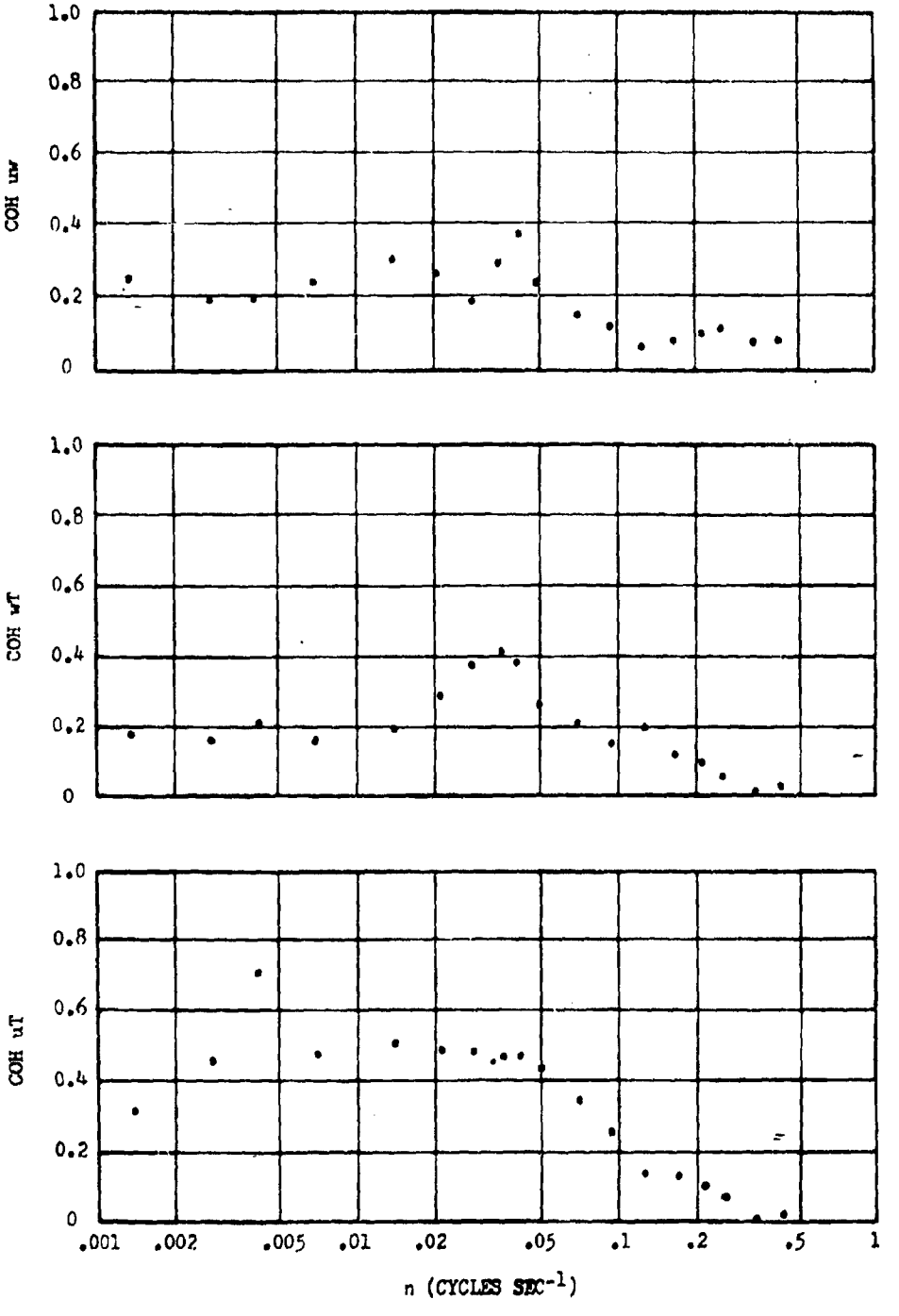

Fig. 21b. Coherence diagrams at a height of 40 m for Run No. 40.

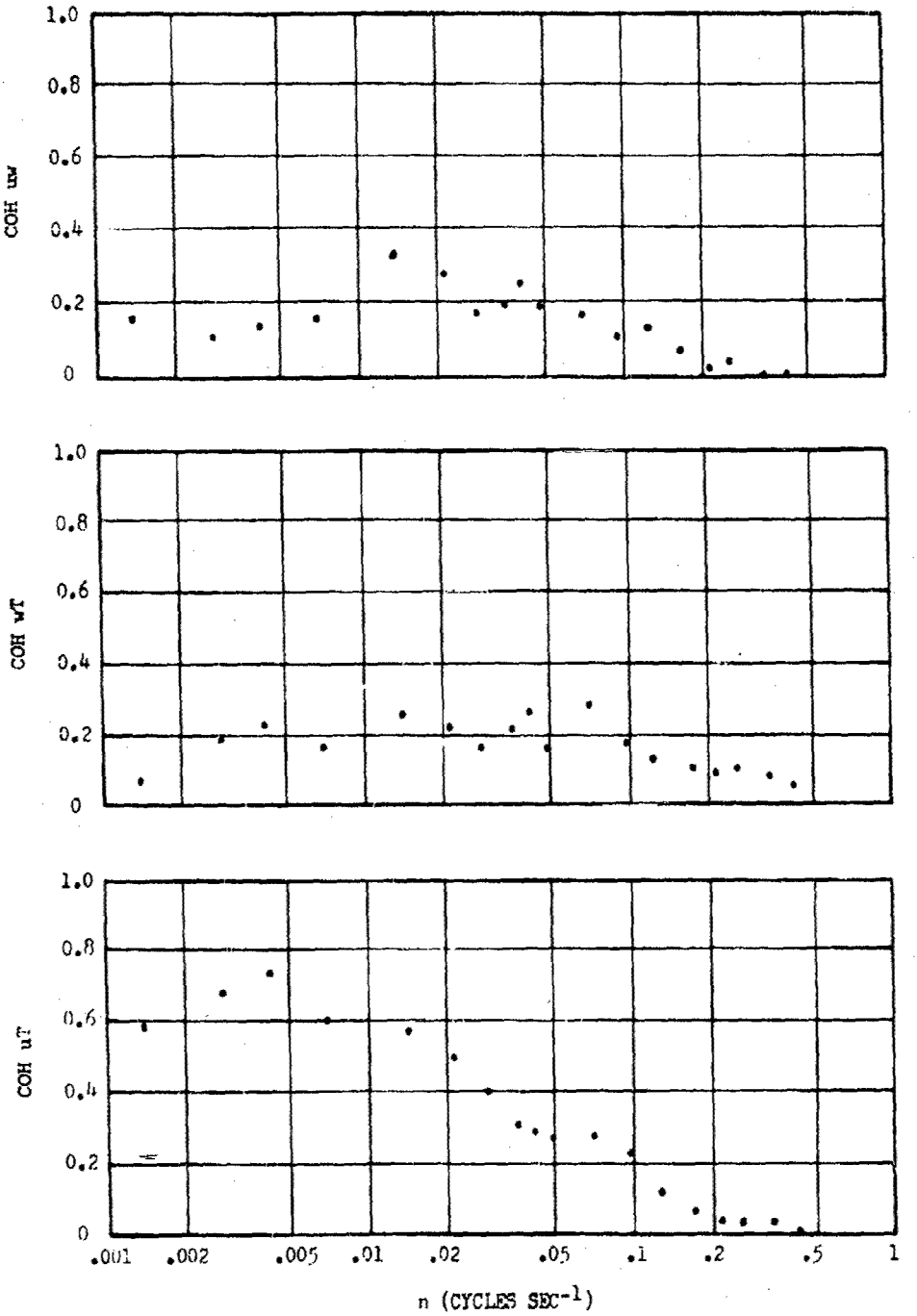

Fig. 22a. Coherence diagrams at a height of 16 m for Run No. 41.

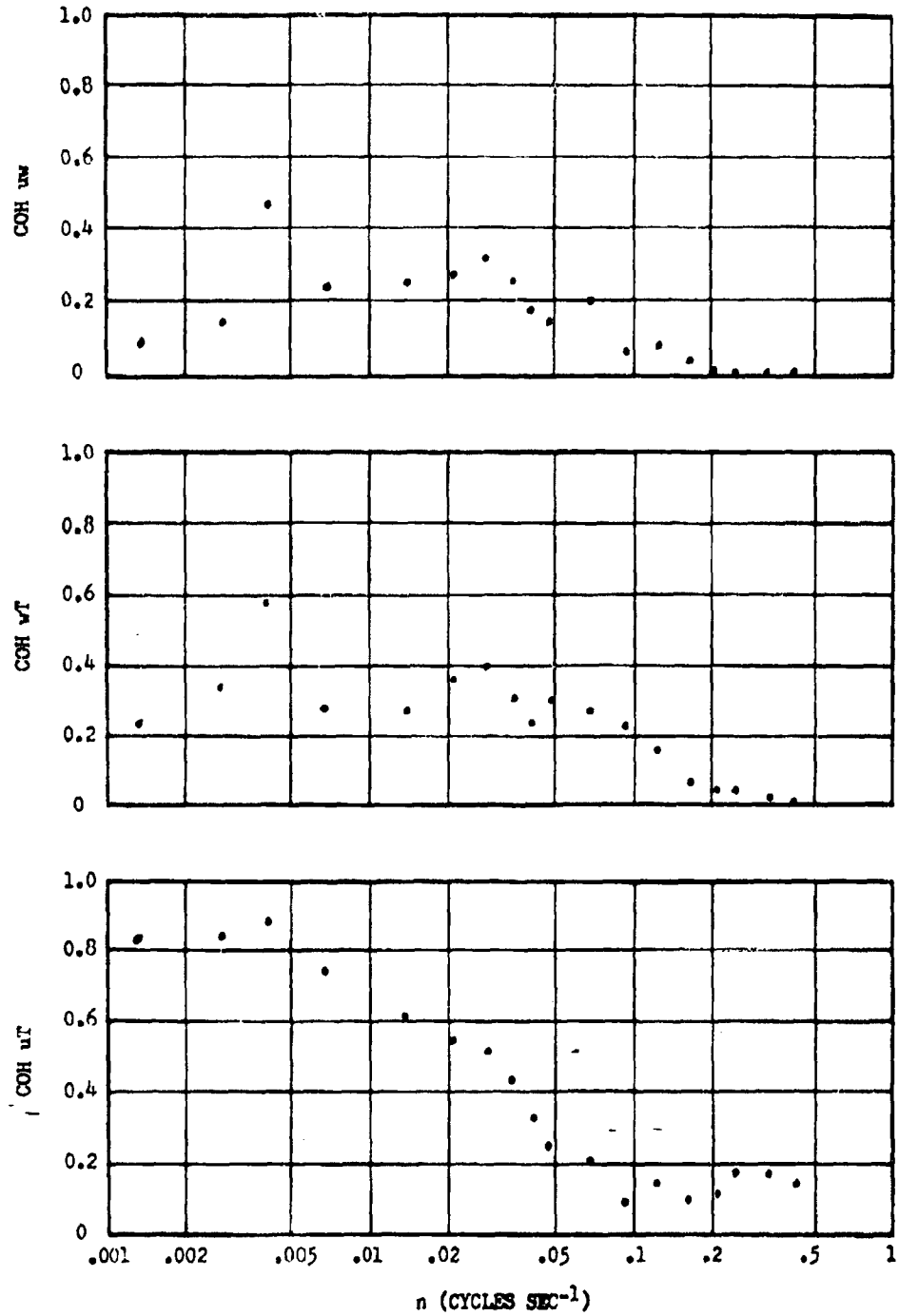

Fig. 22b. Coherence diagrams at a height of 40 m for Run No. 41.

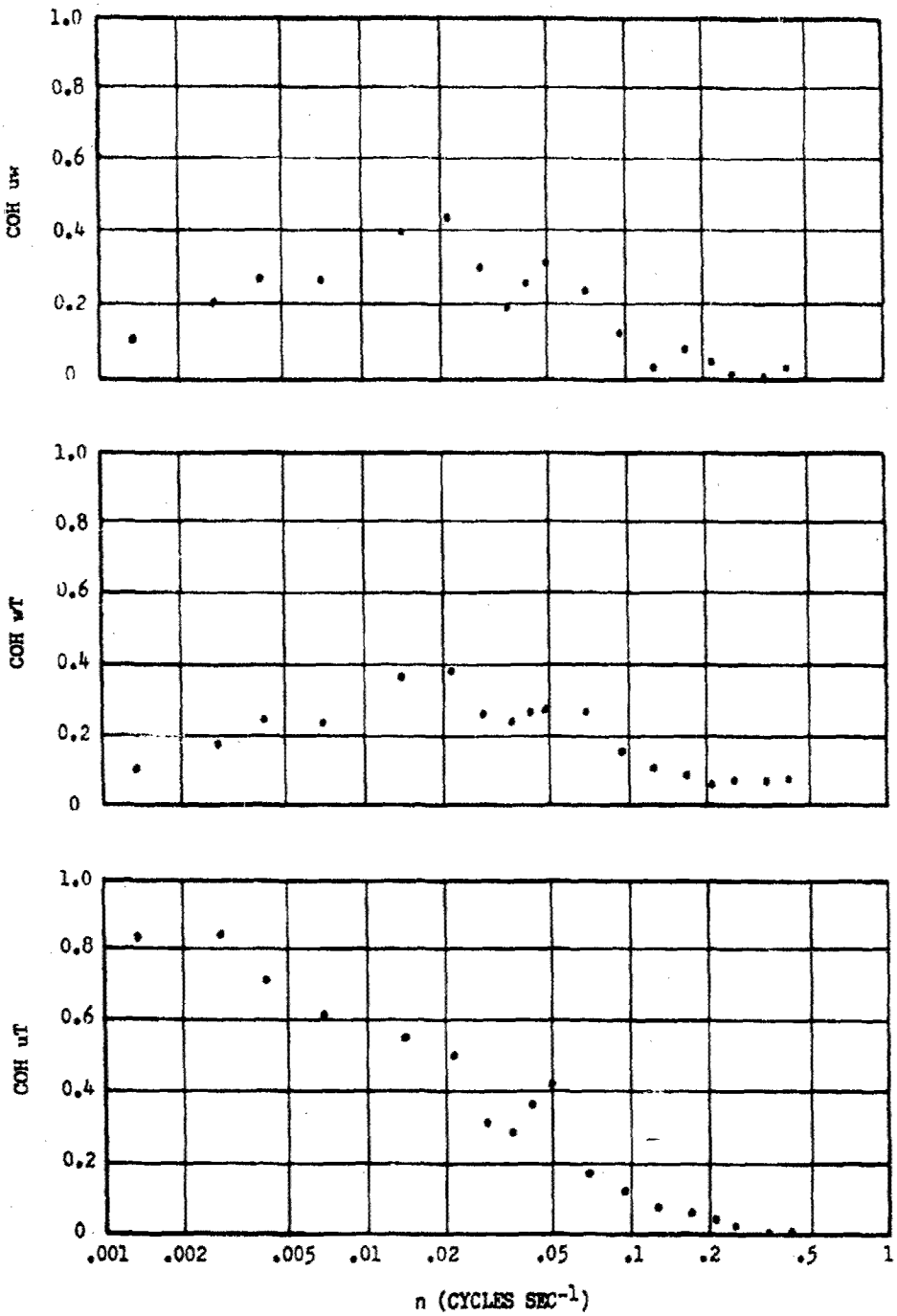

Fig. 23a. Coherence diagrams at a height of 16 m for Run No. 42.

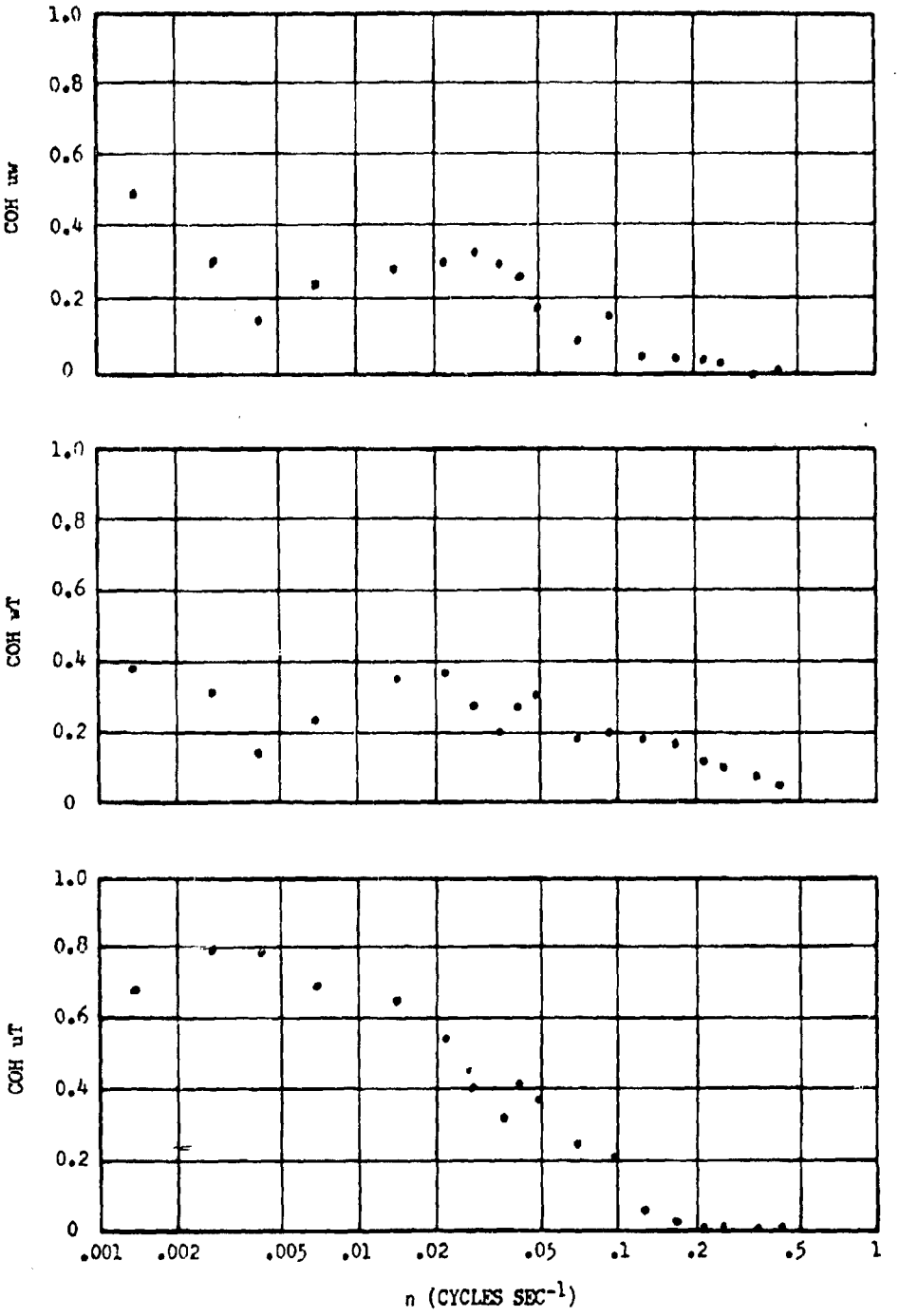

Fig. 23b. Coherence diagrams at a height of 40 m for Run No. 42.

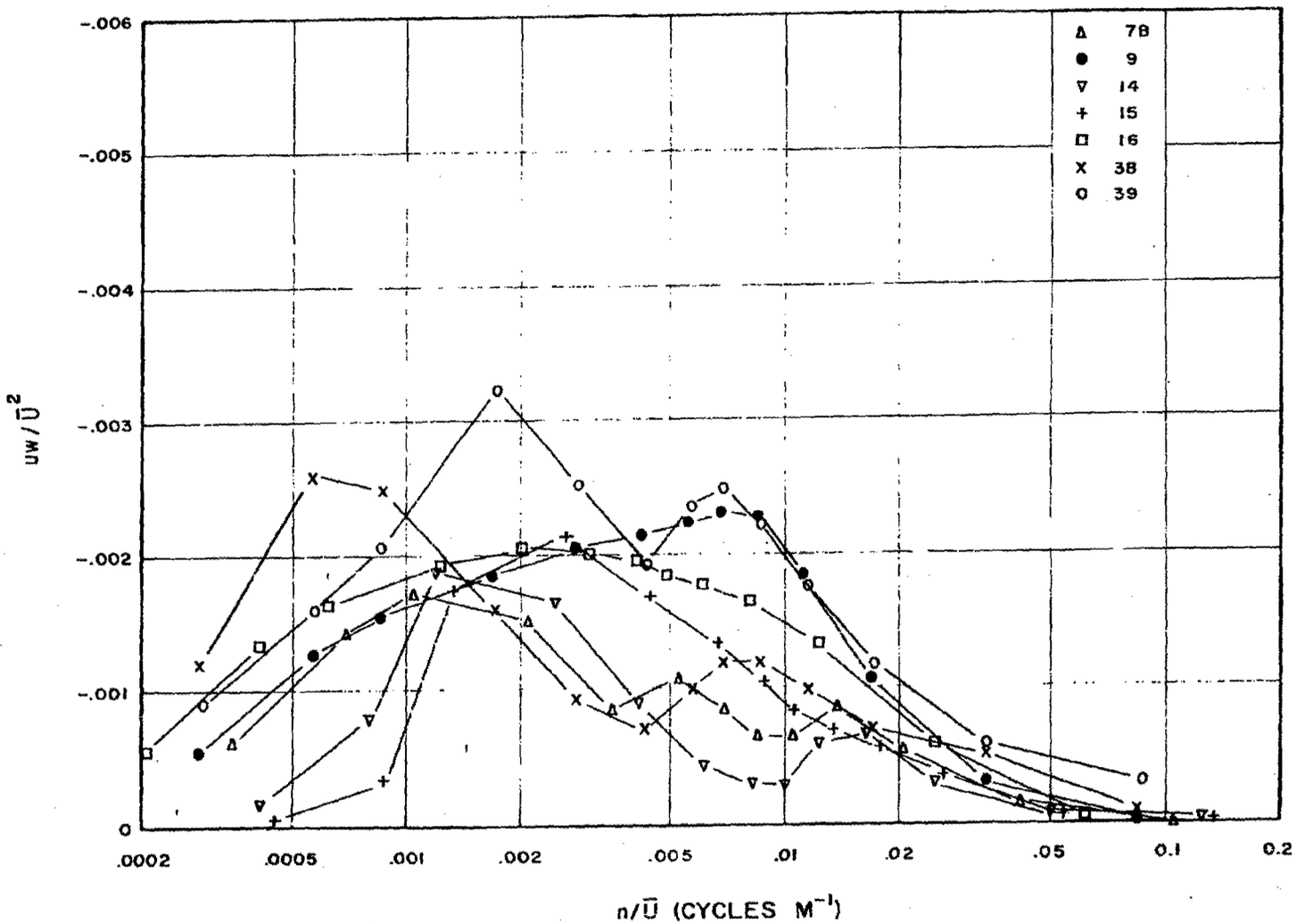

Fig. 24a. Logarithmic cospectra of the vertical flux of momentum at a height of 16 m for the daytime experiments.

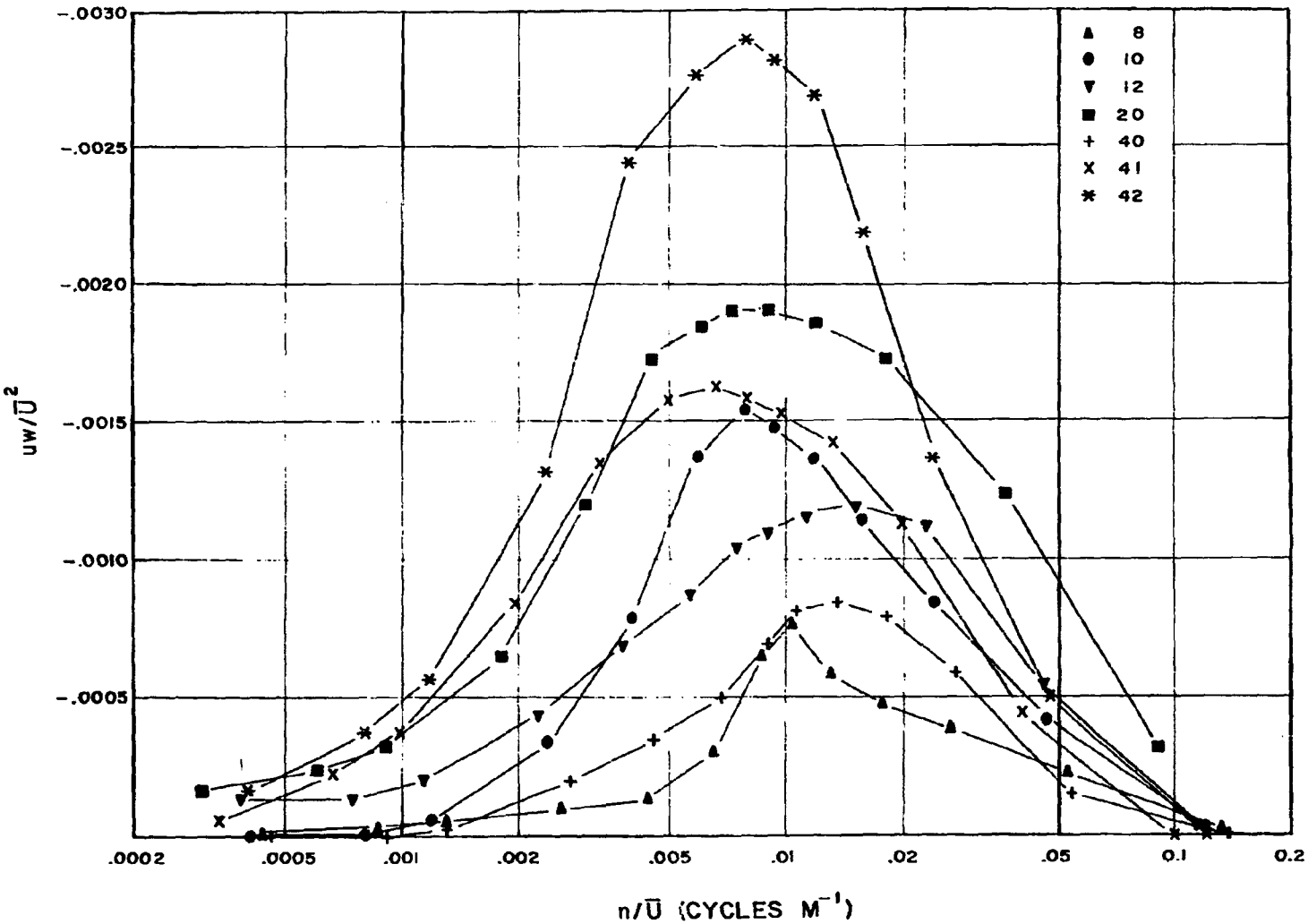

Fig. 24b. Logarithmic cospectra of the vertical flux of momentum at a height of 16 m for the nighttime experiments.

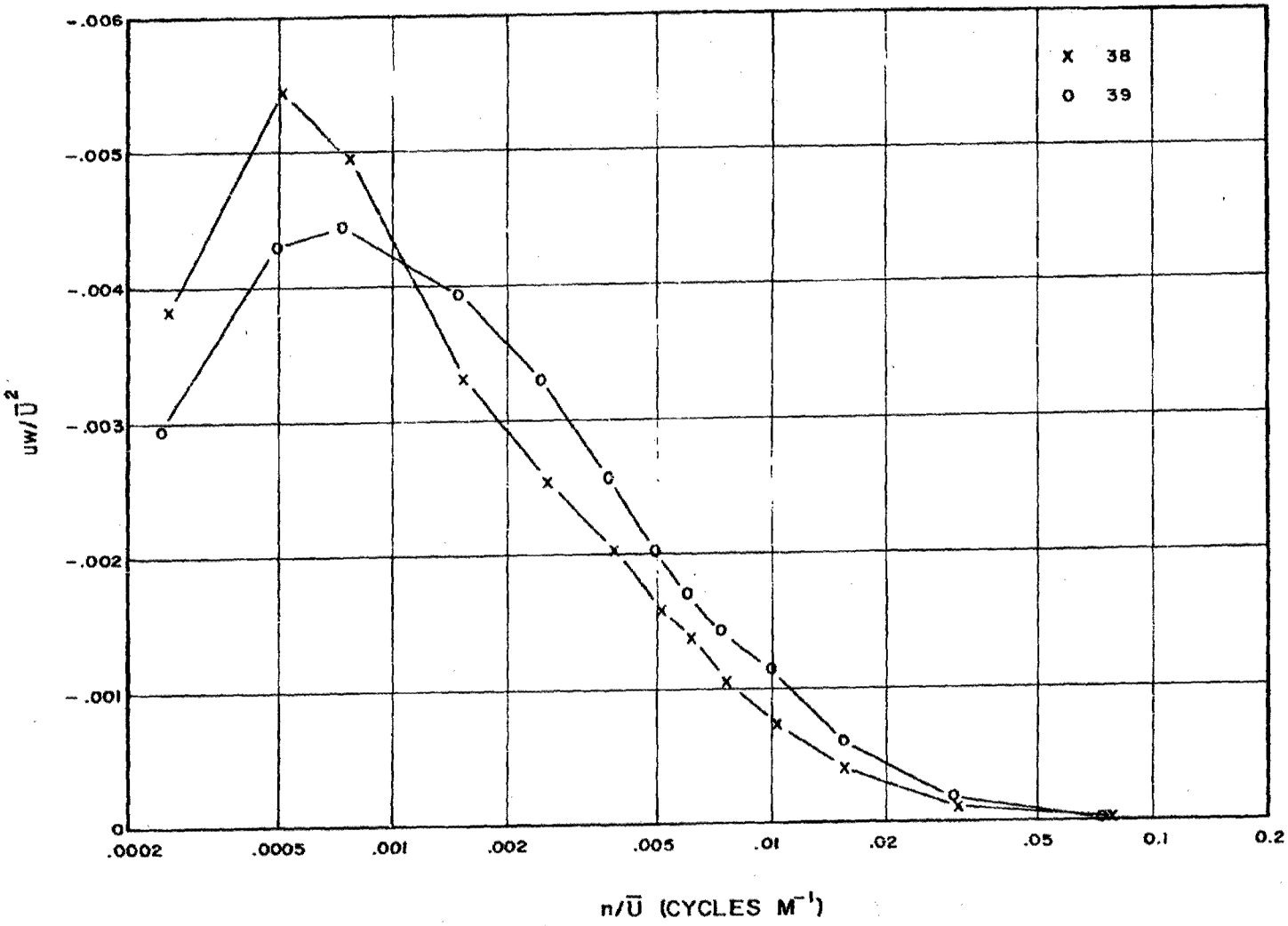

Fig. 24c. Logarithmic cospectra of the vertical flux of momentum at a height of 40 m for the daytime experiments.

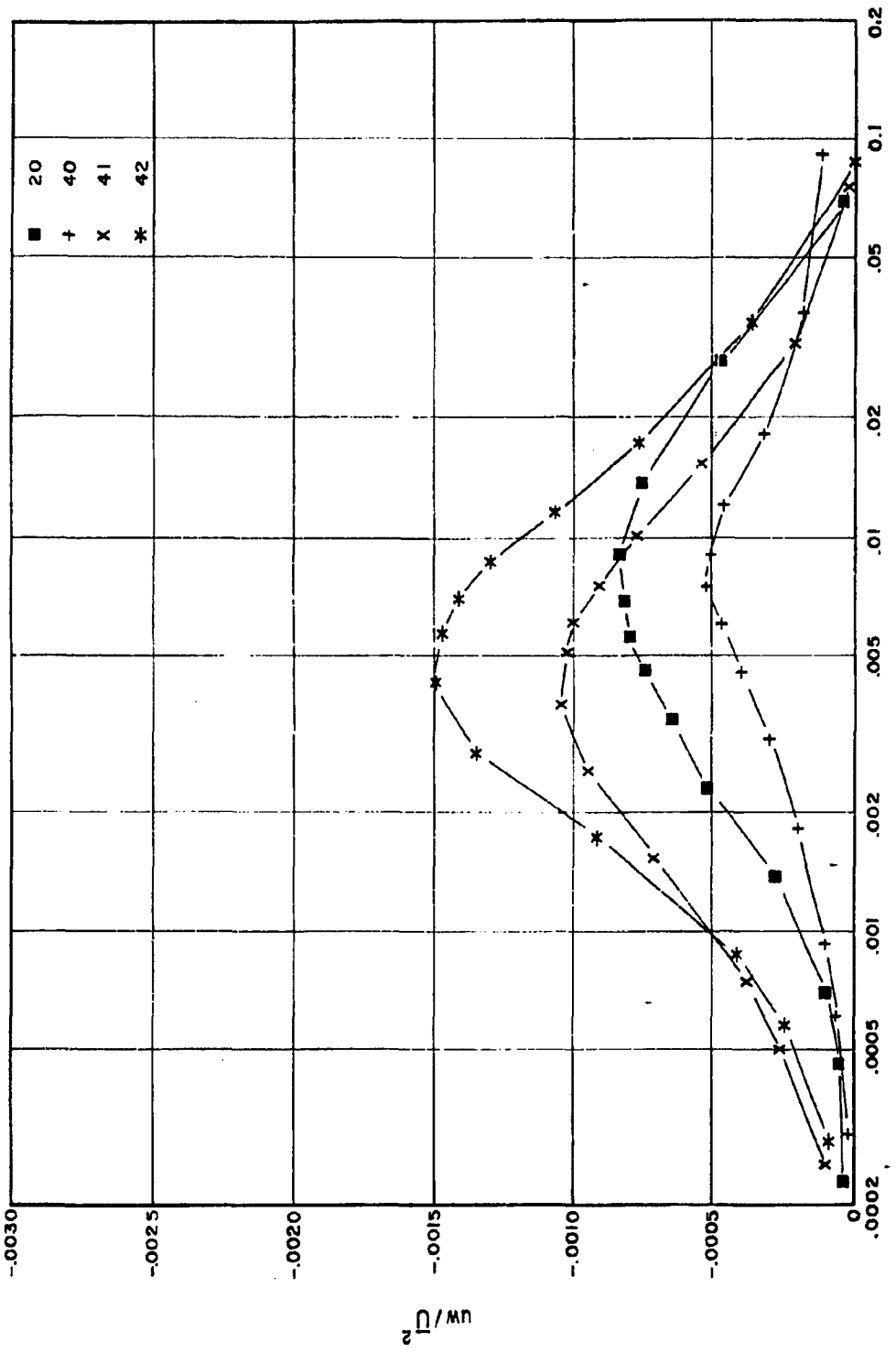

Fig. 24d. Logarithmic cospectra of the vertical flux of momentum at a height of 40 m for the nighttime experiments.

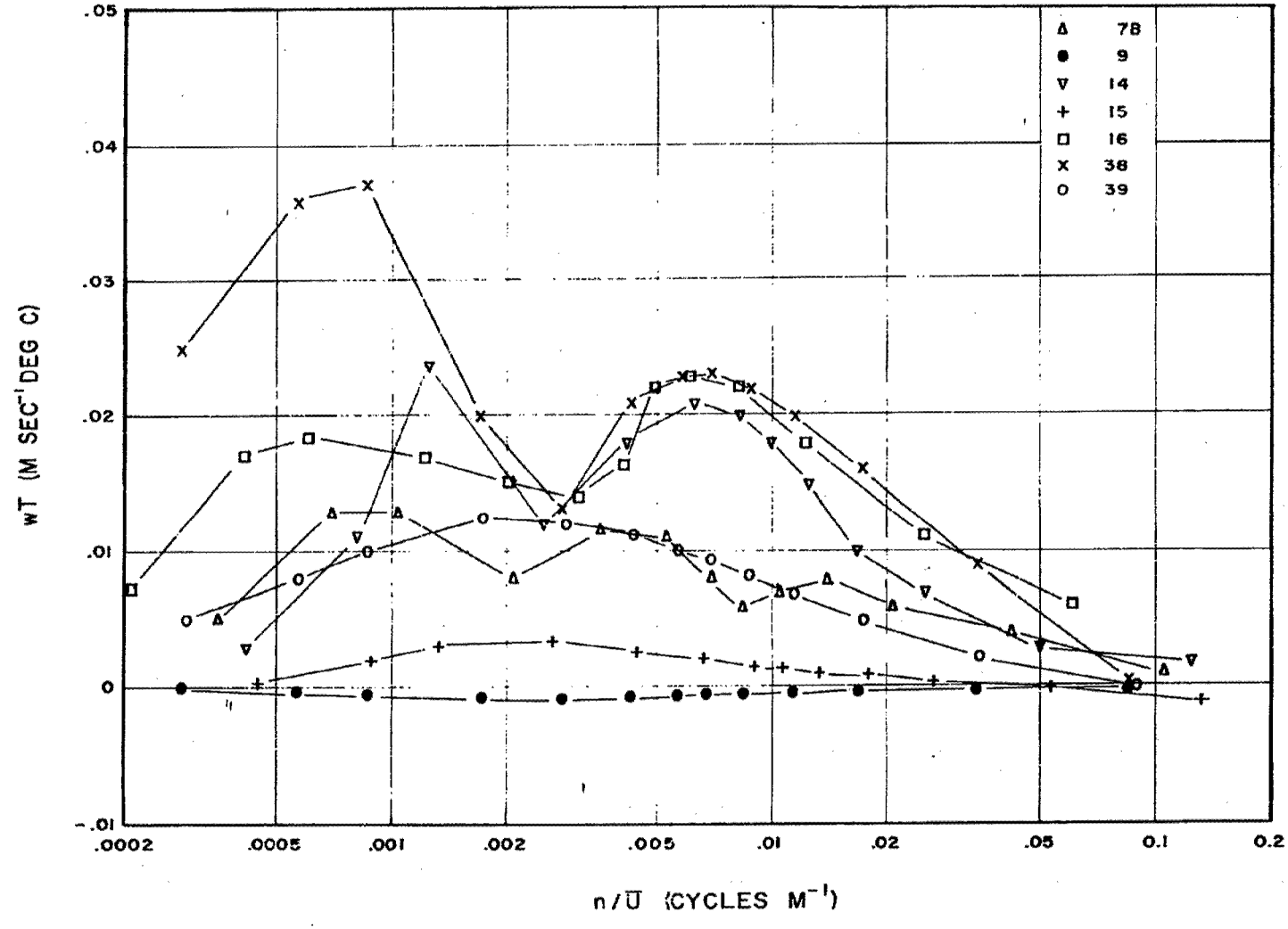

Fig. 25a. Logarithmic cospectra of the vertical flux of temperature at a height of 16 m for the daytime experiments.

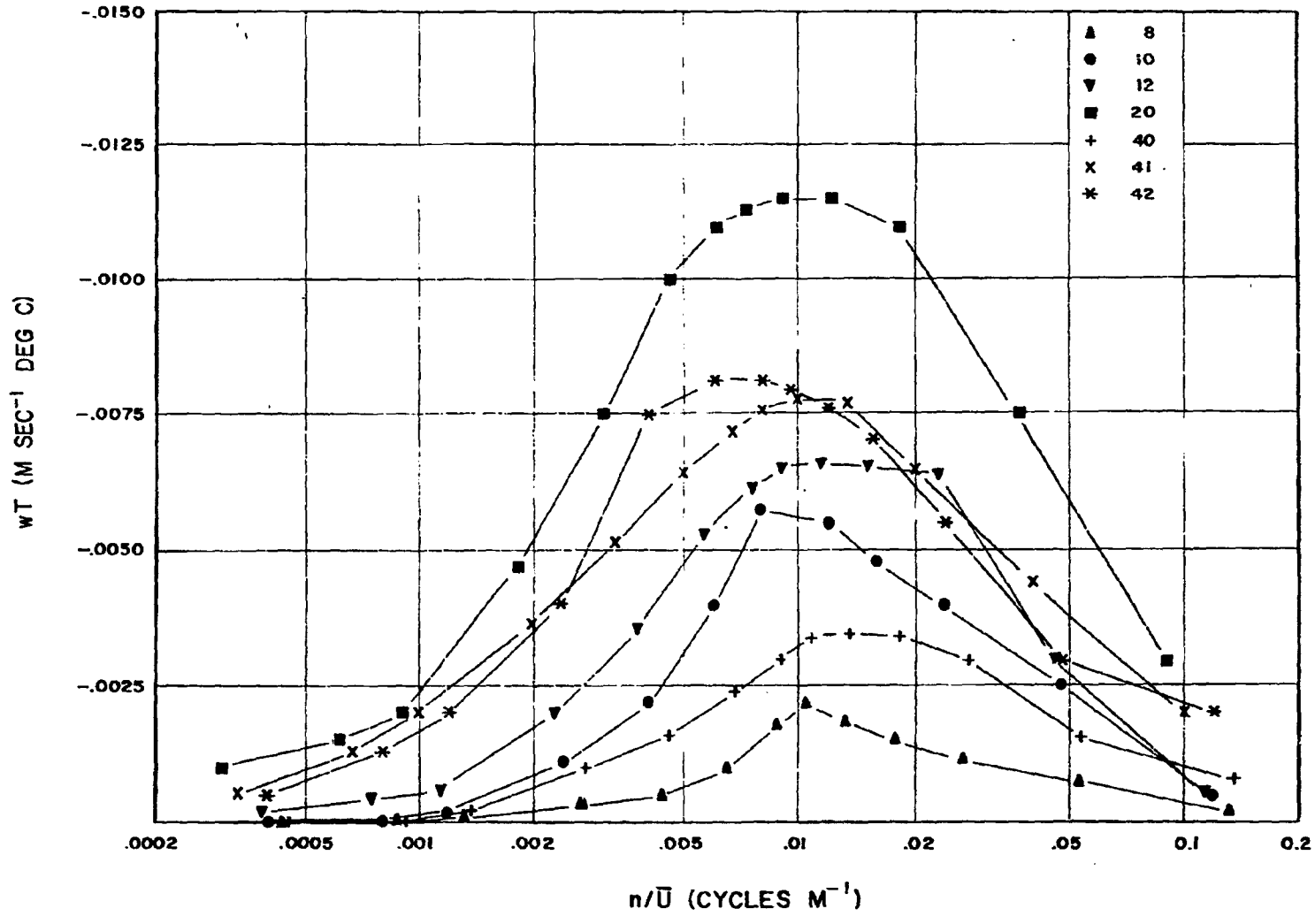

Fig. 25b. Logarithmic cospectra of the vertical flux of temperature at a height of 16 m for the nighttime experiments.

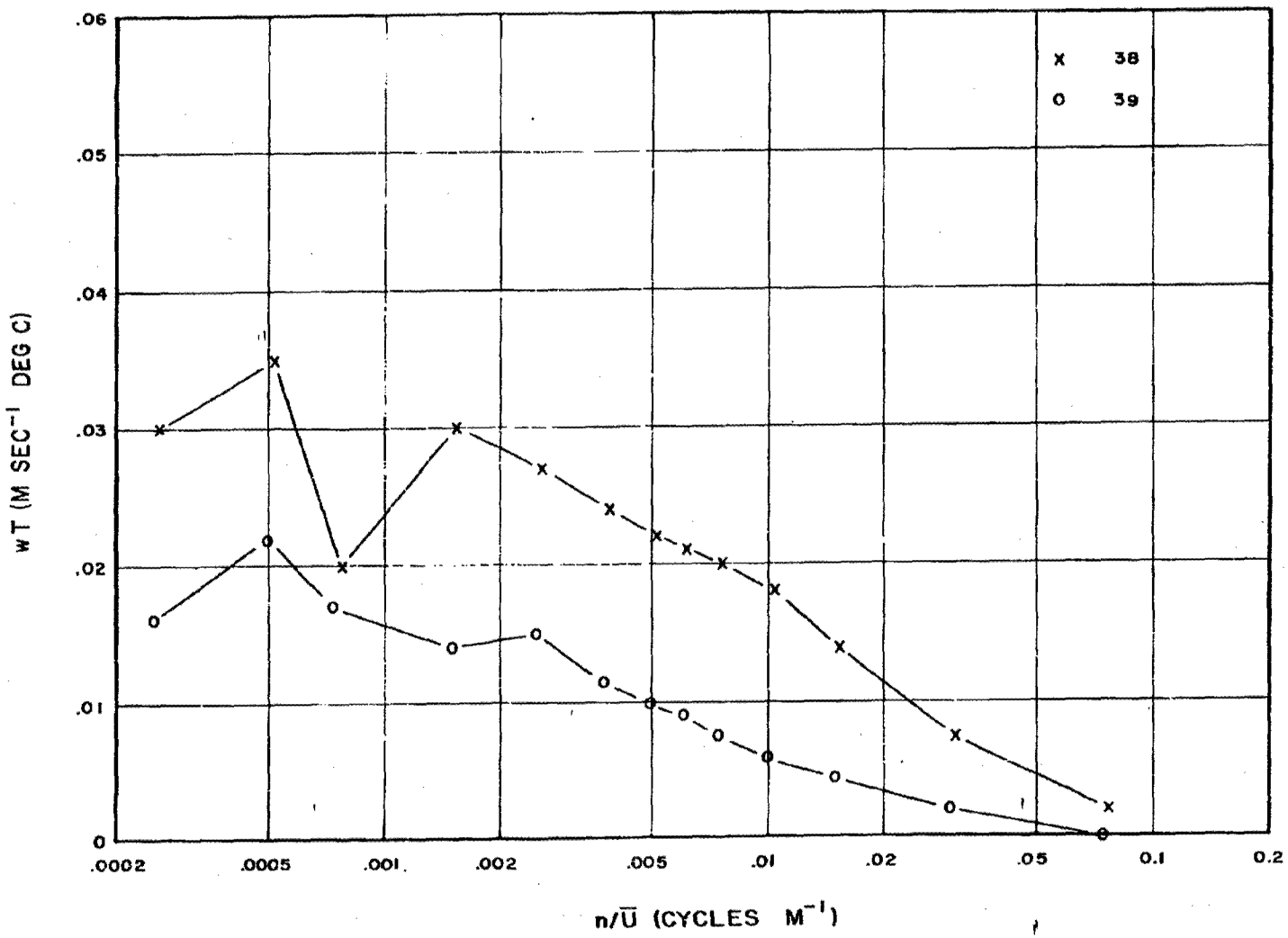

Fig. 25c. Logarithmic cospectra of the vertical flux of temperature at a height of 40 m for the daytime experiments.

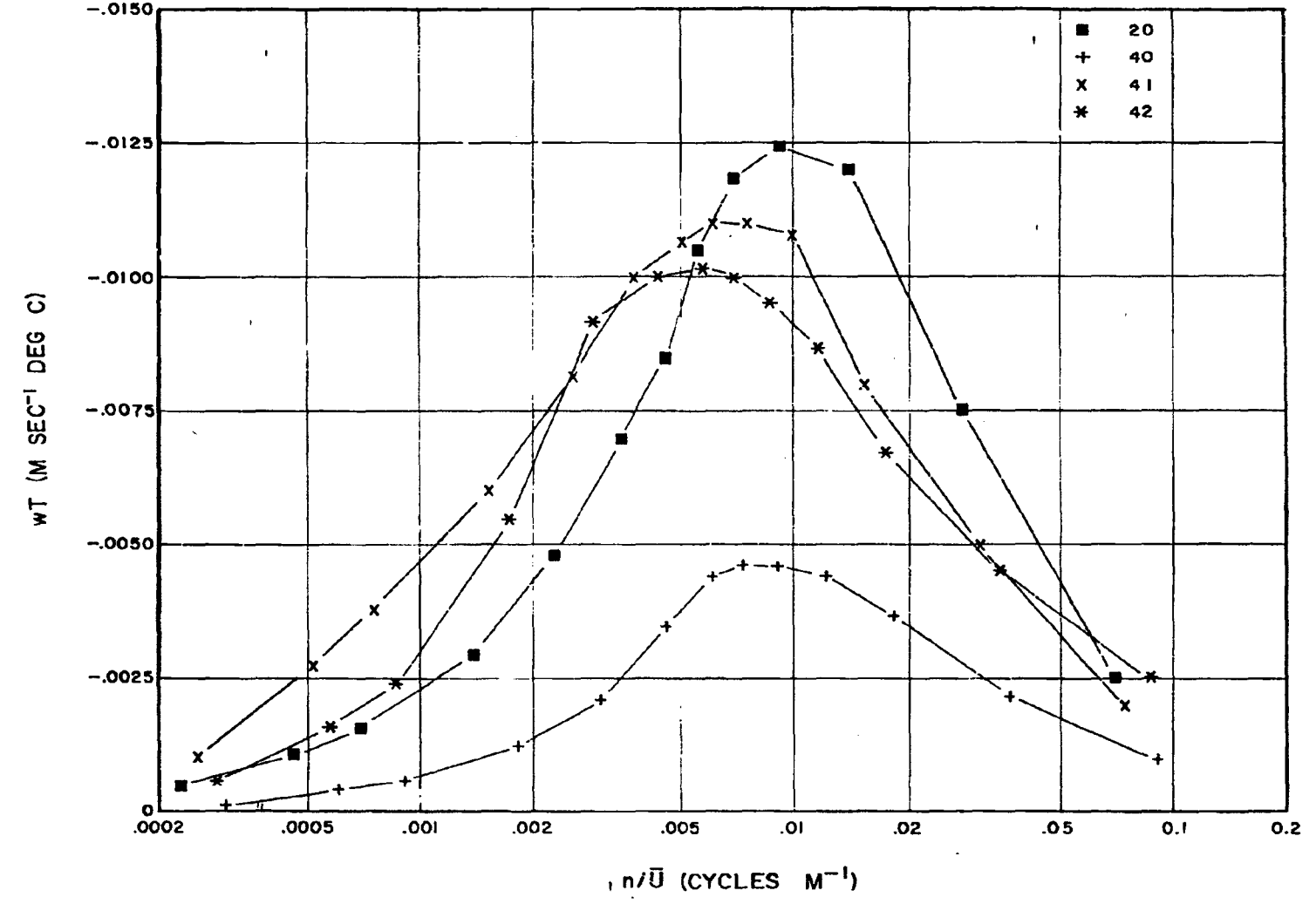

Fig. 25d. Logarithmic cospectra of the vertical flux of temperature at a height of 40 m for the nighttime experiments.

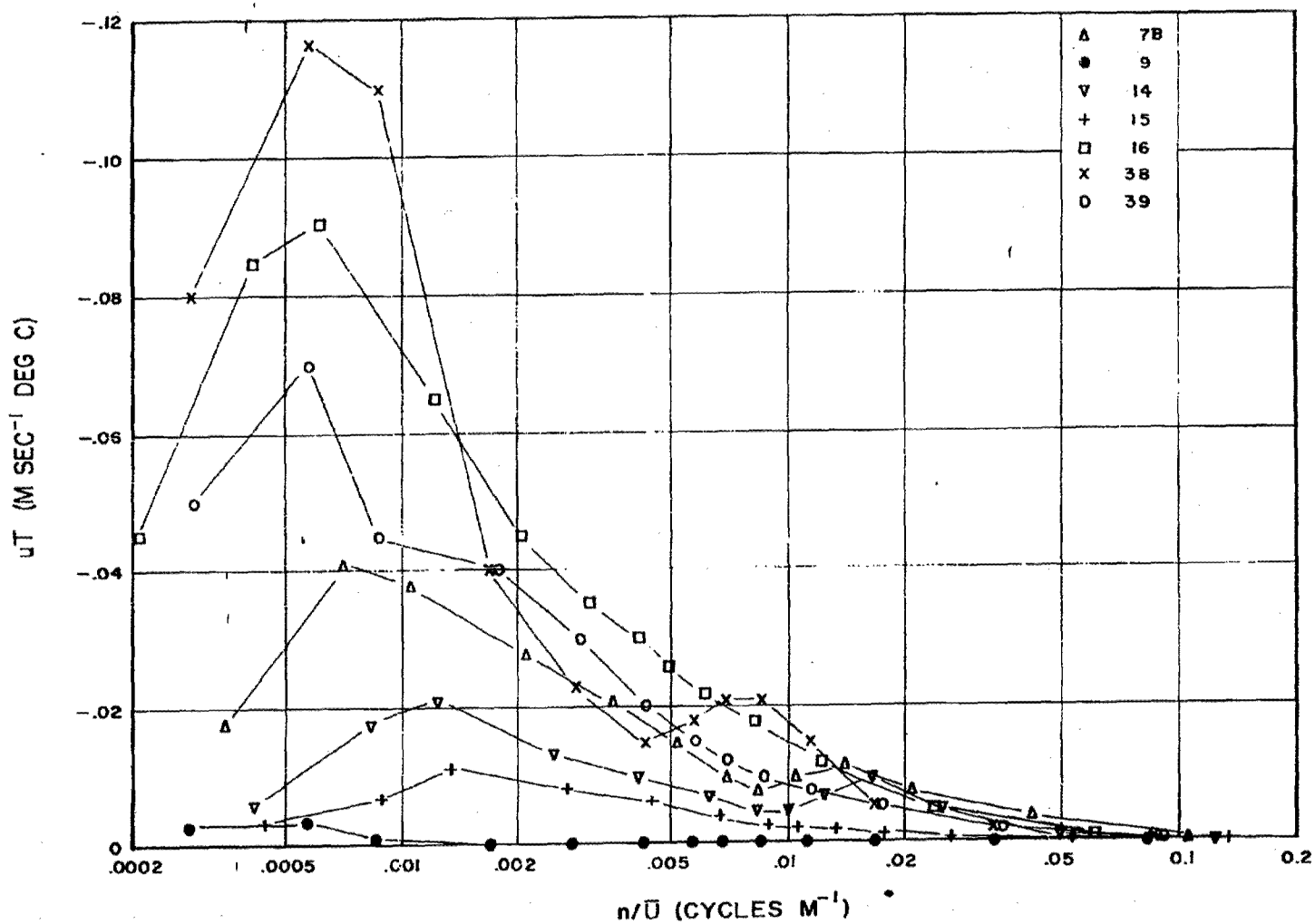

Fig. 26a. Logarithmic cospectra of the horizontal flux of temperature at a height of 16 m for the daytime experiments.

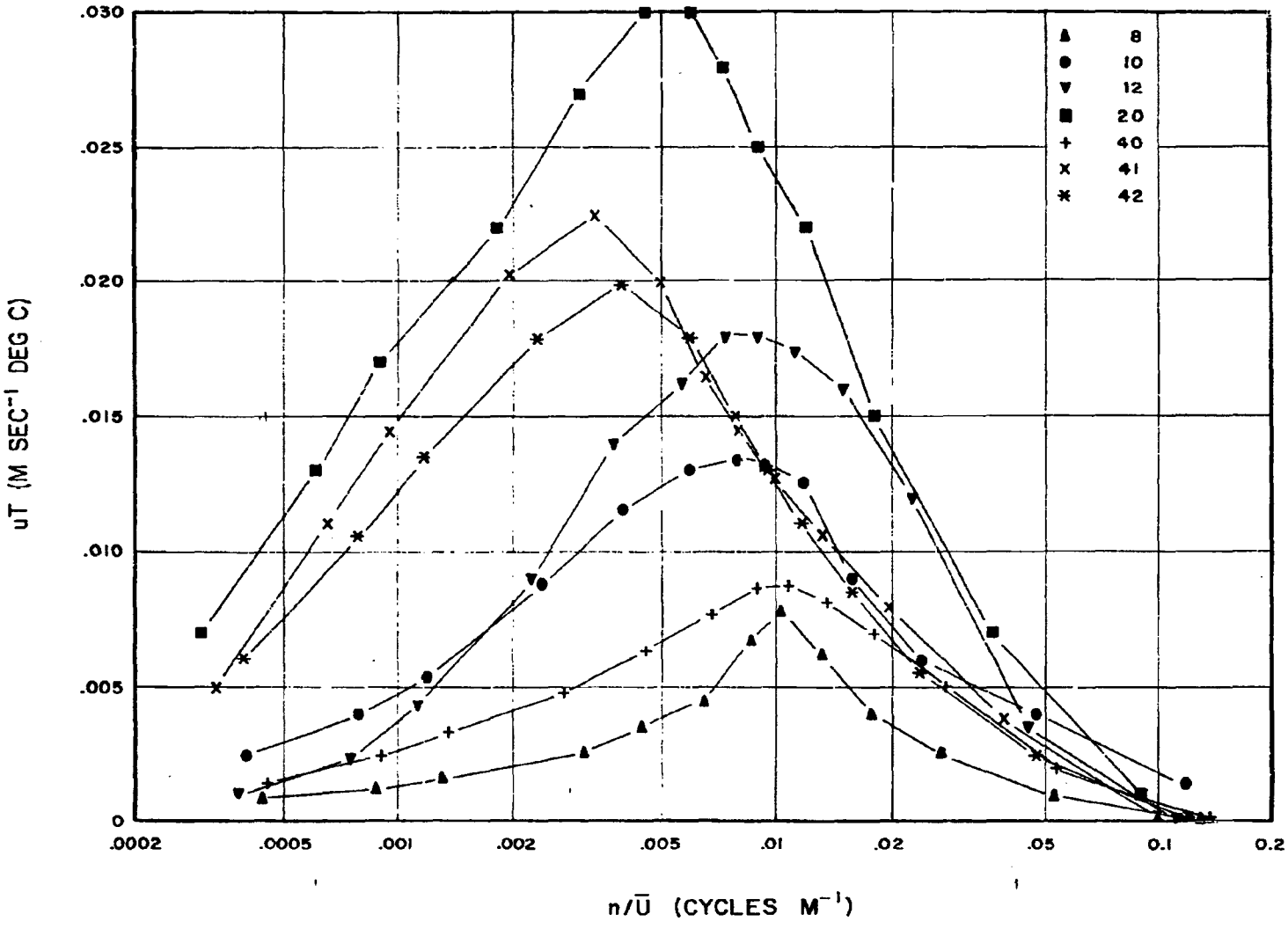

Fig. 26b. Logarithmic cospectra of the horizontal flux of temperature at a height of 16 m for the nighttime experiments.

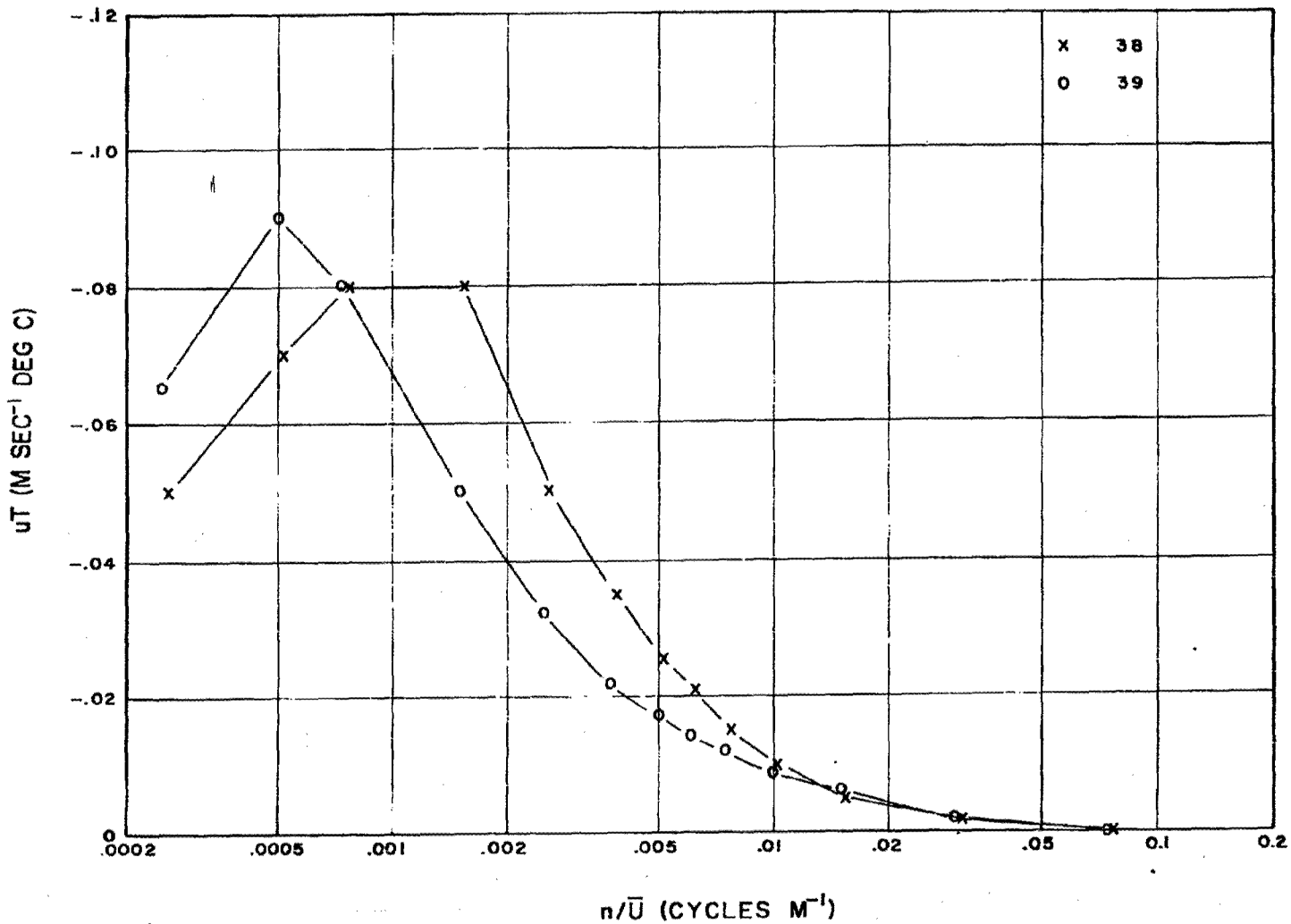

Fig. 26c. Logarithmic cospectra of the horizontal flux of temperature at a height of 40 m for the daytime experiments.

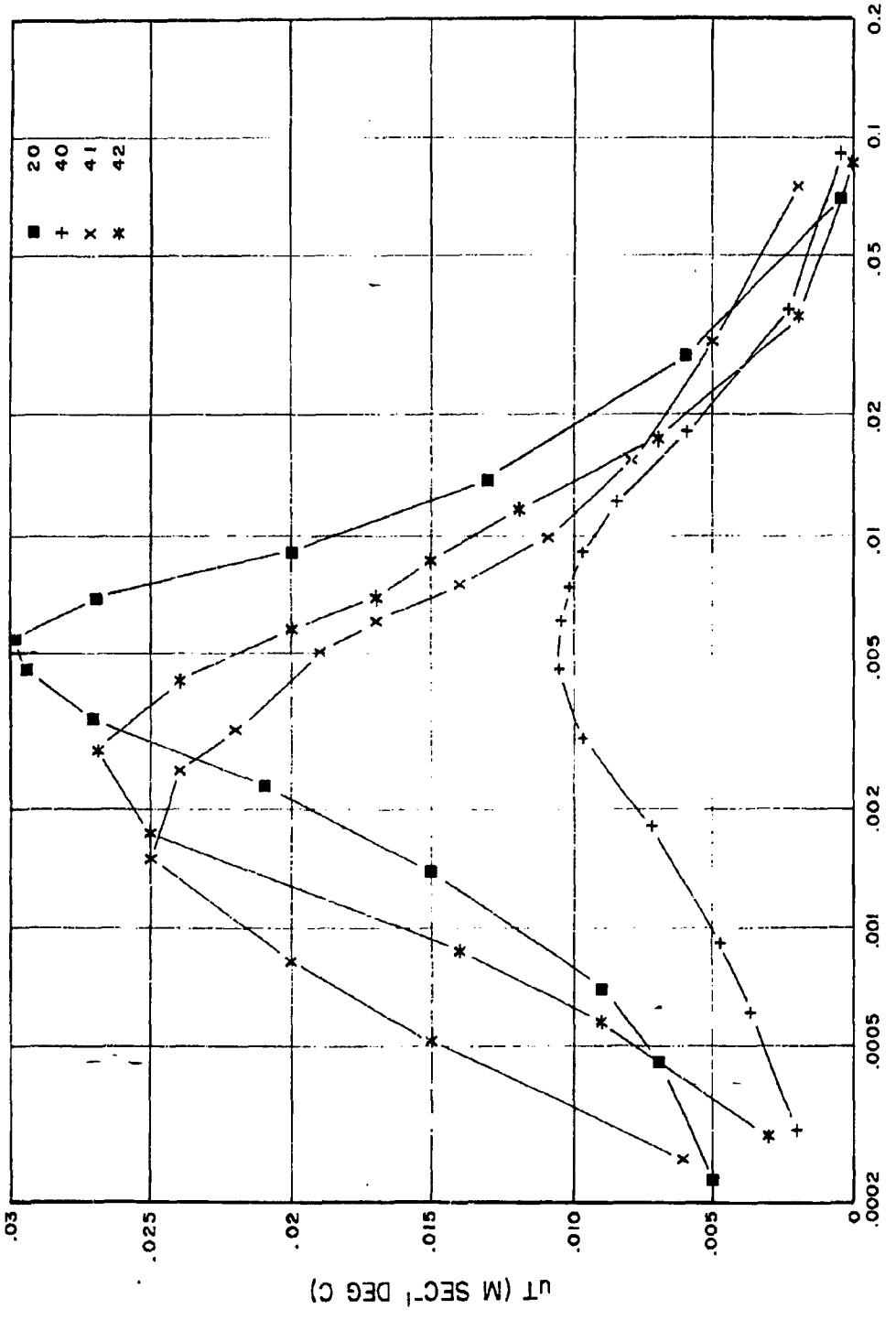

Fig. 26d. Logarithmic cospectra of the horizontal flux of temperature at a height of 40 m for the nighttime experiments.

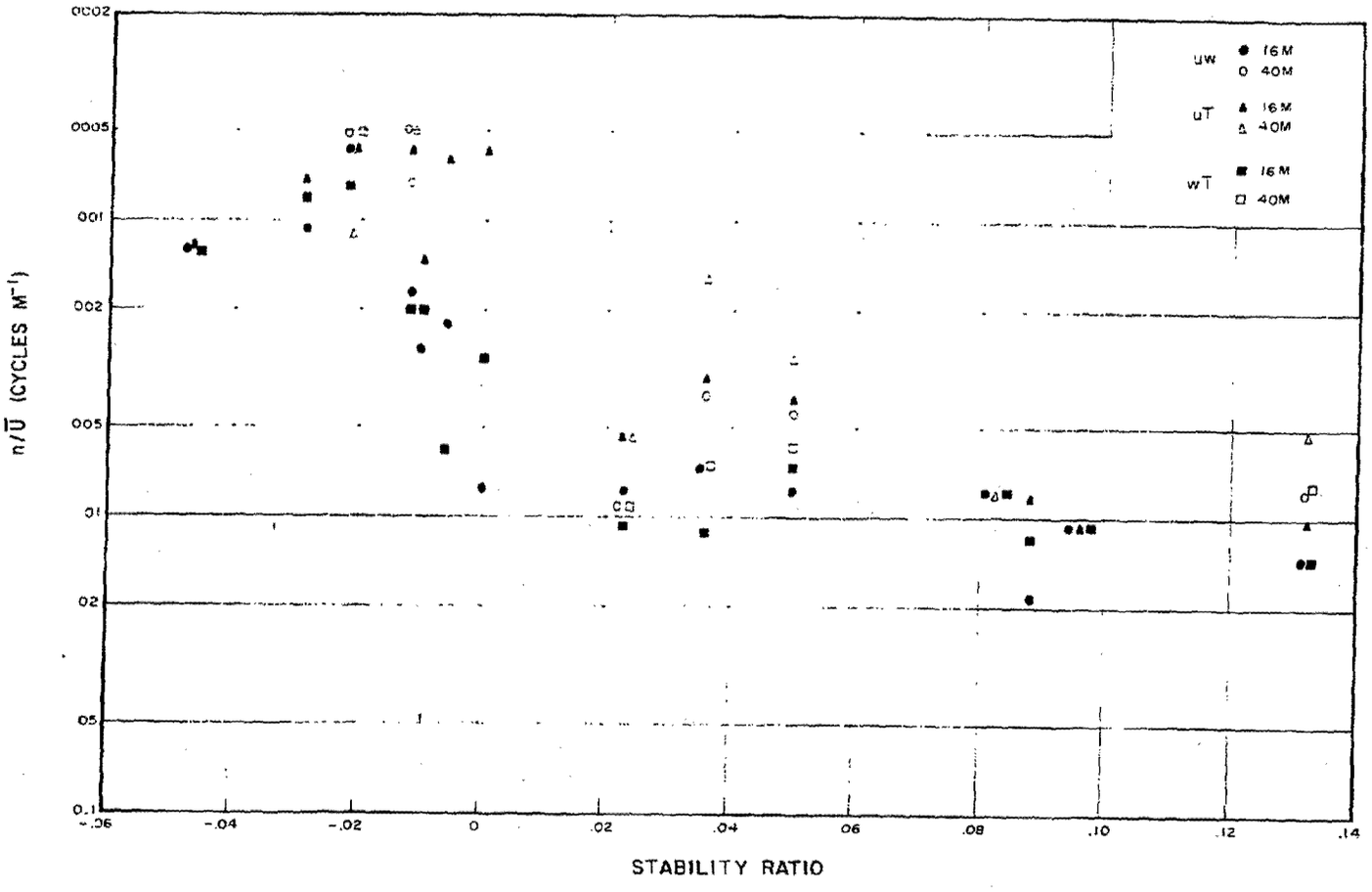

Fig. 27a. Peak frequencies for the uw-, wT-, and uT-cospectra versus the Stability Ratio.

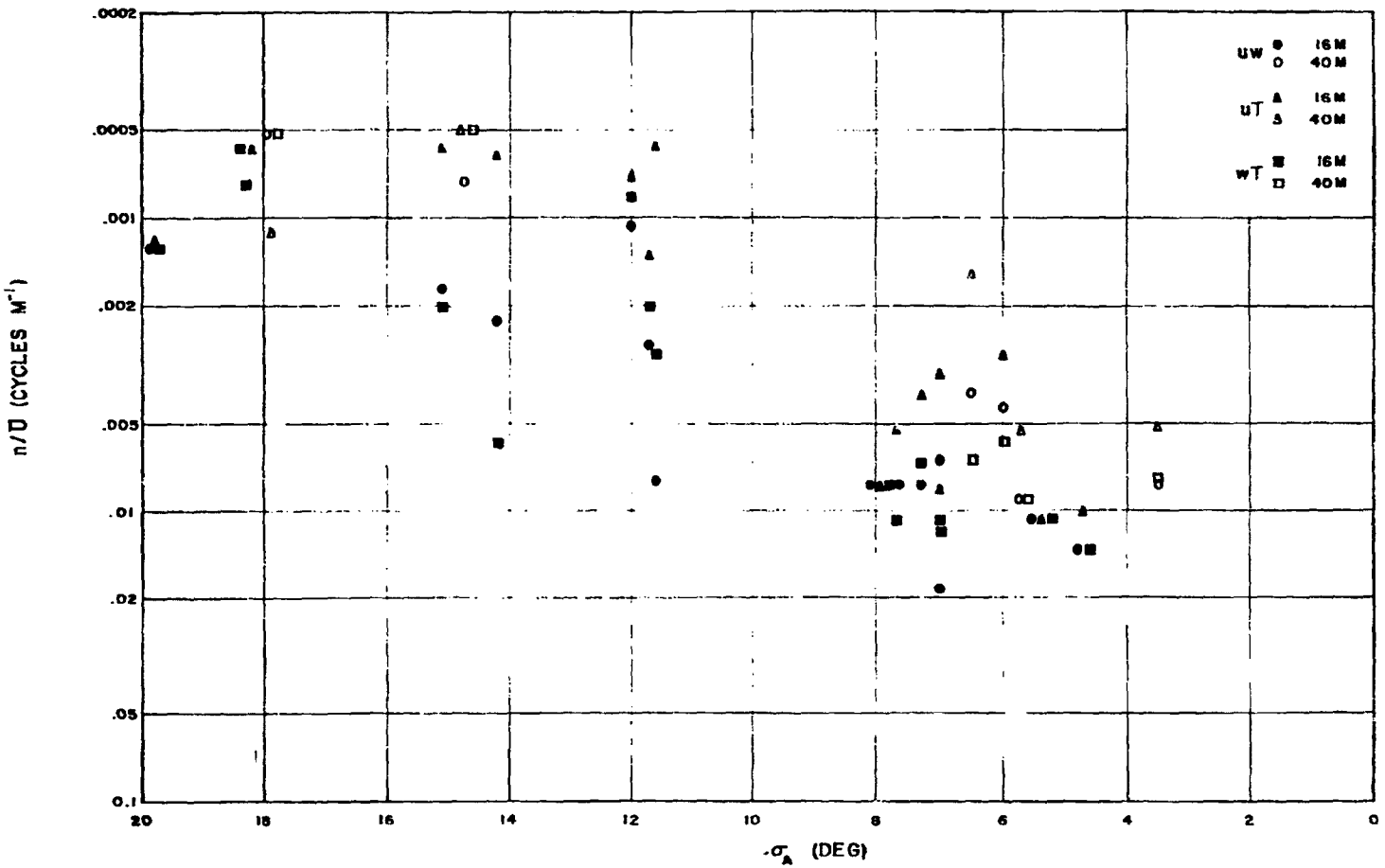

Fig. 27b. Peak frequencies for the uw-, wT-, and uT-cospectra versus the standard deviation of azimuth wind direction.

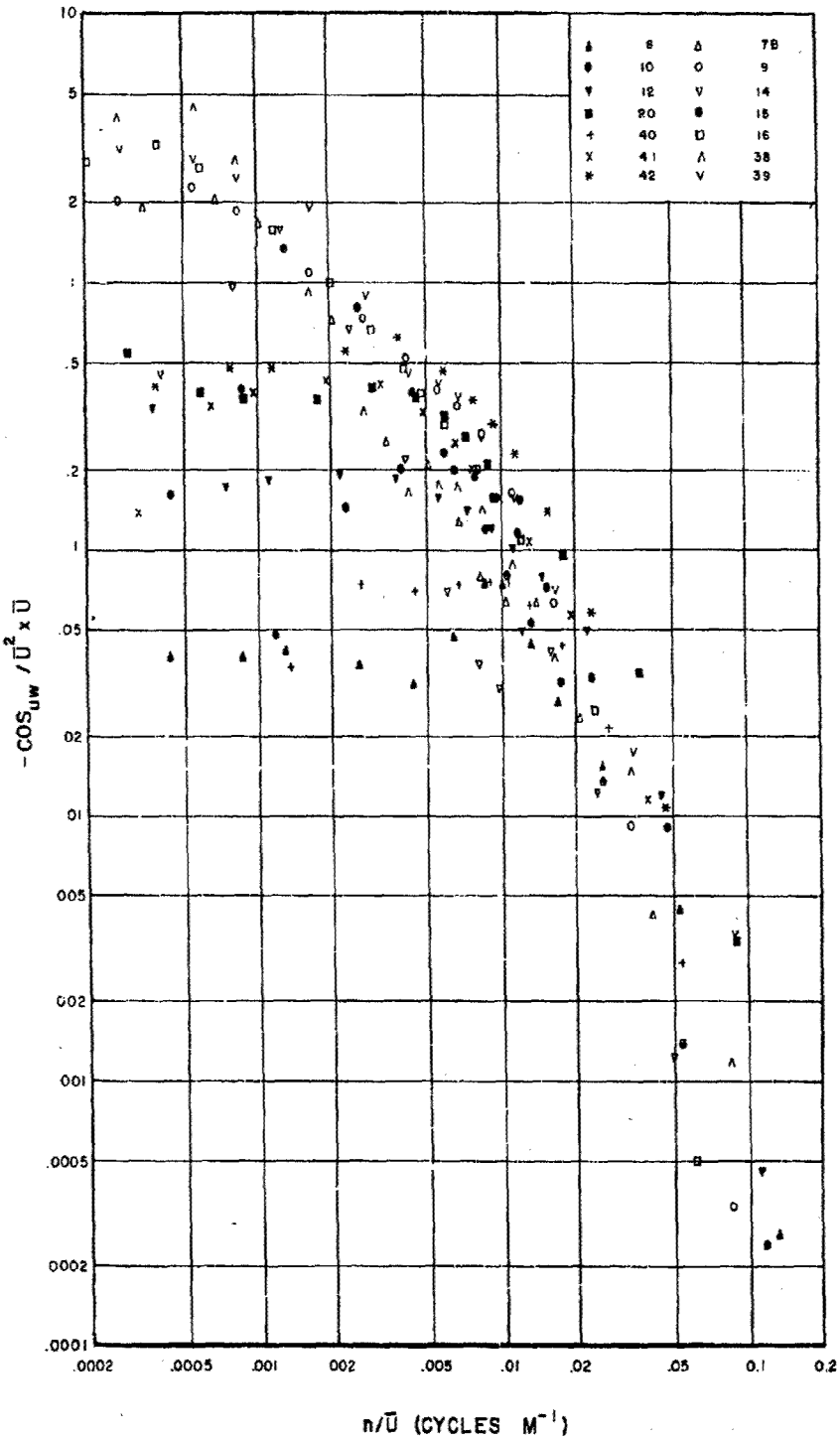

Fig. 28a. Cospectral density of the vertical momentum flux at a height of 16 m.

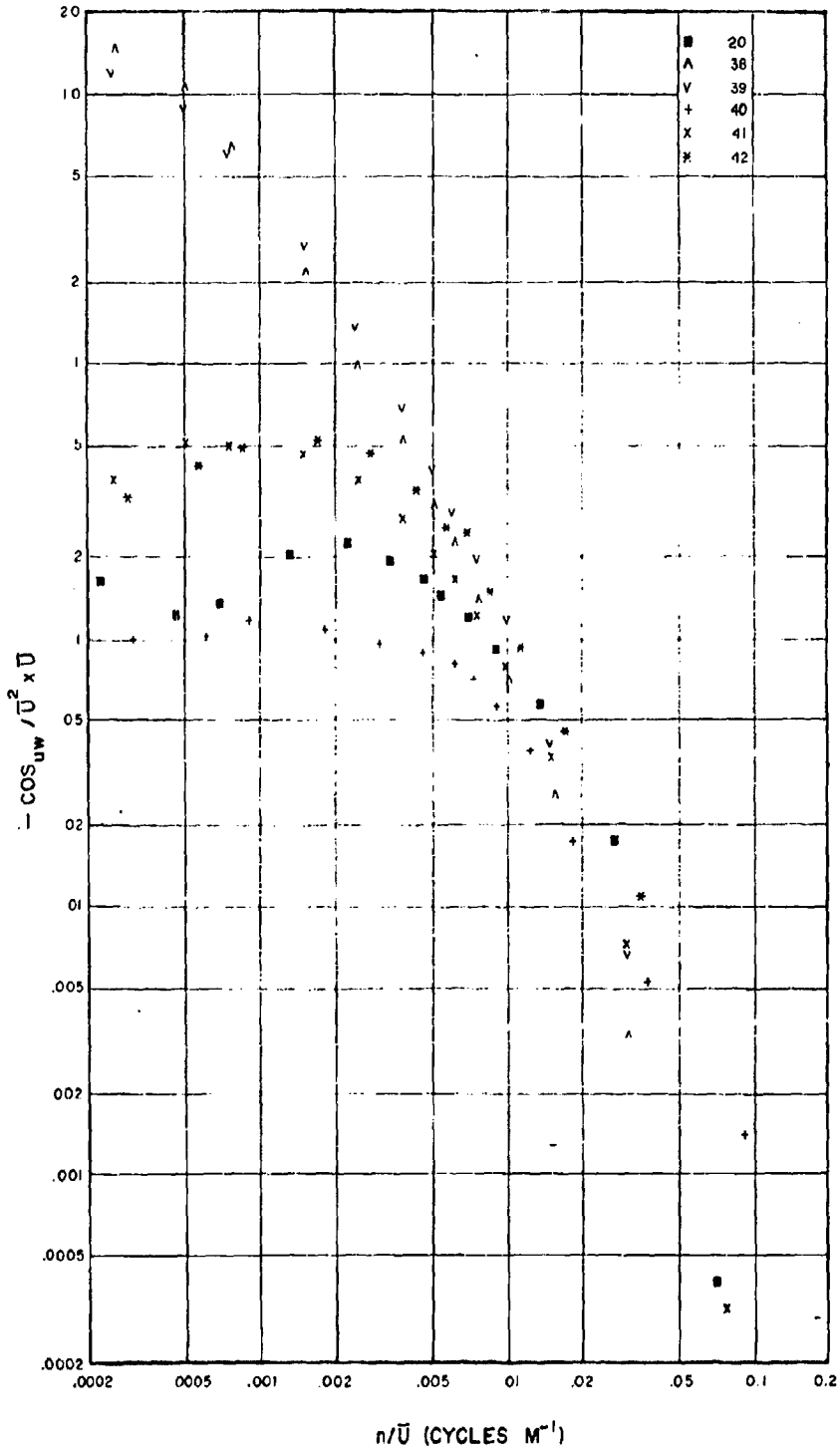

Fig. 28b. Cospectral density of the vertical momentum flux at a height of 40 m.

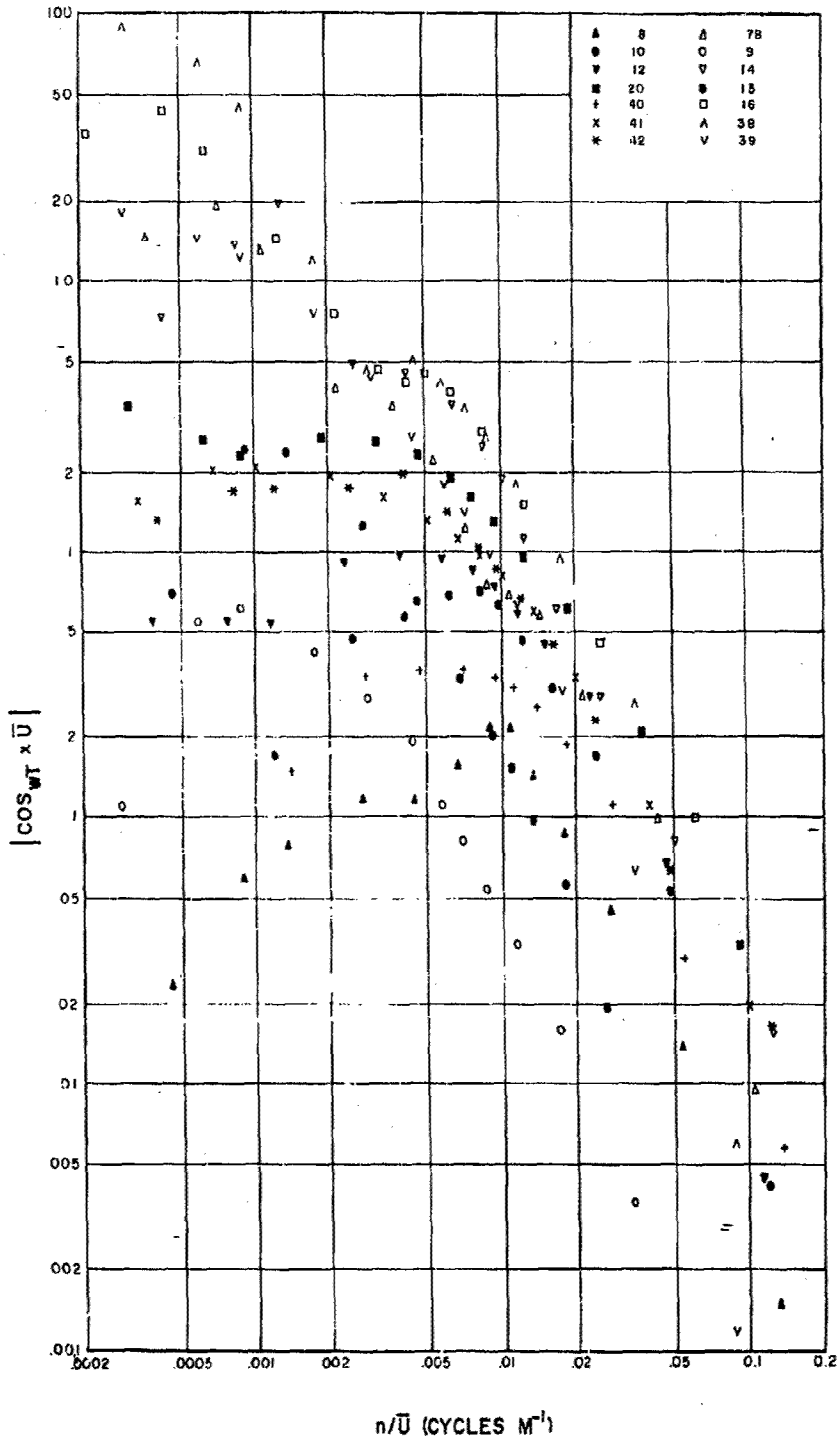

Fig. 29a. Cospectral density of the vertical temperature flux at a height of 16 m.

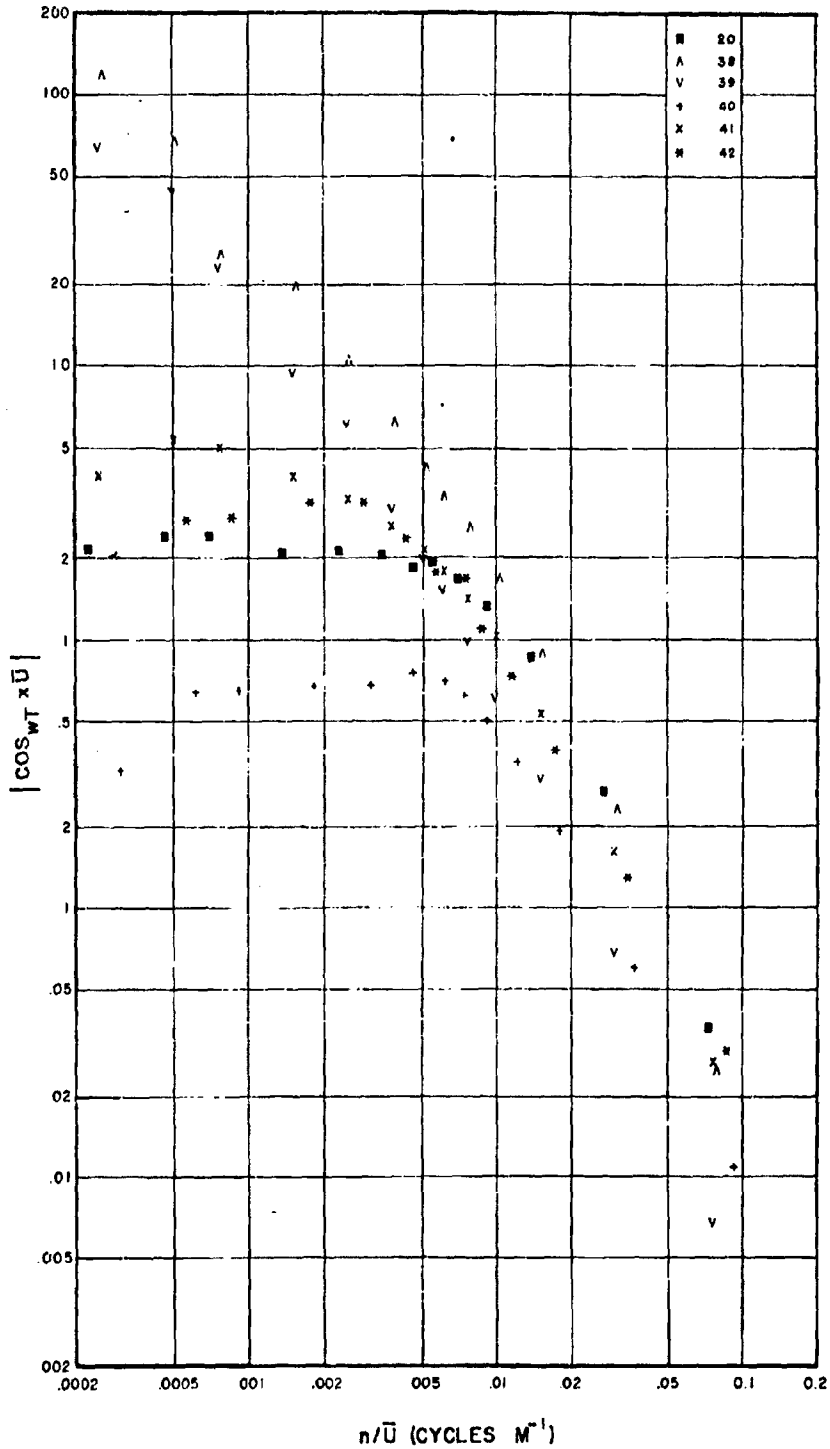

Fig. 29b. Cospectral density of the vertical temperature flux at a height of 40 m.

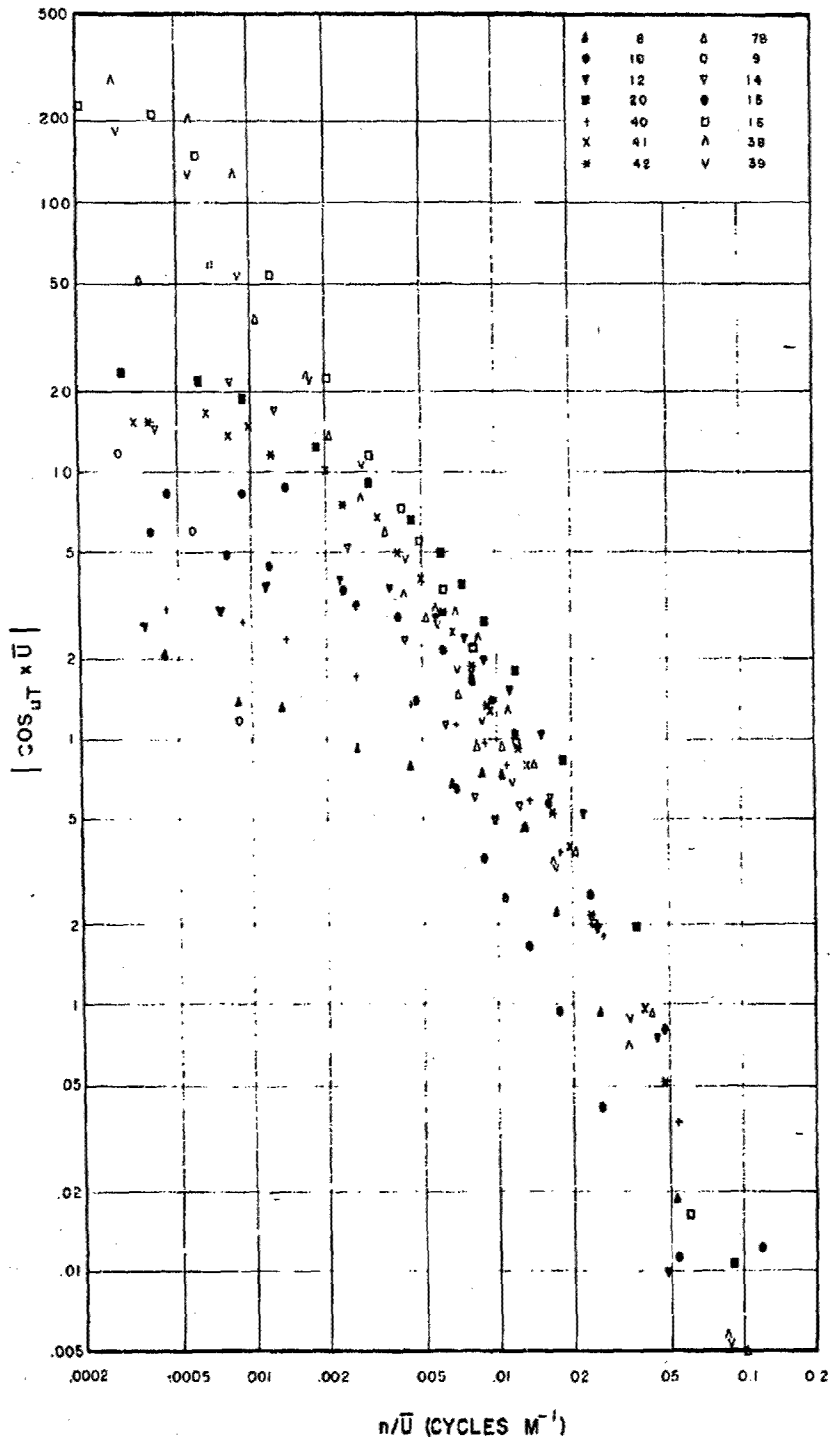

Fig. 30a. Cospectral density of the horizontal temperature flux at a height of 16 m.

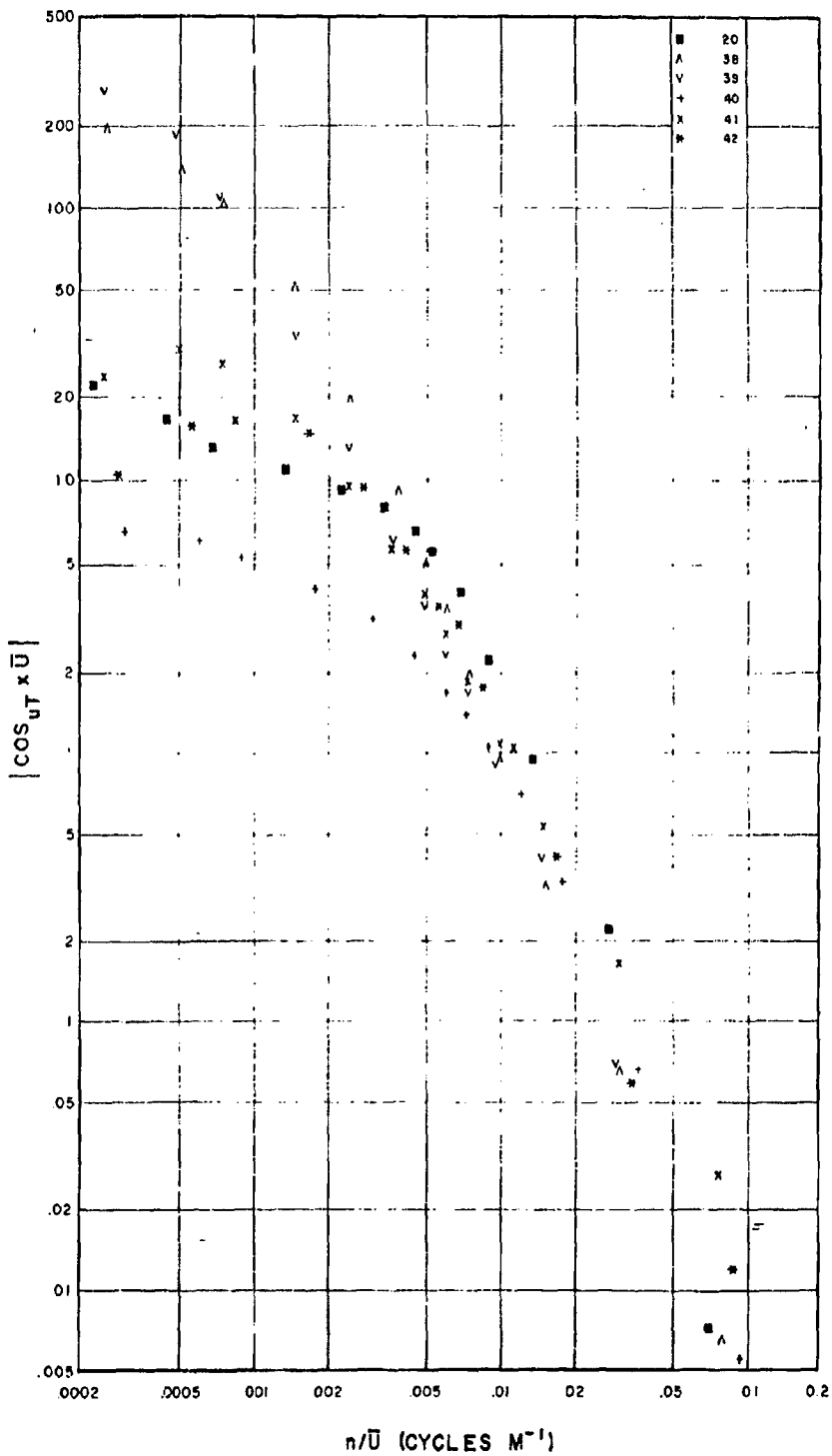

Fig. 30b. Cospectral density of the horizontal temperature flux at a height of 40 m.

REFERENCES

Blackman, R. B., and J. W. Tukey, 1958: The measurement of power spectra from the point of view of communications engineering. Bell Sys. Tech. J., 37, 185-288 and 485-569.

Cramer, H. E., 1959: Measurements of turbulence structure near the ground within the frequency range from 0.5 to 0.01 cycles sec^{-1}. Advances in Geophysics. New York, Academic Press, 6, 75 - 96.

_____, F. A. Record, J. E. Tillman, and H. C. Vaughan, 1961: Studies of the spectra of the vertical fluxes of momentum, heat and moisture in the atmospheric boundary layer. Annual Report under Contract No. DA-36-039-SC-80209, 130 pp.

Dixon, W. J., and F. J. Massey, Jr. 1951: Introduction to Statistical Analysis. New York, McGraw-Hill, 370 pp.

Jones, R. A., 1957: Porton Tech. Paper No. 588, UK Min. of Supply.

Lappe, U. O., B. Davidson, and C. B. Notess, 1959: Analysis of atmospheric turbulence spectra obtained from concurrent airplane and tower measurements. Inst. Aero. Sci. Rep. No.59-44, 33 pp.

Lettau, H. H., and B. Davidson, 1957: Exploring the Atmosphere's First Mile. New York, Pergamon Press, 578 pp.

MacCready, P. B., 1953: Measurement and analysis of atmospheric turbulence. J. Meteor., 10, 325-337.

Monin, A. S., and A. M. Obukhov, 1954: U.S.S.R. Acad. Sci., Works of Geophys. Inst., No. 24(151), 163-187.

Panofsky, H. A., 1962: Scale analysis of atmospheric turbulence at 2 m. Quart. J. roy. meteor. Soc., 88, 57 - 69.

_____, and R. J. Deland, 1959: One-dimensional spectra of atmospheric turbulence in the lowest 100 meters. Advances in Geophysics. New York, Academic Press, 6, 41-64.

_____, and R. A. McCormick, 1954: Properties of spectra of atmospheric turbulence at 100 metres. Quart. J. Roy. meteor. Soc., 80, 546-564.

_____, H. E. Cramer, and V. R. K. Rao, 1958: The relation between Eulerian time and space spectra. Quart. J. Roy. meteor. Soc., 80, 546-564.

Priestley, C. H. B., 1959: Turbulent Transfer in the Lower Atmosphere. University of Chicago Press, 130 pp.

Suomi, V. E., 1957: Energy budget studies at the earth's surface and development of the sonic anemometer for spectrum analysis. AFCRC-TR-56-274, Dept. of Meteorology, Univ. of Wisconsin.

Swinbank, W. C., 1951: The measurement of vertical transfer of heat and water vapor and momentum in the lower atmosphere with some results. J. Meteor., 8, 135-145.

Takeuchi, K., 1962: On the structure of the turbulent field in the surface boundary layer. (To be published by the Meteorology Society of Japan.)

APPENDIX

Table A1. Vertical profiles of 1-hr mean wind speeds. Entries in parentheses are estimated values.

	$\bar{V}$ (m sec^{-1})						
Run No.	7B	8	9	10	12	14	15
Z(m)							
40	5.15	5.89	6.65	5.60	6.54	4.19	4.09
32	4.95	4.99	6.48	5.29	5.91	4.16	4.01
16	4.78	3.82	5.92	4.19	4.42	4.05	3.78
8	4.49	3.28	5.50	3.56	3.59	3.77	3.49
4	4.16	2.88	4.97	3.12	3.19	3.58	3.24
2	3.84	2.35	4.49	2.69	2.77	3.28	2.99
1	3.46	1.92	4.05	2.33	2.38	2.99	2.63
0.5	(3.05)	(1.53)	(3.50)	(1.98)	(2.00)	(2.66)	(2.33)
0.25	(2.60)	(1.13)	(2.97)	(1.68)	(1.62)	(2.32)	(2.02)

Run No.	16	20	38	39	40	41	42
Z(m)							
40	9.04	7.31	6.48	6.69	5.48	6.61	5.80
32	8.80	6.91	6.27	6.31	4.68	5.97	5.18
16	8.20	5.53	6.12	5.81	3.67	5.03	4.21
8	7.56	4.67	5.66	5.30	3.03	4.20	3.50
4	7.00	4.17	5.26	4.96	2.61	3.76	3.16
2	6.37	3.69	4.77	4.49	2.08	3.26	2.74
1	5.70	3.21	4.29	4.00	1.78	2.90	2.41
0.5	(5.07)	(2.72)	(3.77)	(3.53)	(1.56)	(2.55)	(2.10)
0.25	(4.43)	(2.25)	(3.20)	(3.04)	(1.40)	(2.35)	(1.95)

Table A2. Vertical profiles of 1-hr mean air temperatures. Wet-bulb temperatures are enclosed in parentheses and the symbol (m) denotes missing data.

$\bar{T}_D$, $\bar{T}_W$ (C)

Run No.	7B	8	9	10	12	14	15
Z(m)							
40	12.8 (7.0)	10.8 (9.6)	12.3 (8.6)	5.8 (1.8)	4.1 (m)	0.4 (m)	2.0 (m)
32	12.8 (m)	10.7 (m)	12.4 (m)	5.8 (m)	3.9 (m)	0.5 (m)	2.1 (m)
16	13.0 (7.1)	10.3 (9.4)	12.5 (8.7)	5.6 (1.9)	3.4 (m)	0.7 (m)	2.3 (m)
8	13.2 (7.1)	10.0 (9.1)	12.5 (8.7)	5.4 (1.7)	3.1 (m)	0.9 (m)	2.3 (m)
4	13.4 (7.4)	9.7 (8.9)	12.5 (8.7)	5.1 (1.5)	2.7 (m)	1.1 (m)	2.4 (m)
2	13.7 (7.6)	9.2 (8.5)	12.5 (8.7)	4.6 (1.2)	2.2 (m)	1.5 (m)	2.4 (m)
1	14.0 (7.7)	8.8 (8.2)	12.5 (8.7)	3.9 (m)	1.6 (m)	1.8 (m)	2.4 (m)
0.5	14.2 (8.0)	8.4 (7.9)	12.5 (8.8)	3.3 (m)	1.1 (m)	2.1 (m)	2.4 (m)
0.25	14.4 (8.3)	8.2 (7.7)	12.4 (8.8)	2.8 (m)	0.6 (m)	2.4 (m)	2.4 (m)
0.12	14.6 (8.6)	7.9 (7.5)	12.4 (8.9)	2.5 (m)	(m) (m)	2.8 (m)	2.4 (m)

	16	20	38	39	40	41	42
40	9.3 (m)	19.0 (14.6)	8.0 (3.1)	9.7 (m)	7.3 (3.5)	6.6 (3.0)	5.8 (2.7)
32	9.4 (m)	18.9 (14.6)	8.0 (3.1)	9.7 (3.5)	7.2 (3.4)	6.5 (3.0)	5.7 (2.7)
16	9.6 (m)	18.6 (14.5)	8.2 (3.2)	9.8 (3.6)	6.9 (3.3)	6.4 (3.0)	5.6 (2.6)
8	9.8 (4.6)	18.3 (14.5)	8.4 (3.3)	9.8 (3.6)	6.5 (3.1)	6.2 (2.9)	5.4 (2.5)
4	9.9 (4.7)	18.1 (14.4)	8.7 (3.4)	9.9 (3.7)	6.1 (2.9)	6.0 (2.7)	5.2 (2.3)
2	10.1 (4.8)	17.9 (14.4)	9.0 (3.8)	10.1 (4.0)	5.6 (2.7)	5.7 (2.7)	4.9 (2.2)
1	10.4 (4.9)	17.6 (14.4)	9.4 (4.2)	10.3 (4.2)	5.2 (2.6)	5.5 (2.6)	4.6 (2.1)
0.5	10.6 (5.1)	17.3 (14.3)	9.8 (4.7)	10.5 (4.6)	4.8 (2.5)	5.3 (2.6)	4.3 (2.1)
0.25	10.8 (5.3)	17.0 (14.2)	10.1 (5.1)	10.6 (4.8)	4.5 (2.4)	5.0 (2.5)	4.0 (2.1)
0.12	11.0 (5.5)	16.7 (14.2)	10.5 (5.5)	10.8 (5.0)	4.3 (2.3)	4.8 (2.5)	3.8 (2.0)

Table A3. Soil temperature profiles. Measurements in deg C were made immediately preceding and following the 1-hr experiments at two locations (S, N); the values obtained after the experiment are enclosed in parentheses. Average temperature for the 0 to 5 cm layer indicated by separate thermometers is also tabulated. The symbol m denotes missing data. Temperatures at depths of 50 and 100 cm locations, for Runs 38 through 42, are estimates.

Run No.	7B[1]		8	
Depth (cm)	S	N	S	N
1.6	14.1 (16.1)	12.1 (13.2)	6.2 (5.7)	6.8 (6.3)
3.1	11.9 (14.3)	9.2 (11.2)	6.7 (6.3)	7.9 (7.4)
6.2	9.9 (12.1)	8.4 (9.9)	7.6 (7.0)	8.5 (8.0)
12.5	7.9 (9.4)	7.8 (8.6)	9.0 (8.5)	9.0 (8.7)
25.0	7.7 (8.4)	8.0 (8.1)	9.4 (9.1)	8.8 (8.8)
50.0	9.1 (9.0)	8.9 (8.9)	9.2 (9.3)	8.9 (9.0)
100.0	11.4 (11.4)	10.6 (10.6)	11.3 (11.4)	10.5 (10.5)
0-5cm	9.5 (11.2)		6.7 (6.3)	
	9		10	
1.6	12.5 (11.0)	11.0 (10.0)	3.8 (1.9)	5.2 (4.0)
3.1	11.8 (10.8)	10.5 (10.2)	5.1 (3.5)	7.1 (6.1)
6.2	11.3 (10.7)	9.9 (9.9)	6.5 (5.4)	7.9 (7.3)
12.5	10.1 (10.2)	9.2 (9.4)	8.6 (8.0)	8.8 (8.4)
25.0	9.4 (9.6)	8.6 (8.7)	9.3 (8.9)	8.9 (8.9)
50.0	9.3 (9.3)	9.0 (9.0)	9.4 (9.5)	9.1 (9.1)
100.0	11.3 (11.3)	10.4 (10.4)	11.2 (11.2)	10.4 (10.4)
0-5cm	10.6 (9.9)		5.7 (4.5)	
	12		14	
1.6	0.8 (0.3)	2.9 (2.3)	3.0 (4.2)	0.1 (0.9)
3.1	2.2 (1.7)	5.0 (4.5)	2.0 (3.2)	m (m)
6.2	4.0 (3.5)	6.5 (5.9)	0.3 (1.8)	1.4 (1.4)
12.5	7.0 (6.4)	7.9 (7.6)	0.8 (1.2)	m (m)
25.0	8.4 (8.0)	8.8 (8.7)	2.3 (2.3)	4.9 (4.8)
50.0	9.5 (9.5)	9.1 (9.1)	7.1 (7.0)	7.4 (7.4)
100.0	11.2 (11.2)	10.4 (10.4)	10.4 (10.4)	9.7 (9.7)
0-5cm	3.4 (2.9)		m (m)	

[1] Soil temperatures taken at 1030 and 1205 EST

Depth	Run No. 15 S	15 N	16 S	16 N
1.6	2.8 (0.7)	1.0 (0.2)	12.5 (12.0)	9.5 (8.8)
3.1	2.6 (0.2)	0.1 (0.4)	10.6 (11.0)	7.6 (8.5)
6.2	2.2 (1.2)	1.6 (1.8)	9.1 (10.0)	6.8 (7.6)
12.5	1.7 (1.9)	m (m)	7.0 (8.0)	m (m)
25.0	2.4 (2.6)	4.7 (4.7)	6.2 (6.9)	5.7 (5.9)
50.0	6.9 (6.9)	7.3 (7.3)	6.2 (6.3)	5.0 (6.1)
100.0	10.4 (10.4)	9.7 (9.7)	8.7 (8.7)	8.2 (8.2)
0-5cm	m (m)		7.7 (8.1)	
	20		38[2]	
1.6	18.4 (17.1)	19.4 (18.5)	16.0 (16.5)	12.8 (13.2)
3.1	19.2 (18.0)	19.9 (19.1)	16.0 (16.2)	13.0 (13.6)
6.2	20.8 (19.8)	20.8 (20.2)	14.4 (14.8)	11.8 (12.5)
12.5	22.2 (21.5)	21.1 (20.7)	11.8 (12.7)	11.7 (12.2)
25.0	22.5 (22.1)	20.8 (20.6)	11.1 (11.7)	13.2 (13.1)
50.0	19.7 (19.7)	18.4 (18.4)	15.3 (14.9)	16.2 (15.8)
100.0	16.7 (16.7)	16.1 (16.1)	17.1 (17.1)	16.6 (16.6)
0-5cm	20.1 (19.3)		12.2 (12.8)	
	39		40	
1.6	15.5 (12.5)	13.3 (12.2)	6.6 (6.0)	9.0 (8.6)
3.1	14.8 (11.9)	13.8 (13.0)	6.2 (5.5)	9.7 (9.2)
6.2	14.5 (12.8)	13.0 (12.9)	8.1 (7.4)	11.4 (11.0)
12.5	13.3 (13.2)	12.7 (12.9)	11.0 (10.5)	12.3 (12.1)
25.0	12.5 (12.8)	13.4 (13.4)	12.5 (12.1)	13.6 (13.6)
50.0	14.8 (14.8)	15.9 (15.7)	15.0 (15.1)	15.5 (15.5)
100.0	17.1 (17.1)	16.6 (16.6)	17.1 (17.1)	16.6 (16.6)
0-5cm	12.7 (11.6)		8.5 (8.0)	
	41		42	
1.6	5.7 (5.5)	8.5 (8.4)	5.2 (4.8)	8.2 (8.0)
3.1	5.3 (5.1)	9.0 (8.9)	4.9 (4.5)	8.8 (8.5)
6.2	7.1 (6.8)	10.9 (10.7)	6.6 (6.2)	10.6 (10.4)
12.5	10.2 (9.9)	11.9 (11.8)	9.7 (9.4)	11.7 (11.6)
25.0	11.9 (11.7)	13.6 (13.7)	11.5 (11.3)	13.6 (13.6)
50.0	15.1 (15.2)	15.5 (15.6)	15.2 (15.3)	15.6 (15.6)
100.0	17.1 (17.1)	16.6 (16.6)	17.1 (17.1)	16.6 (16.6)
0-5cm	7.8 (7.6)		7.6 (7.2)	

[2] Soil temperatures taken at 1151 and 1316 EST

Table A4. Summary of heat budget estimates in cal cm^{-2} min^{-1} at the air-soil interface.[1] Minus sign indicates the flux is directed away from the interface. Estimates of E_o are obtained from the balance condition. Values of the air heat flux in parenthesis are computed from filtered fast-response data.

Run No.	Net Radiation R_o	Soil Heat Flux S_o	Air Heat Flux Q_o	Evaporative Flux E_o
7B	0.42	-0.07	-0.15	-0.20
8	-0.13	0.02	0.01	0.10
9	0.01	0	0.01	-0.02
10	-0.15	0.06	0.01	0.08
12	-0.15	0.04	(0.03)	(0.08)
14	0.33	-0.02	-0.13	-0.18
15	-0.01	0.04	-0.02	-0.01
16	0.29	-0.03	-0.10	-0.16
20	-0.14	0.04	0.04	0.06
38	0.61	-0.06	-0.27	-0.28
39	0.20	0.02	-0.07	-0.15
40	-0.15	0.05	0.02	0.08
41	-0.16	0.04	0.04	0.08
42	-0.15	0.04	(0.04)	(0.07)

[1] The heat budget equation of the earth-air interface may be written

$$R_o + S_o + Q_o + E_o = 0 ,$$

where R_o = net effect of all radiative processes;
S_o = vertical heat flux in the soil;
Q_o = vertical heat flux in the atmosphere;
and, E_o = heat equivalent of the evaporative flux in moisture in the atmosphere.

The subscript zero denotes the value of the energy fluxes at the interface. The following procedure provides estimates for each of the four terms of the equation. Net radiation, R_o, is measured by a Beckman-

Footnote to Table A4 (continued)

Whitley net radiometer mounted at a height of 1.5 m. For the 1962 observations, net radiation measurements were also made with a small radiometer loaned the project by Dr. Leo J. Fritschen of the U. S. Water Conservation Laboratory, Tempe, Arizona. The soil heat flux, S_o, is determined from the following data: the soil heat flux through the -5 cm level; the change in temperature of the 0 to -5 cm layer of soil; and the heat capacity of the soil within the 0 to -5 cm layer. Beckman-Whitley heat plates and resistance thermometers with a sensitive length of 5 cm are used to measure, respectively, the first two of these quantities. The heat capacity for a particular experiment is calculated from values of the density and specific heat of dried soil samples determined at the start of the field program, and from measurements during the experiment of the fraction of water present in soil samples taken from the 0 to -5 cm layer. Further details of the heat-budget instrumentation and experimental procedure are contained in the Annual Report. The value of Q_o is determined from the 16-m fast-response temperature and wind data, the vertical flux of heat in the 0 to 16-m layer being assumed invariant with height. Values of E_o are obtained by determining the flux required to balance the heat-budget equation.

Table A5. Gross turbulence statistics for unfiltered fast-response data. Wind velocities are in m sec^{-1} and temperatures are in Centigrade. Covariances reflect in-phase contributions only; no quadrature covariances are available. The symbol m denotes missing data.

Run No.	7B (16m)	8 (16m)	9 (16m)	10(16m)	12(16m)	14(16m)	15(16m)
$\bar{U}$	4.78	3.82	5.92	4.19	4.42	4.05	3.76
σ_u	0.886	0.411	1.40	0.590	(m)	1.13	0.899
σ_v	0.982	0.467	1.23	0.508	(m)	1.47	0.723
σ_w	0.428	0.123	0.658	0.255	(m)	0.505	0.381
σ_T	0.418	0.143	0.316	0.457	(m)	0.280	0.140
$\sigma_{u/\bar{U}}$	0.185	0.108	0.236	0.141	(m)	0.272	0.239
$\sigma_{v/\bar{U}}$	0.205	0.122	0.208	0.121	(m)	0.363	0.192
$\sigma_{w/\bar{U}}$	0.090	0.032	0.111	0.061	(m)	0.140	0.101
$\overline{uT}$	-0.1377	0.0392	-0.0924	0.1154	(m)	-0.0553	-0.0649
$\overline{wT}$	0.0857	-0.0039	-0.0059	-0.0070	(m)	0.0754	0.0110
$\overline{vT}$	-0.0445	0.0445	0.0760	0.0244	(m)	0.0261	-0.0265
$\overline{uv}$	0.0226	0.0351	-0.0526	0.0693	(m)	0.2247	0.0135
$\overline{vw}$	-0.0804	0.0036	0.0330	-0.0073	(m)	0.0701	0.0031
$\overline{uw}$	-0.1357	-0.0178	-0.2459	-0.0487	(m)	-0.0565	-0.0817
R (uT)	-0.37	0.67	-0.21	0.43	(m)	-0.18	-0.52
R (wT)	0.48	-0.22	-0.03	-0.06	(m)	0.48	0.21
R (vT)	-0.11	0.18	-0.20	0.11	(m)	0.06	-0.26
R (uv)	0.03	0.18	-0.03	0.23	(m)	0.14	0.02
R (vw)	-0.19	0.07	0.04	-0.06	(m)	0.08	0.03
R (uw)	-0.36	-0.35	-0.27	-0.32	(m)	-0.09	-0.24

Run No.	16(16m)	20(16m)	20(40m)	38(16m)	38(40m)	39(16m)	39(40m)
$\bar{U}$	8.20	5.53	7.31	6.12	6.48	5.81	6.69
σ_u	1.87	0.817	(m)	1.52	1.71	1.56	1.80
σ_v	2.04	0.724	(m)	2.09	2.03	1.50	1.68
σ_w	0.824	0.448	(m)	0.720	1.03	0.669	0.880
σ_T	0.453	0.436	(m)	0.474	0.449	0.236	0.220
$\sigma_u/\bar{U}$	0.228	0.148	(m)	0.248	0.264	0.268	0.269
$\sigma_v/\bar{U}$	0.249	0.131	(m)	0.342	0.321	0.258	0.251
$\sigma_w/\bar{U}$	0.100	0.081	(m)	0.118	0.159	0.115	0.131
$\overline{uT}$	-0.3288	0.0559	(m)	-0.3410	-0.3698	-0.2181	-0.1930
$\overline{wT}$	0.0561	-0.0237	(m)	0.1582	0.2165	0.0425	0.0784
$\overline{vT}$	-0.1787	0.0696	(m)	-0.0978	-0.0465	-0.0248	0.0488
$\overline{uv}$	-0.0115	0.0796	(m)	-0.7613	-0.7085	0.0715	0.3189
$\overline{vw}$	0.2805	-0.0191	(m)	0.0098	-0.0995	0.0297	-0.0930
$\overline{uw}$	-0.5971	-0.1564	(m)	-0.3271	-0.7112	-0.3185	-0.6116
R (uT)	-0.39	0.16	(m)	-0.47	-0.48	-0.59	-0.49
R (wT)	0.15	-0.12	(m)	0.46	0.47	0.27	0.40
R (vT)	-0.19	0.22	(m)	-0.10	-0.05	-0.07	0.13
R (uv)	0	0.13	(m)	-0.24	-0.20	0.03	0.11
R (vw)	0.17	-0.06	(m)	0.01	-0.04	0.03	-0.06
R (uw)	-0.39	-0.43	(m)	-0.30	-0.40	-0.31	-0.39

Run No.	40(16m)	40(40m)	41(16m)	41(40m)	42(16m)	42(40m)
$\bar{U}$	3.67	5.48	5.03	6.61	4.21	5.80
σ_u	0.404	0.495	0.896	0.820	(m)	(m)
σ_v	0.305	0.335	0.616	0.697	(m)	(m)
σ_w	0.210	0.223	0.414	0.464	(m)	(m)
σ_T	0.140	0.173	0.190	0.182	(m)	(m)
$\sigma_{u/\bar{U}}$	0.110	0.090	0.178	0.124	(m)	(m)
$\sigma_{v/\bar{U}}$	0.083	0.061	0.122	0.105	(m)	(m)
$\sigma_{w/\bar{U}}$	0.057	0.041	0.082	0.070	(m)	(m)
$\overline{uT}$	0.0322	0.0407	0.1219	0.0908	0.0404	0.0473
$\overline{wT}$	-0.0097	-0.0113	-0.0218	-0.0307	-0.0260	-0.0284
$\overline{vT}$	0.0028	0.0033	-0.0148	-0.0167	0.0070	0.0110
$\overline{uv}$	0.0183	0.0252	-0.0884	0.0104	-0.0407	0.0025
$\overline{vw}$	-0.0095	-0.0074	-0.0177	-0.0543	-0.0030	-0.0232
$\overline{uw}$	-0.0249	-0.0415	-0.1042	-0.1295	-0.1090	-0.1415
R (uT)	0.57	0.48	0.72	0.61	(m)	(m)
R (wT)	-0.33	-0.29	-0.28	-0.36	(m)	(m)
R (vT)	0.07	0.06	-0.13	-0.13	(m)	(m)
R (uv)	0.15	0.15	-0.16	0.02	(m)	(m)
R (vw)	-0.15	-0.10	-0.07	-0.17	(m)	(m)
R (uw)	-0.29	-0.38	-0.28	-0.34	(m)	(m)

Table A6. Normalized estimates of the cospectral COS and quadrature QUAD contributions to the coherence of uw, wT, and uT for selected field experiments. The sum of COS and QUAD at each frequency n (cycles sec^{-1}) is plotted in Figures 10 through 23b.

(a) uw

n	7B-16M		8-16M		9-16M		10-16M		12-16M	
	COS	QUAD	COS	QUAD	COS	QUAD	COS	QUAD	COS	QUAD
.0017	-.35	.14	.11	.00	.28	.00	.14	.21	.43	.01
.0033	.36	.16	.07	.00	.32	.00	.06	.08	.33	.00
.0050	.43	.10	.07	.03	.25	.01	.06	.01	.30	.00
.0083	.30	.03	.14	.01	.18	.00	.09	.00	.30	.00
.017	.15	.04	.18	.01	.19	.00	.27	.00	.30	.00
.025	.12	.05	.28	.01	.15	.05	.36	.00	.29	.01
.033	.13	.07	.41	.00	.09	.04	.36	.01	.32	.01
.042	.04	.06	.40	.00	.12	.03	.32	.00	.29	.01
.052	.04	.08	.27	.00	.16	.03	.32	.00	.19	.00
.062	.10	.03	.20	.03	.10	.03	.18	.00	.18	.01
.083	.07	.00	.27	.00	.08	.01	.06	.00	.16	.02
.11	.04	.01	.15	.00	.03	.03	.06	.00	.15	.00
.15	.01	.00	.16	.00	.00	.02	.06	.00	.09	.00
.20	.01	.00	.10	.01	.01	.01	.05	.00	.05	.01
.25	.00	.00	.07	.00	.01	.00	.05	.00	.02	.00
.30	.00	.02	.04	.00	.01	.00	.04	.00	.01	.00
.40	.00	.01	.02	.00	.00	.00	.00	.01	.00	.00
.50	.00	.00	.01	.00	.00	.00	.01	.00	.00	.00

n	14-16M		15-16M		16-16M		20-16M		20-40M	
	COS	QUAD	COS	QUAD	COS	QUAD	COS	QUAD	COS	QUAD
.0017	.00	.01	.08	.09	.29	.03	.29	.00	.09	.09
.0033	.01	.01	.12	.12	.31	.02	.31	.00	.13	.10
.0050	.05	.02	.26	.05	.35	.00	.24	.00	.24	.01
.0083	.03	.01	.19	.02	.28	.00	.30	.00	.19	.00
.017	.02	.00	.18	.06	.23	.01	.32	.01	.29	.00
.025	.00	.01	.14	.07	.20	.04	.33	.01	.24	.00
.033	.00	.07	.09	.05	.19	.06	.35	.00	.16	.00
.042	.00	.13	.02	.08	.19	.09	.35	.00	.17	.00
.050	.02	.04	.05	.07	.19	.06	.23	.00	.16	.00
.062	.02	.02	.03	.05	.14	.06	.16	.00	.16	.00
.083	.03	.00	.02	.01	.18	.07	.25	.00	.24	.00
.11	.00	.00	.02	.00	.08	.04	.15	.00	.22	.00
.15	.00	.00	.00	.00	.07	.06	.19	.00	.11	.01
.20	.01	.00	.04	.01	.04	.02	.14	.01	.11	.01
.25	.00	.01	.00	.01	.02	.00	.12	.00	.07	.00
.30	.01	.01	.00	.01	.01	.00	.06	.00	.04	.00
.40	.00	.00	.00	.00	.00	.00	.03	.00	.03	.00
.50	.01	.00	.00	.00	.00	.00	.04	.00	.02	.00

(a) uw

n	38-16M		38-40M		39-16M		39-40M		40-16M	
	COS	QUAD	COS	QUAD	COS	QUAD	COS	QUAD	COS	QUAD
.0014	.10	.02	.35	.05	.21	.02	.45	.00	.02	.05
.0028	.12	.00	.39	.02	.42	.04	.47	.04	.00	.15
.0042	.34	.02	.53	.04	.42	.00	.50	.15	.00	.11
.0069	.15	.00	.31	.01	.27	.00	.40	.01	.08	.02
.014	.13	.02	.16	.02	.25	.03	.27	.00	.17	.01
.021	.05	.04	.08	.02	.12	.05	.23	.03	.14	.00
.028	.02	.07	.08	.01	.15	.01	.23	.00	.15	.00
.036	.05	.12	.10	.02	.25	.01	.15	.00	.22	.00
.042	.10	.13	.12	.01	.22	.03	.08	.01	.23	.02
.049	.05	.10	.03	.00	.17	.08	.09	.00	.20	.01
.069	.03	.06	.02	.02	.15	.05	.05	.01	.22	.00
.094	.01	.03	.01	.01	.04	.00	.01	.02	.10	.01
.12	.01	.01	.02	.02	.06	.00	.01	.00	.09	.02
.17	.02	.00	.00	.00	.03	.02	.02	.00	.03	.01
.21	.02	.00	.00	.00	.03	.01	.01	.00	.00	.01
.25	.02	.00	.01	.00	.04	.00	.00	.00	.00	.00
.33	.00	.01	.00	.00	.02	.00	.00	.00	.00	.00
.42	.01	.00	.00	.00	.01	.00	.02	.00	.01	.00

n	40-40M		41-16M		41-40M		42-16M		42-40M	
	COS	QUAD	COS	QUAD	COS	QUAD	COS	QUAD	COS	QUAD
.0014	.24	.01	.01	.16	.07	.01	.10	.00	.36	.12
.0028	.17	.02	.05	.06	.14	.00	.21	.00	.24	.06
.0042	.19	.00	.14	.02	.39	.06	.14	.12	.14	.00
.0069	.24	.00	.13	.02	/24	.00	.24	.02	.24	.00
.014	.30	.00	.29	.02	.25	.00	.39	.00	.27	.00
.021	.26	.00	.28	.00	.28	.00	.43	.01	.30	.00
.028	.18	.01	.17	.00	.31	.00	.28	.02	.33	.00
.036	.29	.00	.17	.02	.26	.00	.19	.00	.30	.00
.042	.36	.00	.22	.02	.17	.00	.25	.00	.25	.01
.049	.22	.00	.19	.00	.14	.01	.32	.00	.18	.00
.069	.15	.00	.17	.00	.19	.01	.23	.00	.09	.00
.094	.11	.00	.10	.06	.06	.01	.12	.01	.16	.00
.12	.06	.00	.12	.01	.07	.01	.03	.00	.05	.00
.17	.08	.01	.05	.02	.04	.00	.06	.02	.04	.00
.21	.09	.00	.01	.00	.01	.00	.05	.00	.03	.00
.25	.11	.01	.00	.00	.01	.00	.02	.00	.02	.00
.33	.08	.00	.00	.00	.01	.00	.01	.00	.00	.00
.42	.08	.00	.00	.00	.01	.00	.03	.00	.00	.00

(b) WT

n	7B-16M COS	7B-16M QUAD	8-16M COS	8-16M QUAD	9-16M COS	9-16M QUAD	10-16M COS	10-16M QUAD	12-16M COS	12-16M QUAD
.0017	.58	.00	.02	.00	.00	.03	.07	.02	.21	.03
.0033	.64	.00	.01	.02	.04	.03	.00	.01	.29	.00
.0050	.52	.00	.00	.08	.12	.00	.13	.00	.18	.00
.0083	.44	.00	.06	.01	.03	.03	.06	.03	.16	.02
.017	.32	.05	.11	.22	.05	.11	.14	.01	.26	.00
.025	.34	.03	.13	.04	.05	.14	.24	.01	.36	.00
.033	.26	.01	.23	.04	.03	.12	.32	.02	.31	.02
.042	.13	.00	.22	.04	.02	.06	.32	.02	.20	.05
.050	.15	.00	.16	.05	.01	.05	.27	.01	.14	.08
.062	.18	.00	.21	.02	.02	.07	.16	.00	.18	.06
.083	.15	.00	.09	.05	.01	.08	.23	.04	.26	.04
.11	.12	.00	.11	.05	.02	.10	.11	.03	.18	.01
.15	.11	.00	.11	.05	.02	.03	.07	.02	.13	.02
.20	.11	.00	.08	.02	.01	.02	.10	.00	.07	.01
.25	.11	.00	.07	.01	.02	.02	.01	.01	.07	.01
.30	.10	.00	.01	.00	.00	.03	.00	.00	.04	.00
.40	.07	.00	.00	.01	.00	.02	.00	.00	.03	.01
.50	.02	.00	.00	.00	.00	.00	.00	.00	.00	.00

n	14-16M COS	14-16M QUAD	15-16M COS	15-16M QUAD	16-16M COS	16-16M QUAD	20-16M COS	20-16M QUAD	20-40M COS	20-40M QUAD
.0017	.07	.34	.02	.12	.29	.02	.19	.02	.08	.06
.0033	.15	.14	.02	.01	.31	.00	.19	.02	.10	.02
.0050	.62	.01	.28	.00	.38	.00	.12	.00	.06	.00
.0083	.27	.00	.11	.00	.25	.00	.24	.00	.09	.00
.017	.31	.01	.08	.00	.17	.03	.28	.01	.16	.00
.025	.32	.00	.04	.00	.16	.03	.26	.03	.17	.00
.033	.33	.00	.03	.03	.20	.01	.25	.04	.15	.00
.042	.30	.00	.02	.02	.26	.02	.22	.05	.20	.01
.050	.24	.00	.03	.01	.28	.05	.15	.05	.24	.01
.062	.16	.02	.02	.01	.22	.03	.14	.03	.18	.00
.083	.17	.02	.00	.00	.19	.01	.16	.02	.28	.00
.11	.04	.00	.00	.00	.08	.00	.22	.03	.12	.00
.15	.06	.00	.00	.00	.12	.00	.15	.02	.12	.00
.20	.07	.00	.00	.00	.09	.00	.15	.00	.19	.01
.25	.07	.01	.00	.00	.05	.00	.14	.01	.12	.01
.30	.05	.02	.00	.00	.03	.00	.12	.02	.06	.00
.40	.02	.01	.00	.00	.02	.00	.05	.02	.05	.00
.50	.03	.00	.01	.00	.01	.00	.08	.00	.01	.00

(b) wT

n	38-16M		38-40M		39-16M		39-40M		40-16M	
	COS	QUAD	COS	QUAD	COS	QUAD	COS	QUAD	COS	QUAD
.0014	.68	.00	.55	.01	.31	.06	.44	.10	.06	.16
.0028	.53	.00	.35	.02	.37	.06	.34	.14	.00	.21
.0042	.48	.00	.39	.01	.23	.11	.28	.26	.03	.15
.0069	.41	.00	.36	.00	.22	.03	.31	.03	.06	.05
.014	.13	.00	.21	.00	.20	.02	.23	.03	.18	.02
.021	.12	.01	.14	.01	.17	.00	.21	.00	.19	.00
.028	.23	.01	.14	.01	.20	.00	.17	.02	.18	.02
.036	.24	.00	.20	.01	.23	.02	.16	.05	.22	.09
.042	.23	.00	.22	.00	.17	.01	.10	.03	.23	.06
.049	.20	.00	.19	.00	.17	.01	.11	.00	.22	.05
.069	.16	.00	.20	.00	.13	.00	.01	.01	.16	.05
.094	.11	.01	.02	.00	.04	.00	.08	.00	.16	.00
.12	.15	.00	.01	.00	.01	.02	.04	.00	.11	.00
.17	.13	.00	.09	.00	.08	.00	.02	.00	.12	.00
.21	.07	.00	.07	.02	.04	.00	.01	.00	.06	.00
.25	.05	.01	.05	.01	.02	.00	.01	.00	.04	.01
.33	.04	.00	.02	.00	.01	.00	.01	.00	.06	.00
.42	.03	.00	.02	.00	.00	.00	.01	.00	.04	.00

	40-40M		41-16M		41-40M		42-16M		42-40M	
	COS	QUAD	COS	QUAD	COS	QUAD	COS	QUAD	COS	QUAD
.0014	.10	.09	.08	.00	.23	.01	.11	.00	.25	.12
.0028	.08	.08	.17	.02	.31	.03	.18	.00	.21	.10
.0042	.18	.03	.14	.09	.51	.07	.15	.10	.11	.03
.0069	.16	.00	.12	.05	.27	.00	.21	.03	.24	.00
.014	.19	.00	.18	.09	.26	.01	.34	.03	.35	.00
.021	.29	.01	.17	.06	.35	.01	.38	.01	.36	.01
.028	.38	.00	.11	.06	.40	.00	.26	.00	.26	.02
.036	.41	.00	.18	.04	.31	.00	.24	.00	.20	.00
.042	.38	.01	.24	.02	.23	.00	.26	.02	.26	.01
.049	.26	.00	.12	.04	.30	.01	.25	.03	.29	.02
.069	.21	.00	.25	.04	.27	.00	.26	.01	.16	.02
.094	.15	.00	.17	.06	.22	.01	.16	.00	.19	.01
.12	.19	.00	.12	.02	.15	.01	.08	.03	.17	.01
.17	.12	.00	.11	.00	.06	.01	.09	.00	.14	.02
.21	.10	.00	.10	.00	.05	.00	.07	.00	.11	.00
.25	.06	.00	.10	.00	.05	.00	.08	.00	.10	.00
.33	.02	.00	.09	.00	.03	.00	.08	.00	.08	.00
.42	.04	.00	.06	.00	.01	.00	.08	.00	.05	.00

(c) uT

n	7B-16M COS	7B-16M QUAD	8-16M COS	8-16M QUAD	9-16M COS	9-16M QUAD	10-16M COS	10-16M QUAD	12-16M COS	12-16M QUAD
.0017	.59	.25	.27	.07	.37	.02	.34	.00	.25	.11
.0033	.57	.24	.17	.06	.19	.00	.50	.00	.35	.02
.0050	.46	.25	.40	.04	.04	.05	.54	.00	.40	.05
.0083	.46	.09	.36	.01	.11	.01	.42	.01	.50	.01
.017	.34	.15	.40	.04	.00	.01	.45	.02	.53	.01
.025	.27	.04	.39	.06	.00	.02	.42	.02	.50	.00
.033	.13	.03	.48	.05	.00	.03	.36	.04	.49	.00
.042	.09	.00	.53	.06	.00	.00	.32	.02	.40	.01
.052	.14	.03	.46	.10	.01	.01	.37	.00	.31	.01
.062	.21	.02	.30	.12	.01	.01	.24	.00	.30	.02
.083	.20	.00	.26	.08	.00	.00	.16	.01	.31	.00
.11	.13	.00	.15	.11	.00	.01	.07	.02	.19	.00
.15	.04	.00	.17	.04	.01	.00	.14	.00	.09	.02
.20	.10	.00	.11	.03	.00	.00	.08	.00	.04	.01
.25	.04	.01	.08	.03	.00	.00	.12	.00	.01	.00
.30	.01	.03	.05	.02	.00	.00	.16	.00	.00	.00
.40	.02	.00	.02	.01	.00	.00	.23	.00	.00	.00
.50	.03	.00	.03	.01	.00	.00	.03	.00	.00	.00

n	14-16M COS	14-16M QUAD	15-16M COS	15-16M QUAD	16-16M COS	16-16M QUAD	20-16M COS	20-16M QUAD	20-40M COS	20-40M QUAD
.0017	.03	.33	.30	.07	.66	.07	.71	.00	.78	.00
.0033	.05	.32	.23	.08	.62	.08	.85	.00	.62	.02
.0050	.11	.20	.28	.12	.70	.03	.83	.00	.45	.01
.0083	.05	.06	.24	.06	.58	.01	.71	.00	.62	.00
.017	.05	.07	.17	.14	.38	.03	.61	.02	.51	.01
.025	.02	.00	.13	.08	.26	.05	.51	.03	.44	.00
.033	.01	.03	.05	.05	.22	.08	.46	.04	.40	.00
.042	.02	.05	.02	.02	.15	.13	.40	.07	.44	.00
.050	.05	.07	.04	.00	.17	.13	.35	.09	.41	.00
.062	.14	.02	.03	.00	.17	.03	.33	.06	.24	.00
.083	.06	.00	.01	.00	.08	.01	.31	.05	.24	.00
.11	.01	.00	.01	.02	.07	.01	.15	.00	.18	.01
.15	.00	.00	.03	.00	.01	.01	.09	.01	.09	.03
.20	.00	.01	.01	.33	.02	.00	.08	.01	.15	.01
.25	.01	.00	.00	.00	.01	.00	.05	.01	.07	.01
.30	.06	.00	.00	.00	.00	.00	.02	.01	.02	.01
.40	.22	.00	.00	.00	.00	.00	.01	.00	.01	.00
.50	.25	.00	.01	.00	.00	.00	.00	.00	.00	.00

(c) uT

n	38-16M COS	38-16M QUAD	38-40M COS	38-40M QUAD	39-16M COS	39-16M QUAD	39-40M COS	39-40M QUAD	40-16M COS	40-16M QUAD
.0014	.31	.17	.31	.33	.58	.11	.60	.06	.52	.00
.0028	.36	.10	.26	.28	.65	.10	.72	.05	.64	.00
.0042	.50	.03	.42	.08	.63	.07	.69	.05	.46	.02
.0069	.34	.02	.36	.04	.54	.04	.56	.03	.51	.00
.014	.26	.06	.40	.08	.42	.12	.44	.11	.50	.00
.021	.11	.03	.28	.03	.29	.07	.41	.04	.40	.01
.028	.05	.07	.22	.01	.23	.09	.31	.03	.34	.07
.036	.06	.04	.18	.03	.21	.09	.09	.00	.42	.04
.042	.17	.05	.22	.02	.19	.07	.15	.00	.41	.01
.049	.12	.06	.13	.00	.17	.02	.18	.00	.36	.00
.069	.03	.07	.03	.02	.19	.00	.14	.02	.33	.02
.094	.01	.02	.01	.01	.13	.02	.23	.00	.24	.00
.12	.02	.00	.03	.00	.07	.01	.13	.00	.20	.00
.17	.01	.00	.02	.00	.08	.02	.09	.02	.08	.00
.21	.03	.02	.02	.00	.06	.00	.05	.00	.05	.00
.25	.02	.01	.03	.00	.05	.00	.03	.00	.04	.00
.33	.01	.01	.01	.00	.02	.01	.01	.00	.02	.00
.42	.00	.00	.00	.00	.00	.00	.05	.00	.00	.00

n	40-40M COS	40-40M QUAD	41-16M COS	41-16M QUAD	41-40M COS	41-40M QUAD	42-16M COS	42-16M QUAD	42-40M COS	42-40M QUAD
.0014	.31	.00	.54	.05	.74	.09	.82	.01	.68	.00
.0028	.45	.01	.67	.02	.82	.02	.83	.01	.79	.00
.0042	.69	.00	.73	.01	.88	.00	.71	.00	.78	.00
.0069	.48	.00	.57	.03	.74	.00	.58	.03	.67	.01
.014	.50	.01	.52	.05	.60	.01	.46	.09	.61	.03
.021	.46	.04	.46	.05	.49	.04	.42	.03	.52	.03
.028	.44	.05	.32	.09	.50	.01	.28	.04	.38	.02
.036	.45	.02	.22	.10	.42	.00	.24	.05	.32	.01
.042	.47	.00	.20	.09	.32	.00	.35	.01	.41	.00
.049	.43	.01	.20	.05	.25	.00	.37	.05	.35	.02
.069	.32	.02	.28	.08	.20	.00	.16	.01	.24	.01
.094	.26	.01	.23	.00	.09	.01	.12	.00	.20	.01
.12	.13	.01	.11	.00	.14	.00	.07	.01	.06	.00
.17	.11	.02	.07	.00	.10	.00	.05	.01	.02	.01
.21	.10	.00	.04	.00	.12	.00	.04	.00	.01	.00
.25	.07	.00	.03	.00	.17	.00	.03	.00	.01	.00
.33	.01	.00	.04	.00	.17	.00	.01	.00	.00	.00
.42	.02	.00	.01	.00	.14	.00	.00	.00	.00	.00

INDEX OF DISTRIBUTION
METEOROLOGICAL RESEARCH REPORTS

Reports are furnished for information and retention. When no longer required, reports should be destroyed in accordance with current regulations.

	Nr Cys
Chief Signal Officer Department of the Army ATTN: SIGRD-4c Washington 25, D. C.	1
Chief, U.S. Army SigC Operations Research Office The Johns Hopkins University Washington 25, D. C.	1
Commanding Officer U.S. Army Signal R and D Lab ATTN: Chief, Met Div: Surveillance Fort Monmouth, New Jersey	2
President U.S. Army Signal Board Fort Monmouth, New Jersey	1
Commandant U.S. Army Signal School ATTN: Weather Br, DST Fort Monmouth, New Jersey	1
Commanding Officer, U.S.Army Signal Missile Support Agency ATTN: Chief, Missile Met. Div. White Sands, New Mexico	2
Commanding General U.S. Continental Army Command ATTN: ATSIG Fort Monroe, Virginia	1
Deputy for Defense Research and Engineering Office of the Secretary of Defense ATTN: Geophysical Sciences Washington 25, D. C.	1
Commandant U.S. Army Command and General Staff College ATTN: Archives Fort Leavenworth, Kansas	1
President U.S. Army Artillery Board Fort Sill, Oklahoma	1
Commandant U.S. Army Artillery and Missile School ATTN: Metro Div, Target Acquisition Dept Fort Sill, Oklahoma	1
Chief of Ordnance Department of the Army ATTN; ORDTU Washington 25, D.C.	1
Chief of Ordnance Department of the Army ATTN: ORDTB Washington 25, D.C.	1
Commanding General U.S. Army Ordnance Missile Command ATTN: Staff Assistance Div, Signal -Office (ORDXM-DR) Redstone Arsenal, Alabama	1
Commander U.S. Army Rocket and Guided Missile Agency ATTN: T and E Laboratory Redstone Arsenal, Alabama	1

Commander
U.S.Army Rocket and Guided
Missile Agency
ATTN: ORDXR-ODT
Redstone Arsenal, Alabama 1

Chief, Research and Development
Department of the Army
ATTN: CRD/M, Army Research Off.
Washington 25, D. C. 2

Commanding General
U.S. Continental Army Command
ATTN: ATINT D and D Div
Weather Branch
Fort Monroe, Virginia 2

Commanding General
U.S. Continental Army Command
ATTN: 16th Weather Squadron
USAF Air Weather Service
Fort Monroe, Virginia 1

Commanding Officer
Army Research Office--Durham
Duke Station
Durham, North Carolina 1

Chief Chemical Officer
Department of the Army
ATTN: R and D Command
Washington 25, D. C. 1

Director
U.S. Army Chemical Corps Opns
Research Gp
U.S. Army Chemical Center
Edgewood, Maryland 1

Commanding Officer
U.S. Army Chemical Corps Proving
Ground
ATTN: Chief, Meteorology Div
Dugway, Utah 2

The Quartermaster General
Department of the Army
ATTN: Research Br, R & E Div
Washington 25, D. C. 1

Commanding Officer
U.S. Army Quartermaster R and E
Command
ATTN: EPR Div
Natick, Massachusetts 1

Chief of Engineers
Department of the Army
ATTN: Chief, Engineer R and D Div
Washington 25, D. C. 1

Commander
U.S. Army Ballistics Missile Agency
ATTN: Director Research Laboratory
(ORDAB-RR)
Redstone Arsenal, Alabama 1

Commanding General
White Sands Missile Range
ATTN: Office of Ordnance Mission
(ORDBS-CM-SS)
White Sands, New Mexico 1

Commanding General
Aberdeen Proving Ground
ATTN: U.S. Army Ballistic Research
Laboratories
Fort George Meade, Maryland 1

Armed Services Technical Information
Agency
Arlington Hall Station
Arlington 12, Virginia 10

Director, Geophysical Research
Directorate
USAF Cambridge Research Center
Hanscom Field
Bedford, Massachusetts 1

Commander
USAF Air Weather Service
Scott Air Force Base, Illinois 1

Commander
2d Weather Group
USAF Air Weather Service
Langley Field, Virginia 1

Commander
U.S. Naval Research Laboratory
(Code 7100)
Washington 25, D.C. 1

Officer-in-Charge
U.S. Naval Weather Research Facility
U.S. Naval Air Station
Norfolk, Virginia 1

Commanding Officer
U.S. Army Corps of Engineers
ATTN: SIPRE
1215 Washington Avenue
Wilmette, Illinois 1

Commanding Officer
U.S. Army Corps of Engineers
ATTN: Army Mobility Research Center
Vicksburg, Mississippi 1

Chief of Transportation
Department of the Army
ATTN: CAD-E
Washington 25, D.C. 1

Chief of Transportation
Department of the Army
ATTN: TCCAD-E
Washington 25, D.C. 1

Commanding Officer
U.S. Army Transportation R & E Command
ATTN: Chief, Tech Svcs Div
Fort Eustis, Virginia 1

Chief, Radio Propagation Lab
U.S. National Bureau of Standards
Boulder, Colorado 1

Chief, Fallout Studies Branch
Division of Biology and Medicine
Atomic Energy Commission
Washington 25, D. C. 1

Director, Soil and Water Conservation Division
Agricultural Research Service
U.S. Dept. of Agriculture
Beltsville, Maryland 1

Director, Pacific Southwest Forest and Range Experiment Station
U.S. Dept. of Agriculture Forest Service
P.O. Box 245
Berkeley 1, California 1

Executive Secretary
American Meteorological Society
45 Beacon Street
Boston 8, Massachusetts 1

Director, National Center for Atmospheric Research
University of Colorado
Boulder, Colorado 1

Commander
U.S. Navy Electronics Laboratory
ATTN: Dr. M. Halstead
San Diego 52, California 1

Officer-in-Charge
Meteorological Curriculum
U.S. Naval Post Graduate School
Monterey, California 1

Director, Atmospheric Sciences Program
National Science Foundation
Washington 25, D. C. 1

Chief
U.S. Weather Bureau
Washington 25, D. C. 7

Chief
National Aeronautics and Space Administration
Washington 25, D. C. 1

Director, Federal Aviation Agency
Bureau of Research & Development
ATTN: Records Officer
Washington 25, D. C. 1

Director, National Research Council
National Academy of Sciences
2101 Constitution Avenue
Washington 25, D. C. 1

Director, Meteorology Dept.
Pennsylvania State University
University Station, Pa. 1

Director, Meteorology Department
St. Louis University
St. Louis, Missouri 1

Dept of Oceanography & Met
The Agricultural & Mechanical
College of Texas
College Station, Texas 1

Director, Meteorology Department
University of Washington
Seattle, Washington 1

Director, Meteorology Department
University of Wisconsin
Madison, Wisconsin 1

Director, Meteorology Department
University of Arizona
Tucson, Arizona 1

Director, Meteorology Department
University of California at
Los Angeles
Los Angeles 24, California 1

Director, Meteorology Department
The University of Chicago
Chicago 37, Illinois 1

Director, Meteorology Department
Cornell University
Ithaca, New York 1

Director, Meteorology Department
Florida State University
Tallahassee, Florida 1

Director, Department of Civil
Engineering
Johns Hopkins University
Baltimore 18, Maryland 1

Director, Meteorology Department
Massachusetts Institute of Technology
Round Hill Field Station
South Dartmouth, Mass 1

Dept of Civil Engineering
Colorado State University
Fort Collins, Colorado 1

Dept. of Soils
University of Wisconsin
ATTN: Dr. C.B. Tanner
Madison, Wisconsin 1

Department of Agricultural Chemistry
and Soils
University of Arizona
ATTN: Dr. D.M. Anderson
Tucson, Arizona 1

Department of Agronomy
Utah State University
ATTN: Dr. S.A. Taylor
Logan, Utah 1

Department of Geophysics
Washington University
St. Louis, Missouri 1

Meteorology Department
University of Hawaii
Honolulu, Hawaii 1

Atmospheric Science Branch
Scientific Research Institute
Oregon State College
Corvallis, Oregon 1

Department of Meteorology
University of Utah
Salt Lake City, Utah 1

Department of Agronomy
Iowa State University
ATTN: Dr. R.H. Shaw
Ames, Iowa 1

Electrical Engineering Research Laboratory
The University of Texas
Austin, Texas 1

Department of Soils
University of Missouri
Columbia, Missouri 1

Meteorology Department
San Jose State College
San Jose, California 1

Commanding General
ATTN: SIGPG AGAC
U.S. Army Electronic Proving Ground
Fort Huachuca, Arizona 43

Director, Geophysical Research Directorate
USAF Cambridge Research Center
ATTN: CRZD
Hanscom Field
Bedford, Massachusetts 2

Director, Meteorology Dept.
Massachusetts Institute of Technology
Cambridge 37, Mass 1

Director, Meteorology Dept
University of Michigan
Ann Arbor, Michigan 1

Director, Meteorology Dept
New York University
University Heights
New York 53, New York 1

Department of Irrigation
University of California
Davis, California 1

Dept of Agricultural Engineering
University of California
ATTN: Dr. F. A. Brooks
Davis, California 1

University of Minnesota
ATTN: Dean Spilhouse
Minneapolis, Minnesota 1

Director, U.S. Salinity Laboratory
P.O. Box 672, ATTN: Dr. L.A. Richards
Riverside, California 1

Director, Southern Piedmont Soil Conservation Field Station
U.S. Department of Agriculture
P.O. Box 33
Watkinsville, Georgia 1

Director, U.S. Water Conservation Lab
Agricultural Research Service
U.S. Department of Agriculture
Route 2, Box 816-A
Tempe, Arizona 1

Soil and Water Conservation Research Division
Agricultural Research Service
U.S. Department of Agriculture
Cornell University, Bailey Hall
Ithaca, New York 1

Department of Meteorology
University of Wisconsin
Madison, Wisconsin 1

Massachusetts Institute of Technology, Round Hill Field Station, South Dartmouth, Massachusetts

STUDIES OF THE SPECTRA OF THE VERTICAL FLUXES OF MOMENTUM, HEAT, AND MOISTURE IN THE ATMOSPHERIC BOUNDARY LAYER

By Dr. Harrison E. Cramer, Dr. Frank A. Record, and Mr. James E. Tillman
Final Report, April 1962

112 pages, 66 illus.

(Contract DA-36-039-SC-80239)

This report deals with the investigation of the spectra of the vertical fluxes of momentum, heat and water vapor in the atmospheric boundary layer under various thermal stratifications and surface roughness.

UNCLASSIFIED

1. Micrometeorology
2. Turbulence Studies
3. Spectral Analyses
4. Fast-Response Meteorological Instrumentation

UNCLASSIFIED

Massachusetts Institute of Technology, Round Hill Field Station, South Dartmouth, Massachusetts

STUDIES OF THE SPECTRA OF THE VERTICAL FLUXES OF MOMENTUM, HEAT, AND MOISTURE IN THE ATMOSPHERIC BOUNDARY LAYER

By Dr. Harrison E. Cramer, Dr. Frank A. Record, and Mr. James E. Tillman
Final Report, April 1962

112 pages, 66 illus.

(Contract DA-36-039-SC-80239)

This report deals with the investigation of the spectra of the vertical fluxes of momentum, heat and water vapor in the atmospheric boundary layer under various thermal stratifications and surface roughness.

UNCLASSIFIED

1. Micrometeorology
2. Turbulence Studies
3. Spectral Analyses
4. Fast-Response Meteorological Instrumentation

UNCLASSIFIED

Massachusetts Institute of Technology, Round Hill Field Station, South Dartmouth, Massachusetts

STUDIES OF THE SPECTRA OF THE VERTICAL FLUXES OF MOMENTUM, HEAT, AND MOISTURE IN THE ATMOSPHERIC BOUNDARY LAYER

By Dr. Harrison E. Cramer, Dr. Frank A. Record, and Mr. James E. Tillman
Final Report, April 1962

112 pages, 66 illus.

(Contract DA-36-039-SC-80239)

This report deals with the investigation of the spectra of the vertical fluxes of momentum, heat and water vapor in the atmospheric boundary layer under various thermal stratifications and surface roughness.

UNCLASSIFIED

1. Micrometeorology
2. Turbulence Studies
3. Spectral Analyses
4. Fast-Response Meteorological Instrumentation

UNCLASSIFIED

Massachusetts Institute of Technology, Round Hill Field Station, South Dartmouth, Massachusetts

STUDIES OF THE SPECTRA OF THE VERTICAL FLUXES OF MOMENTUM, HEAT, AND MOISTURE IN THE ATMOSPHERIC BOUNDARY LAYER

By Dr. Harrison E. Cramer, Dr. Frank A. Record, and Mr. James E. Tillman
Final Report, April 1962

112 pages, 66 illus.

(Contract DA-36-039-SC-80239)

This report deals with the investigation of the spectra of the vertical fluxes of momentum, heat and water vapor in the atmospheric boundary layer under various thermal stratifications and surface roughness.

UNCLASSIFIED

1. Micrometeorology
2. Turbulence Studies
3. Spectral Analyses
4. Fast-Response Meteorological Instrumentation

UNCLASSIFIED